Fall 12-20-2019

HIV-1 Elimination in Humanized Mice

Hang Su
University of Nebraska Medical Center

HIV-1 Elimination in Humanized Mice

by

Hang Su

A Dissertation

Presented to the Faculty of

the Graduate School in the University of Nebraska Medical Center

in Partial Fulfillment of the Requirements

for the Degree of Doctor of Philosophy

Department of Pharmacology and Experimental Neuroscience

Under the Supervision of Professor Howard E. Gendelman

University of Nebraska Medical Center

Omaha, Nebraska

October 2019

Supervisory Committee:

Prasanta K. Dash, Ph.D.

Tatiana K. Bronich, Ph.D.

Larisa Y. Poluektova, M.D., Ph.D.

Angie Rizzino, Ph.D.

Samuel M. Cohen, M.D., Ph.D.

Acknowledgements

First of all, I would like to thank my mentor Dr. Howard E. Gendelman, for all these years' unconditional guidance and support. His foresight in science keeps us at the frontier of the field and shows us the way of thinking. His hard working motivates us to expand our limitations and complete missions that once seemed impossible. He always immerses his wisdom in his humor and teaches us to be optimistic about life. His passion in science encourages us to pursue and succeed in what we do.

I would like to thank my committee members Drs. Prasanta K. Dash, Tatiana K. Bronich, Larisa Y. Poluektova, Angie Rizzino, and Samuel M. Cohen for their consistent guidance, suggestions, and support over the years. I want to specially thank Dr. Dash for his day-to-day supervision, training, and support. I appreciate his support as both a mentor and close friend. I would like to thank Dr. Poluektova and Dr. Santhi Gorantla for their support on both science and daily life through the years. I would like to thank all the former and current Gendelman's lab members for their all-time support and friendship, which includes but not limited by Drs. Mariluz Arainga, Divua Prakash, Midhun Ben Thomas, Bhavesh Kevadiya, Saumi Mathews, JoEllyn McMillan, Benson Edagwa, R. Lee Mosley, Charles Schutt, Kate Olson, Weizhe Li, Tian Zhou, Brady Sillman, Zhiyi Lin, James R. Hilaire, Aditya N. Bade, Ibrahim Ibrahim, Mary Banoub and Denise Cobb, Diana Palandri, Mahmudui Hasan, Jonathan Herskovitz, Tanmay Kulkarni, Insiya Mukadam, Brendan Ottemann, Dhruvkumar Soni, Sruthi Sravanam, Yan Cheng, Lili Guo, Li Wu, Weimin Wang, and Edward Makarov.

I would like to thank the Chinese Scholarship Council and UNMC fellowship for the financial support during my PhD training. I would like to thank the committee and friends in UNMC MD/PhD program for your support and friendship. I would like to thank all administrative staff at UNMC Graduate Studies and Department of Pharmacology and Experimental Neuroscience for the many years of support. I would like to thank the staff in UNMC core research and animal facilities for their support.

I would like to thank my parents, Guobin Su and Yanbin Liu, for their understanding, love, support, and sacrifice. They always supported me on whatever I choose to do and put me first above all else. I wouldn't be who I am without them. I also wouldn't survive without my friends on and off campus. Their lifelong friendship is invaluable treasure. One person is too small. I am only standing here because all of you around me.

Hang Su

October 2019

Abstract

HIV-1 Elimination in Humanized Mice

Hang Su, Ph.D.

University of Nebraska Medical Center, 2019

Supervisor: Howard E. Gendelman, M.D.

Human immunodeficiency virus type one (HIV-1) exclusively infects humans and chimpanzees. Therefore, animal models are required for all investigations of viral pathogenesis, therapy and cure. Immunodeficient mice transplanted with human hematopoietic stem cells, termed humanized mice, support the development of multiple human cell lineages throughout the cell's life span. To this end, we used humanized mice to evaluate the dynamic changes of host immunologic and viral profiles during both acute and chronic HIV-1 infection. We identified the temporal and spatial distribution of HIV-1 cell and tissue compartment infections and outlined correlations made between viral progression and host immunity by comparing two different humanized mouse models. Based on the discovery of early viral set-points, we developed a paradigm for a potential 'HIV-1 cure' by sequential administration of long-acting slow-effective release antiretroviral therapy (LASER ART) and CRISPR-Cas9 treatments. HIV-1 elimination was achieved in a third of dual-treated humanized mice after exhaustive works to detect HIV-1 and its gene products in peripheral blood, brain, lung, liver, spleen, kidney, gut, and bone marrow (BM). This was done by sensitive nested and digital-droplet PCR and RNAscope tests. Immune function was preserved in animals where HIV-1 was eliminated. In vivo viral outgrowth assay (VOA) was employed to confirm HIV-1 elimination by adoptive transfer of donor splenocytes and BM cells into naïve humanized mice. While

virus was successfully recovered from HIV-1 control, LASER ART or CRISPR-Cas9 alone treated animals virus could not be recovered in recipients transplanted from a third of the dual-treated “cured” animals. We further characterized the impact of humanized mice-based VOA in viral isolation assay by expanding the sample sizes. We observed that replication-competent HIV-1 persisted in multiple tissues even when plasma viral load was undetectable and virus can be readily recovered from naïve humanized mice. We demonstrate that in vivo VOA using humanized mice is a sensitive assay system to interrogate replication competent HIV-1 and can be employed to determine viral eradication from donor samples. To this end, we used the humanized mouse model to study HIV-1 tissue compartmentalization, interrogate HIV-1 eradication employing innovative technologies, and assess HIV-1 elimination using humanized mice-based VOA, which will facilitate future translational studies.

Table of Contents

List of Figures

Chapter 2

Chapter 3

Chapter 4

List of Tables

Chapter 2

Chapter 4

List of Abbreviation

AIDS acquired immune deficiency syndrome

HIV human immunodeficiency virus

ART antiretroviral therapy

GALT gut-associated lymphoid tissue

TSCM T stem cell memory

TCM T central memory

TTM T transitional memory

TEM T effector memory

TMM T migratory memory

TRM tissue T resident memory

TTD T terminally differentiated

FDC follicular dendritic cell

TFH follicular CD4+ helper T cells

HPC hematopoietic progenitor cell

VL viral load

CSF cerebrospinal fluid

SIV simian immunodeficiency virus

NHP non-human primate

HLA human leukocyte antigen

TRIM5α tripartite motif-5alpha isoform

APOBEC3G apolipoprotein beta mRNA-editing enzyme catabolic polypeptide 1-like protein G

HSC hematopoietic stem cell

NSG NOD.Cg-Prkdc^{scid}IL2rg^{tm1Wjll}/Sz

NOG NOD.Cg-Prkdc^{scid}Il2rg^{tm1Sug}

NRG NOD-Rag1^{tm1Mom}IL2rg^{tm1Wjll}/Sz)

BM Bone marrow

PK pharmacokinetic

PD pharmacodynamic

DTG dolutegravir

NMDTG nanoformulated myristyl DTG

hu-PBL human peripheral blood lymphocyte

CAB cabotegravir

HSCT hematopoietic stem cell transplantation

GvHD graft versus host disease

PTC posttreatment controller

LRA latency-reversing agent

HMTi histone methyltransferase inhibitor

HDACi histone deacetylase inhibitors

PKC protein kinase C

P-TEFb positive transcription elongation factor b

SMACm second mitochondrial activator of caspases mimetic

Bcl-2 B cell lymphoma 2

CTL cytotoxic T lymphocyte

PD1 programmed cell death protein 1

CTLA4 cytotoxic T lymphocyte antigen 4

TIM3 T cell immunoglobulin mucin receptor 3

LAG3 lymphocyte activation gene 3 protein

PDL1 PD1 ligand

bNAb broadly neutralizing antibody

ADCC antibody-dependent cellular cytotoxicity

TLR7 toll-like receptor 7

CAR-T chimeric antigen receptor T cell

SHIV simian-human immunodeficiency virus

ZFN zinc finger nuclease

TALEN transcription activator-like effector nuclease

CRISPR clustered regularly interspaced short palindromic repeat

HSPC hematopoietic stem/progenitor cell

gRNA guide RNA

LASER ART long acting slow effective release ART

VOA viral outgrowth assay

$TCID_{50}$ 50% tissue culture infective doses

IRB Institutional Review Board

IACUC Institutional Animal Care and Use Committee

FACS fluorescence-activated cell sorting

PPIB Human peptidylprolyl isomerase B

SEM standard error of the mean

DL detection limit

IPA Ingenuity Pathway Analysis

3TC lamivudine

ABC abacavir

RPV Rilpivirine

EDTA ethylenediaminetetraacetic acid

ddPCR droplet digital PCR

PHA/IL-2 phytohemaglutinin/interleukin-2

CCR5 β-chemokine receptor type 5

iPSCs induced pluripotent stem cells

GC genome copy

qVOA quantitative viral outgrowth

mVOA mouse viral outgrowth assay

TR total recipient

SR spleen recipient

BR BM recipient

ATI antiretroviral therapy interruption

HAART highly active antiretroviral therapy

CAB cabotegravir

VLP virus-like particle

Chapter 1 Introduction

1.1 HIV-1 reservoirs

The wide spread use of antiretroviral therapy (ART) has heralded a remarkable milestone for the treatment of human immunodeficiency virus type one (HIV-1) infection. Disease morbidity and mortalities have been reduced significantly and infection is now medically manageable with viremia suppressed to undetectable levels. Also, there is preservation of CD4+ T cell and global immune function (1-3). This includes, but is not limited to, the maintenance of fully functional circulating and tissue $CD4^+$ T cells (4, 5). However, ART requires life-long uninterrupted treatments. This is as a consequence of HIV-1 persistence as latent replication-competent genomic integrated provirus. Such HIV-1 infected cells persist with an average half-life of 44 months. This occurs with or without suppressive ART. It is estimated to take up to 70 years for complete viral decay (6). Underlying the need for continuous ART is the speed of viral rebound that typically ensues within 2 weeks after antiretroviral drug (ARV) discontinuation (7-9). Therefore, viral reservoirs are the major obstacle towards securing an HIV-1 cure.

HIV-1 reservoirs are a pool of infected cells containing replication-competent viral sequence whereas extremely low or no viral antigens are expressed. HIV-1 reservoirs are distributed in human body across a broad range of cell (principally CD4+ T cells) and tissue (gut-associated lymphoid tissue (GALT), spleen, lymph nodes, brain, genitourinary system and lung, see below) **(Figure 1.1).** The best characterized HIV-1 reservoir is resting CD4+ T cells, of which most are present with a memory phenotype. Memory T cells can be further allocated to stem cell memory (TSCM), central memory (TCM), transitional memory (TTM), effector memory (TEM), migratory memory (TMM), tissue resident memory (TRM) and terminally differentiated (TTD) cells (10, 11). While individual memory T cell

type contributes to HIV-1 reservoirs to different degrees, TCM is considered as a major source of viral latency (10, 11). Monocyte-macrophages also play a prominent role in HIV-1 latency that viral DNA/RNA and antigens can be detected in patients after long-term effective ART (12, 13). Macrophages are long-lived and resistant to cytotoxic T lymphocytes-mediated killing which make them ideal candidates as HIV-1 reservoirs (14). Other cell types such as dendritic cells, epithelial cells, and hematopoietic stem/precursor cells may also serve as HIV-1 reservoirs that need further investigation (10, 15).

Tissues represent major HIV-1 sanctuaries where tremendous amounts of viral susceptible immune cells reside along with limited ART penetration (16). While peripheral CD4+ T lymphocytes are easy to access in the clinic and have been extensively interrogated as the surrogate of HIV-1 reservoirs, it is noteworthy that more than 98% of total body CD4+ T lymphocytes reside throughout variant tissues (17). Tissue-derived macrophages have also been reported to harbor latent HIV-1 (18, 19). GALT and lymph nodes, which are the most accessible tissue samples in the clinic, have been employed as surrogates to determine HIV-1 tissue infection in patients. GALT is one of the earliest breached organs during acute HIV-1 infection. Studies have discovered active viral replication and depletion of memory CD4+ T cell during early HIV/SIV infection (20). Persistence of viral DNA/RNA was observed in GALT even after years of effective ART (21, 22). Early viral invasion of lymph nodes has been reported in humans (23). Lymph nodes are characterized as diverse viral susceptible immune cells, lower ART concentrations, and resistance to cytotoxic CD8+ T cells and NK cells surveillance. Altogether lymph nodes are an ideal sanctuary maintaining HIV-1 replication under treatment (24). Recently the follicular dendritic cell (FDC) network that locates in the lymphoid tissues has drawn attention as an

HIV-1 shelter. The FDC system traps viral particles that facilitates infection of massive immune cells that are located, especially follicular CD4+ helper T cells (TFH) and follicular regulatory T cells (TFR) which support active HIV-1 infection and maintain HIV-1 latency during ART (25, 26). This emphasizes the significance of lymphoid tissues such as GALT, lymph nodes, and spleen as HIV-1 tissue reservoirs. Compared to the other two, spleen viral infection is much under studied due to difficulty of sample access. Using simian immunodeficiency virus-infected macaque model spleen is identified as an active viral infection site as well as viral sanctuary during ART (27). Lung and liver contain plentiful HIV-1 susceptible cells, especially myeloid-derived macrophages (alveolar macrophages and Kupffer cells). Although there is evidence showing that both tissues harbor HIV-1 in untreated patients (28, 29), their contribution to systemic viral persistence under highly suppressive ART is unclear. Studies have found that viral compartmentalization existed between lung, liver and peripheral blood (29, 30). In addition, viral particles were successfully recovered from tissue-specific macrophages in patients with controlled viremia (31), suggesting that myeloid cells may represent the major HIV-1 reservoirs in these two organs. The long-lived hematopoietic progenitor cells (HPCs) located in bone marrow hold the potential of self-renewal and differentiation to different cellular lineages that can serve as HIV-1 reservoirs as soon as they start to express major HIV-1 receptor CD4 and co-receptors CCR5 and CXCR4 (32). Although it remains unclear if hematopoietic stem cells maintain HIV-1 latency, persistent viral infection was observed in both untreated and ART-treated bone marrow cells (32, 33). HIV-1 is also tracked in other tissue types such as kidney where multiple cell types were found susceptible to viral infection (34). However, the contribution of various anatomical sites to HIV-1 latency

needs further investigation. Lamers el al. scrutinized 229 autopsy samples from 20 HIV-1 patients who received ART and exhibited low or undetectable plasma viral load (VL) and cerebrospinal fluid (CSF) prior to death. A wide spectrum of tissue types was covered including brain, aorta, colon, kidney, liver, lung, lymph nodes, spleen, and testis. Surprisingly, although HIV-1 tissue distribution varies between patients, viral DNA was recovered from all the participants (35). This report confirmed that HIV-1 persists in tissues under long-term effective ART even when plasma VL is undetected. Development of strategies that can target and eliminate tissue HIV-1 infection is critical to achieve HIV-1 cure.

1.2 Animal models for studies of HIV-1 pathogenesis

HIV-1 is a species-specific pathogen that only infects humans and chimpanzees (36-38). Therefore, a major obstacle in investigating the pathophysiology and assessing novel treatment of HIV-1 and AIDS rests on the development of animal models that readily reflect virus-to-host interactions as in human. HIV-1 originates from its counterpart simian immunodeficiency virus (SIV) that infects non-human primates (NHPs) symptomatically or asymptomatically depending on viral strains and host species (39). Therefore, SIV-infected macaques including three most commonly used species, rhesus macaques (*Macaca mulatta*), pigtailed macaques (*Macaca nemestrina*), and cynomolgus macaques (*Macaca fascicularis*), have become valuable tools to study HIV-1 infection. Indeed, with a similar immune system, NHP models have successfully recapitulated major symptoms of HIV-1 infection in human including CD4+ T cell depletion, peripheral and tissue viral replication, viral control under functional CD8+ T cell and ART administration,

establishment and reversal of viral latency, and development of AIDS (40). Additionally, NHPs provide more accessible tissue sample acquisition, controlled experimental design (infection, treatment, and treatment interruption), and tests of novel regimens and techniques not easily done in humans. NHP models have extended our understanding of HIV/AIDS pathobiology and facilitated our progress on HIV-1 cure. However, it is noteworthy that SIV and HIV are still genetically different viruses with only 53% sequence identity (41). This reflects on the different compositions of human leukocyte antigen (HLA) genes between HIV and SIV that account for viral antigen recognition and cellular restriction factors such as tripartite motif-5alpha isoform (TRIM5α) and apolipoprotein beta mRNA-editing enzyme catabolic polypeptide 1-like protein G (APOBEC3G) that affect viral entry into cells (39). Altogether, these factors lead to more rapid disease progression in SIV-infected rhesus macaque than in HIV-infected human. It may also explain many failures during reproduction of SIV discoveries in HIV. In addition, high cost of NHPs significantly impedes the usage of this model in large scalable studies that require assessment of multiple experimental parameters. Therefore, small murine models, namely humanized mice, have been developed to compensate these limitations.

The principle of generating humanized mice is to reconstitute human CD34+ hematopoietic stem cells (HSCs) that are isolated from fetal livers or umbilical cord blood into murine with immunodeficient background such as NSG (NOD.Cg-Prkdc^{scid}IL2rg^{tm1Wjll}/Sz), NOG (NOD.Cg-Prkdc^{scid}Il2rg^{tm1Sug}), and NRG (NOD-Rag1^{tm1Mom}IL2rg^{tm1Wjll}/Sz) (42). Multiple lineages of human immune cells including T cells, B cells, NK cells, monocytes/macrophages, and dendritic cells can be established and sustained in mouse peripheral blood as well as various tissues including brain, lung, spleen,

kidney, liver, gut, and bone marrow (BM). To this end, these humanized mice can be used as a platform to support human disease studies (e.g. HIV-1). For relative low expense and short lifespan (about 1 year) of animals, humanized mice are more accessible, easier to scale up, and can be employed for reasonable long periods of studies.

Using HIV-1 infected human CD34+ HSCs-reconstituted NSG (hu-HSC) mice, our lab observed a sustained CD4+ T cell decrease in both peripheral blood and tissues (spleen and BM) as detected in clinical patients (43). Multiple forms of HIV-1 DNA and RNA was identified in a broad spectrum of tissues including BM, spleen, lung, gut, brain, kidney, and liver. We further analyzed dynamic changes of numbers and distributions of cell subtypes including CD34+ progenitor cells, monocyte-macrophages, dendritic cells, regulatory CD4+ T cells, and memory T cells (stem cell memory, naïve memory, central memory, and effector memory) and identified HIV-1 infection in each individual cell types. Our discoveries using humanized mice either paralleled with what has been observed in HIV-1 infected patients or provided new insights of HIV-1 pathophysiology. Together it demonstrated that humanized mouse models are valid platforms that recapture the characteristics of HIV-1 infection. We further employed humanized mice to evaluate the pharmacokinetic (PK) and pharmacodynamic (PD) profiles of parent ART and house-made modified ART (a HIV-1 integrase inhibitor dolutegravir (DTG) in this case). In the initial screen, a single dose of intramuscular (IM) injection of native DTG or prodrug DTG (nanoformulated myristyl (NMDTG) in this case) was administered to human peripheral blood lymphocytes (hu-PBLs)-reconstituted NSG mice. Animals were infected at either 2 or 4 weeks after treatment and kept for another 10 days before sacrifice. NMDTG exhibited superior PK and PD profiles over native DTG as shown by sustained higher levels of parent

drug in both peripheral blood and multiple tissues (spleen, gut, liver, lung, and kidney) and lower HIV-1 expression was observed in NMDTG-treated animals compared to native DTG-treated animals. Similar results were confirmed when NMDTG was tested using hu-HSC mice (44). In addition, the characteristics of other drugs, e.g. nanoformulated cabotegravir (CAB), were also successfully assessed using humanize mouse model (45). Together, humanized mice have been demonstrated as a valid laboratory tool to investigate preclinical virology, immunology, pathogenesis, therapy, and potential eradication of HIV-1.

1.3 Strategies for HIV-1 cure

ART has led to considerable success on maintaining HIV-1 suppression and relatively normal immune function which combines to render a nearly normal life expectancy in patients. However, ART does not eradicate HIV-1 reservoirs that drive viral rebound upon ART discontinuation. In addition, cells that are considered HIV-1 reservoirs are usually long lived such as memory CD4+ T cells which withhold a half- life up to 4 years. At this rate, it will take 73 years to naturally eradicate a reservoir size of 10^6 cells (46). As a result, ART requires life-long adherence that renders the patients of treatment-associated side effects and toxicities along with high expenses and stigma associated with the disease. To this end, an HIV-1 cure is highly urged in the community. To date, there have been only 2 cases of HIV-1 cure, the “Berlin patient” and the “London patient” who underwent similar procedures (47, 48). Both patients received allogeneic hematopoietic stem cell transplantation (HSCT) from the respective donor with a homozygous mutation in the HIV coreceptor CCR5 (CCR5Δ32/Δ32) for the treatment of tumorous malignancy.

Both patients underwent ART interruption later after the procedures and have remained viral remission for 10 and 2 years, respectively (47, 48). While the news remains exciting, it is unrealistic to put millions of HIV-1 patients into aggressive chemotherapy/irradiation and highly risky HSCT. Indeed, at least 6 other cancer patients who went through similar procedures died within 12 months after transplantation due to cancer relapse, graft versus host disease (GvHD), or other comorbidities (49). Nevertheless, these two cases demonstrated that HIV-1 cure can be realized when viral reservoirs are completely eliminated (the so-called "sterilizing cure") that is assumed to have happened to both patients. What can be implied is that a smaller HIV-1 reservoir size may lead to delayed viral rebound and even long-term viral remission in the absence of ART, namely functional cure. This was demonstrated in the "Mississippi child" case who acquired perinatal HIV-1 infection and started ART at 30 hours after birth. Treatment was discontinued by the parents at age of 18 months and a delayed viral rebound until 27 months later was achieved, indicating limited amounts of HIV-1 reservoirs achieved by early ART administration may set up a foundation for long-term viral control (50). Reduction of HIV-1 latency burden was also observed in early treated adults (51). In this study, HIV-1 latency was found to be established within 2 weeks of infection. However, compared to untreated patients, individuals who started ART at early stage had much lower levels of total and integrated HIV-1 DNA that represented a smaller size of HIV-1 latency. In addition, lower viral reservoir level is correlated to prolonged viral remission (52). In the VISCONTI cohort, patients, termed posttreatment controllers (PTCs), initiated ART during acute HIV-1 infection and maintained viral suppression for several years upon treatment interruption (53). It is noteworthy that early ART alone does not eliminate HIV-1 infection. In a recent

report, patients that initiated ART during Fiebig I stage (positive HIV-1 RNA, negative HIV-1 antigen/antibody) (54) that is considered the earliest stage of infection all experienced rapid viral rebound following treatment interruption (55). The median rebound time was 26 days which is no different from general populations that undergo ART intervention (56, 57). Even so, early ART successfully prevents HIV-1 transmission, limits viral escape, improves immune function, and reduce HIV-1 associated morbidity and mortality in the long run. Therefore, early treatment set the foundation for HIV-1 cure which might be achieved when other strategies are combined.

HIV-1 reservoirs remain latent in ART-treated individuals with minimal to no viral transcription/translation, needed to evade immune surveillance and ART responses (58). To expose the footprint of reservoirs, an approach termed “shock and kill” was developed that implements latency-reversing agents (LRAs) to reawaken dormant virus (shock) from latently-infected cells and induces viral and/or immune-mediated cell death (kill), while sustained ART prevents newly produced virus from infecting healthy cells (59). HIV-1 latency is maintained through several mechanisms including HIV-1 integration site and orientation, DNA methylation and histone deacetylation, lack of key transcription factors, inhibition of transcriptional elongation, and others (60). To target each mechanism, respective reagents were developed including histone methyltransferase inhibitors (HMTi), histone deacetylase inhibitors (HDACi), protein kinase C (PKC) agonists, positive transcription elongation factor b (P-TEFb) activators, and disulfiram. Because many of these compounds are developed and already implemented in cancer and other medical field, researchers were able to accelerate their clinic tests on antiviral functions after *in vitro* and *ex vivo* evaluations. Currently, there are over 160 chemicals identified as LRAs that have

been tested preclinically or clinically in small scale (59, 61-63). To date, while certain LRAs are able to induce cell-associated HIV-1 RNA transcription and/or plasma HIV-1 RNA production, no reductions in HIV-1 reservoirs or delay in viral rebound have been met. Major concerns and suggested improvements have been proposed (59, 62, 64). First, the mechanisms by which present LRAs may affect infected and uninfected cells would cause generalized disturbance of homeostasis. Therefore, the dose, quantity, and frequency of LRAs needs cautious consideration and inevitably compromises their latency-reversing function (65). New generations of small molecules such as second mitochondrial activator of caspases mimetic (SMACm) acting on alternative pathways have exhibited partial immune activation while preserving efficacy for HIV-1 reactivation (59). Also, some of these compounds synergized with current LRAs on viral reactivation and remain front runners for clinical trials. It is noteworthy that these newly developed molecules are not viral unique emphasizing the continuous demand of more specific LRAs with high potency and minimal side effects. HIV-1 reservoirs distinguish themselves from healthy cells through their apoptosis-resistant characteristics (63). Cummins et al. demonstrated that co-treatment with a major apoptotic inhibitor, the B cell lymphoma 2 (Bcl-2) antagonist venetoclax, in αCD3/αCD28-treated cells from virally suppressed patients could induce preferential killing of HIV-1 infected cells, with minimal death of uninfected cells. More importantly, cell-associated viral DNA was significantly reduced upon dual-treatment compared to αCD3/αCD28 treatment alone (66). This virus-specific elimination strategy, named "prime, shock, and kill", needs further *in vivo* evaluation. Lack of efficacy is another shortcoming of current LRAs that reflects on both short half-lives and reactivation incompetency. Stochastic reactivation of HIV-1 latency requires repeated stimulation to

shrink reservoir size (67) and the activation effect is likely correlated to LRA concentrations (65). These, in combination, demand a high dose frequency and volume of LRAs leading to potential toxicity (59).

Nanotechnology offers a solution by formulating regimens into nanosuspensions that can prolong drug half-lives and reduce dosing frequencies (68, 69). In both preclinical and clinical studies, nanoformulated long acting ART has shown superior drug retention, release, and tissue penetration with minimal side effects when compared to native ART (70-73). Nanoformulation of LRAs is much under developed. Buehler et al. engineered self-assembling vault nanoparticles containing bryostatin-1 that exhibited HIV-1 reactivation and cell activation function using J-Lat cell line as latency model (74). Kovochich et al. showed that lipid nanoparticle-encapsulated bryostatin-2 enhanced HIV-1 latency reversal from J-Lat cells compared to conventional regimens (75). Notably, co-delivery of ART and LRA by nanoparticles, simultaneously reversed HIV-1 latency and prevented viral spread (75, 76). Further interrogation of such a co-delivery system towards reducing HIV-1 reservoirs should be pursued. Although there is still a long way to go before the realization of clinical use of nanoformulation on HIV-1 treatment, it is an appealing direction in terms of easing patients' life, improving clinical adherence, and lowering potential drug toxicity and side effects. Heterogeneity of HIV-1 reservoirs makes it unlikely for a single LRA to act on all hidden targets. Indeed, a given LRA exhibited high variability on viral reactivation using different primary and patients' cell samples while a specific cell model also reacts diversely upon distinct LRAs (77, 78). To overcome this hurdle, LRA combinations with variant mechanisms can be implemented that has shown enhanced viral reactivation compared to individual LRA alone *in vitro* and *ex vivo*

(79, 80). In addition, by using drug combinations, single drug dose can be reduced. Co-formulation and co-delivery systems through nanocarriers could also be developed to simplify treatments.

Another concern for unsuccessful “shock and kill” is suboptimal “killing” of latently infected cells (80). Competent CTLs are prominent in HIV-1 surveillance as observed in initial viral control during acute infection, greater potency in elite controller that are able to naturally maintain viral suppression without taking cART, and rapid viremia rebound in SIV-infected macaques upon CD8+ T cell depletion (81). Nevertheless, during chronic infection, CTLs then become functionally exhausted featuring increased expression of immune checkpoint markers such as programmed cell death protein 1 (PD1), cytotoxic T lymphocyte antigen 4 (CTLA4), T cell immunoglobulin mucin receptor 3 (TIM3), and lymphocyte activation gene 3 protein (LAG3). PD1 is one of the best characterized immune checkpoint molecules. Under physiological conditions, upon T cell activation PD1 expression is increased to avoid excessive immune stimulation for maintaining biological homeostasis. Nevertheless, overexpression of PD1 causes immune ‘exhaustion’ that impairs effector function and leads the organisms less defensive against diseases (82). PD1 ligand (PDL1) expression is broadly upregulated in several cancer types to escape immune control (83) whereas the inhibition of PD1/PDL1 pathway restores T cell function and mitigates tumor progress (84). Since T cells are the major targets of HIV and also undertake direct antiviral responses, it is not surprising to observe an upregulation of PD1 on both CD4+ and CD8+ T cells in untreated HIV patients (85, 86). However, upon ART, PD1 expression is reduced on CD4+ and CD8+ T cells, demonstrating that sustained antigen exposure is pivotal for PD1 expression and immune exhaustion (87). In SIV

infected rhesus macaques, the blockade of PD1 using anti-PD1 antibody resulted in the expansion of HIV specific CD8+ T cells presenting enhanced antiviral function, leading to decreased plasma viral load as well as prolonged animal survival (88). In addition, a recent report demonstrated that PD1 blockade synergized with ART by improving CD8+ T cell proliferation, restoring CD8+ T cell function, and enhancing viral suppression in SIV infected macaques. By far, there is only one clinical study applying anti-PDL1 antibody on treated HIV infected patients without malignancy in which increased HIV-specific CD4+ and CD8+ T cells were observed after antibody infusion (89). PD1/PDL1 molecules also contribute to HIV latency. A positive correlation was identified between the frequency of PD1+ cells and the size of HIV reservoirs (90). Within memory CD4+ T cells from ART treated patients, HIV DNA was enriched in PD1 high compared to PD1 low expressing cells, indicating PD1 level may play a major role in maintaining HIV persistence (91). Blockade of PD1 was suggested to destabilize the HIV reservoirs whereas whether or not PD1 inhibition can affect reservoir size and potential viral cure needs further investigation. Broadly neutralizing antibodies (bNAbs) is another potent tool for clearance of free HIV-1 or infected cells through binding of Fc region and subsequent cellular phagocytosis and antibody-dependent cellular cytotoxicity (ADCC) (92). In HIV-1 infected untreated patients, bNAbs have demonstrated capacity to reduce plasma viremia (93, 94). However, when bNAbs were administered to viral suppressed patients, no change of peripheral CD4+ T cells total and integrated HIV-1 DNA was observed (94). This could be due to a lack of viral expression in HIV-1 reservoirs that are required for bNAbs to recognize in order to clear. Therefore, it is rational to combine LRAs and bNAbs in an attempt to limit HIV-1 reservoirs. To this end, Borducchi et al. employed a combination of GS-9620 (a toll-like

receptor 7 (TLR7) agonist) and bNAb PGT121 in acute simian-human immunodeficiency virus (SHIV)-infected macaques during ART and plasma VL was monitored for 196 days after treatment interruption. While viral rebound was observed in 11/11, 10/11, and 9/11 of positive controls, GS-9620, and PGT121 single treated animals, respectively, only 6/11 animals rebounded from dual-treated group (95). How this combinational strategy will affect HIV-1 latency in human is under active pursuit (NCT02850016 and NCT03041012).

While efforts devoted to developing new LRAs and combinational strategies continue, alternative timing of LRA administration is worth investigation. As mentioned above, although ART initiation during early HIV-1 infection successfully reduces reservoir size it alone does lead to viral elimination. Studies also showed that viral sequences from remained reservoirs and relapse are highly similar to that isolated shortly before ART started (55, 96, 97). This indicates that although early ART does not prevent latency formation it successfully halts viral evolution that eases designs for further latency targeting. The question that remains lies on how to maximally diminish the setup reservoir pool as ART is initiated. Although HIV-1 latency is established rapidly upon infection, it is relatively unstable as shown by quick turnover of viral DNA before treatment initiates (98). This is likely due to a pro-inflammatory environment along with highly expressed viral antigen that favors T-cell activation and hinders the formation of HIV-1 latency. One can speculate that adding LRA to ART during early HIV-1 infection may further restrain viral reservoir size compared to ART alone (99, 100). Notably, “earlier” ART intervention may not necessarily be “better” for developing effective antiretroviral immune responses (101). Such early intervention blunts the generation of HIV-1 specific CTLs that may explain the failure of viral control upon ART interruption in early treated patients (55). To

overcome this challenge, immune enhancers such as bNAbs , therapeutic vaccine, and chimeric antigen receptor T cells (CAR-T) can be adopted to induce cytotoxic T cell responses as mentioned above (95). To be noted, although ART was started early at 7 days post-infection in this study, GS-9620 and PGT121 were administered during chronic infection when viral reservoirs are relatively stable. A higher rate of viral remission might be achievable if both reagents were applied during early infection when viral latency was not readily established. To this end, it holds promise that an early interfering cocktail containing LRA, immunotherapy, and ART can maximize latency restriction, if not complete eradication and can optimally filter reservoir populations with limited diversity for subsequent selective destruction, e.g. gene therapy as discussed below.

Gene editing technology deploys various biological enzymes such as zinc finger nucleases (ZFN), transcription activator-like effector nucleases (TALEN), and clustered regularly interspaced short palindromic repeats (CRISPR), to modify the host genome in the manners of gene regulation, gene knock-in and knock-out, and epigenetic modulation (102). Current ART targets HIV-1 transcription and translation levels but does not affect viral sequences that integrate into the host genome. Nevertheless, complete HIV-1 eradication requires clearance of each individual virus that likely happened in the “Berlin patient” and “London patient”. Therefore, gene editing could be the final solution to achieve an HIV-1 cure. Following the success of the first ever HIV-1 cure through HSCT of CCR5 mutated cells, the field was highly interested in the modification of CCR5 expression from patients’ autologous T cells. In a phase 1 study, CD4+ T cells isolated from HIV-1 suppressed patients were engineered to delete CCR5 expression using ZFN ex vivo and infused back to patients (103). The primary goal of the study was achieved which

proved the capability and safety of gene editing of human cells. Even though during ART interruption, all the patients experienced HIV-1 rebound, CCR5-modified CD4+ T cells exhibited resistance to viral infection and sustained in both peripheral blood and mucosal tissues with a mean half-life of 48 weeks. CCR5 modification on hematopoietic stem/progenitor cells (HSPCs) was also realized using ZFN or CRISPR/Cas9 technology that subsequently differentiated into multilineages of human cells resistant to HIV-1 infection. Primary studies using humanized mouse models demonstrated that animals engrafted with CCR5-modified cells presented better CD4+ T cell reservation and lower HIV-1 amplification compared to animals engrafted with CCR5-unmodified cells (104, 105). The development of CRISPR/Cas9 system eases the design and improves the specificity and efficiency of gene editing. CRISPR/Cas9 is composed of two working machineries that the guide RNA (gRNA) is designed to complement specific target sequence while the Cas9 enzyme excises the respective sequence (106). To enhance excision efficiency, multiple gRNA targeting different portions of the aiming sequence can be deployed. Indeed, HIV-1 excision from host genome by CRISPR/Cas9 has been demonstrated in *in vitro*, *ex vivo*, and small animal models (107, 108). While so far none of the techniques alone is able to eliminate HIV-1 infection, gene therapy could add the final punch to the residual viral reservoirs when the majority has already been cleared. Based on this hypothesis, we conducted a proof-of-concept study using a combinational strategy through sequential treatment of ART in the form of long acting slow effective release ART (LASER ART) and CRISPR/Cas9 targeting of the LTR-Gag region to infected humanized mice (109). For the first time, we achieved a complete elimination of HIV-1 in a subset of infected humanized mice, as demonstrated by the absence of viral

DNA/RNA from both peripheral blood and multiple tissue compartments along with failure of viral recovery using both *in vitro* and *in vivo* viral outgrowth assays (VOAs). This study provides the possibility of achieving HIV-1 cure through combinatorial treatments containing gene editing.

Challenges to achieve complete HIV-1 elimination remain. Different combination strategies should be exercised to optimize for a 100% cure rate. Off-target effects, side effects, and potential toxicities of each individual therapy and drug-drug interaction should be cautiously evaluated before moving into humans. While multiple arms targeting HIV-1 elimination are advancing rapidly including pharmacological approaches, immune boosting, and genome editing, HIV-1 cure is no longer a fantasy but an achievable goal.

Chapter 2 Immune Activations and Viral Tissue Compartmentalization During Progressive HIV-1 Infection of Humanized Mice

2.1 Abstract

Human immunodeficiency virus type one (HIV-1) tissue compartments are established soon after viral infection. However, the timing in which virus gains a permanent foothold in tissue and the cellular factors that control early viral-immune events are incompletely understood. These are critical events in studies of HIV-1 pathogenesis and in the development of viral reservoirs after antiretroviral therapy. Moreover, factors affecting the permanence of viral-tissue interactions underlie barriers designed to eliminate HIV-1 infection. To this end we investigated the temporal and spatial viral and host factors during HIV-1 seeding of tissue compartments. Two humanized NOD.Cg-Prkdc^{scid} IL2rg^{tm1Wjl}/SzJ mouse models were employed. In the first, immune deficient mice were reconstituted with human CD34+ cord blood hematopoietic stem cells (HSC) (hu-HSC) and in the second mice were transplanted with adult mature human peripheral lymphocytes (hu-PBL). Both, in measure, reflect relationships between immune activation and viral infection as seen in an infected human host. Following humanization both mice models were infected with HIV-1_{ADA} at 10^4 50% tissue culture infective doses. Viral nucleic acids and protein and immune cell profiles were assayed in brain, lung, spleen, liver, kidney, lymph nodes, bone marrow, and gut from 3 to 42 days. Peripheral CD4+ T cell loss began at 3 days together with detection of HIV-1 RNA in both mouse models after initiation of HIV-1 infection. HIV-1 was observed in all tested tissues at days 3 and 14 in hu- PBL and HSC mice, respectively. Immune impairment was most prominent in hu-PBL mice. T cell maturation and inflammation factors were linked directly to viral tissue seeding in both mouse models. We conclude that early viral tissue compartmentalization provides a roadmap for investigations into HIV-1 elimination.

2.2 Introduction

Following the introduction of antiretroviral therapy (ART) in the mid-1990s, remarkable progress was made towards reducing disease morbidities and mortality during a life-long human immunodeficiency virus type one (HIV-1) infection (1-3). While ART efficiently controls viremia and preserves immune function (4) it does not eradicate infection (110). Recent discoveries suggested that HIV-1 persistence is established within two weeks of viral exposure (111). Thus, complete understanding of viral tissue compartmentalization needs be made in efforts to eliminate HIV-1 infection.

To reflect the temporal and spatial challenges of human infection, animal models must reflect essential features of HIV-1 pathobiology in its human host (112). Insights into HIV-1 transmission and tissue distribution were made through studies of simian immunodeficiency virus (SIV) infection of nonhuman primates (113, 114). However, there are limitations in study. *First,* SIV and HIV are genetically and biologically distinct (41). *Second,* divergent viral and host factors affect progression to the acquired immune deficiency syndrome which commonly occurs more rapidly during SIV than HIV (41). Therefore, an HIV-1 susceptible animal model would be preferable for studies that reflect human infection. To such ends, humanized mouse models were developed. These models received engraftment of human cells into immunodeficient rodents resulting in the establishment of a functional human immune systems and tissue microenvironment that support long-term HIV-1 replication in target cells and tissues (115). Studies conducted by our group and others using such humanized mice have provided new insights into HIV-1 virology, immunology, pathology, therapeutics, and modes of viral eradication (45, 71, 116-118). However, to date, limited studies were performed to dissect when and to what

extent HIV-1 establishes persistent infection in tissue compartments. If this information is gleamed they could prove instrumental in developing improved antiretroviral therapies.

In our prior works, chronic HIV-1 infected CD34+ hematopoietic stem cell (hu-HSC) reconstituted NOD.Cg-Prkdc^{scid} Il2rg^{tm1Wjl}/SzJ (NSG) mice were investigated (119-121). They were used successfully to identify viral replication patterns and virus-induced injuries in diverse cell and tissue types. In the current study, attempts were made to better understand the temporal and spatial dynamics of viral seeding that followed HIV-1 inoculation. To this end we tracked early viral footprints in tissue compartments. To compare how the host microenvironment could affect viral seeding we used both infected adult peripheral blood lymphocyte (hu-PBL) and hu-HSC mouse models. Animals were evaluated in parallel after infection and were necropsied at days 3, 5, 7, 14, 28, and 42. Results showed that peripheral CD4+ T cells decreased rapidly in infected hu-PBL mice with viral detection in all tissues within 3 days of infection. In contrast, in hu-HSC mice virus was detected in gut, kidney, spleen, lung, liver, and lymph nodes and in brain only by 14 and 28 days. HIV-1 nucleic acids and proteins demonstrated that the viral life cycle was completed in both humanized mice. Transcriptomic analysis demonstrated substantive immune activation and pro-inflammatory signature in hu-PBL compared to HSC mice that paralleled viral tissue compartmentalization. These data, taken together, demonstrate the dynamics and extent of HIV-1 tissue infections and its link to human immunity in relevant humanized mouse models of viral infection.

2.3 Materials and Methods

2.3.1 Ethics Statement

All animal studies were performed in compliance with UNMC institutional policies and the National Institutes of Health guidelines for laboratory animal housing and care, and were approved by the Institutional Animal Care and Use Committee of UNMC. Human monocytes were isolated by leukapheresis from HIV-1/2 and hepatitis seronegative donors exempt from UNMC Institutional Review Board (IRB) review. Human CD34+ hematopoietic stem cells were isolated from umbilical cord blood which is also exempt from UNMC IRB.

2.3.2 Generation and HIV-1 infection of humanized mice

NSG mice were purchased from the Jackson Laboratory (Bar Harbor, ME) and housed under pathogen-free conditions in accordance with ethical guidelines for the care of laboratory animals at the National Institutes of Health and the University of Nebraska Medical Center. All experimental protocols were approved by the University of Nebraska Medical Center Institutional Animal Care and Use Committee (IACUC).

To generate human CD34+ mice, the new born NSG mice were irradiated at a 1Gy by a RS 2000 biological irradiator (Rad Source Technologies Inc.), followed with intrahepatic engraftment of human CD34+ HSCs that were isolated from human cord blood. Humanization of the animals was monitored monthly from peripheral blood using flow cytometry analysis on human cell markers. At 20-22 weeks of age, a total of 31 animals with replicate levels of human cell reconstitution were selected then divided into uninfected (n=5) and HIV-1 infected mouse groups (n=26). The latter animals were infected intraperitoneally with HIV-1_{ADA} at 10^4 $TCID_{50}$ and then randomly distributed into groups

that were sacrificed at days 3 (n=5), 5 (n=5), 7 (n=5), 14 (n=5), 28 (n=3), and 42 (n=3) post viral challenge for further immune and viral analysis.

Adult human PBL mice were generated by intraperitoneal injection of adult human peripheral blood lymphocytes purified from HIV-1 seronegative donor leukopaks into 8-week old NSG mice at 25×10^6 PBLs/mouse. Ten days after engraftment, animal humanization was confirmed by flow cytometry. In total, 28 mice with replicate numbers of engrafted human cells were divided into uninfected (n=4) and HIV-1 infected groups (n=24) used for analyses. HIV-1_{ADA} challenge was given intraperitoneally at 10^4 $TCID_{50}$. Infected animals were then randomly distributed into groups that were sacrificed at days 3, 5, 7 and 17 (n= 6, 5, 5 and 8) after viral infection for further immune and viral evaluations.

2.3.3 Flow cytometry

Peripheral blood was collected at designated time points into EDTA-coated tubes by cardiocentesis at the study end. Cellular phenotypes were analyzed for human antigens CD45, CD3, CD19, CD4, CD8, and CD14 (BD Pharmingen, San Diego, CA) using the fluorescence-activated cell sorting (FACS) system BD LSR2 (BD Immunocytometry Systems, Mountain View, CA) system. CD45+ human cells were gated from total lymphocytes. The percentages of $CD4^+$ and $CD8^+$ cells were obtained from the gate set for human CD3+ T cells. Results were analyzed using FlowJo software (BD Pharmingen, San Diego, CA).

2.3.4 Viral load analyses

Plasma samples were isolated from animal peripheral blood by centrifugation. Plasma HIV-1 RNA levels were measured using an automated COBAS Amplicor System

V2.0/Taqman-48 system (Roche Molecular Diagnostics, Basel, Switzerland) as per the manufacturer's instructions.

2.3.5 Nucleic acid extraction and quantification

Animal tissues were homogenized using a Qiagen Tissue Lyser II followed with total nucleic acids (DNA and RNA) extraction with Qiagen All Prep DNA/RNA Mini Kit (QIAGEN). Serial dilutions of HIV-1 DNA from the ACH-2 cell line, which contains one integrated viral copy per cell, served as the standard control (122). Tissue HIV-1 RNA was first reverse-transcribed to complementary DNA using a cDNA synthesis kit (Invitrogen, MA) (123). HIV-1 DNA and RNA were quantified by semi-nested real-time PCR as previously described (121). The first round of the PCR was performed on a conventional PCR machine (T100 Thermal Cycler, BioRad, CA). The products were subsequently applied to the second round real-time PCR using TaqMan fluorescent probes on an ABI Prism 7000 real-time PCR machine (Applied Biosystems, MA). The expression levels of tissue HIV-1 DNA and RNA were normalized to those for the human CD45 gene (Life Technology, CA). The sensitivity of our assay is around 10 copies.

2.3.6 RNAscope

RNAscope was performed on 5-μm thick paraffin-embedded spleen sections (Advanced Cell Diagnostics, Hayward, CA) according to the manufacturer's instructions. Anti-sense HIV-1 Clade B probe designed for targeting 854–8291 base pairs of HIV-1 sequence was used for viral detection. Positive signals were expressed as single or clusters of brown dots. Human peptidylprolyl isomerase B (PPIB) was applied as controls for human genome. All the images were captured for 40X magnification.

2.3.7 Immunohistochemistry

Tissue samples were collected at the time of animal autopsy, fixed with 4% paraformaldehyde, and embedded in paraffin. Tissue sections of 5-um thickness were cut and immuno-stained with HLA-DR (clone CR3/43, 1:100, DAKO, Carpinteria, CA) and HIV-1 p24 (1:10, DAKO) antibodies. The DAKO EnVision polymer-based system was used for staining development, and all the sections were counterstained with Mayer's hematoxylin (116). Images were obtained with a Nuance EX camera fixed to a Nikon Eclipse E800 microscope using Nuance software (Cambridge Research & Instrumentation, Woburn, MA). Human HLA-DR images were taken at 20× magnifications and HIV-1p24 images were captured at 40× objective magnifications.

2.3.8 Human mRNA analysis of immune responses

Humanized mouse spleen was harvested at animal necropsy followed with total RNA isolation using an RNease Mini Kit (QIAGEN). Complementary DNA (cDNA) was generated using a cDNA synthesis kit (Invitrogen, MA) and subscribed to RT^2 PCR arrays for T & B cell activation analysis (QIAGEN). Quantitative RT-PCR was performed on an Master cycler® ep realplex as per the manufacturer's instructions (Eppendorf) and analyzed using RT^2 Profiler PCR Array web-based data analysis software, version 3.5 (QIAGEN). Gene networks analysis was performed using Ingenuity Pathway Analysis (QIAGEN).

2.3.9 Statistical analyses

Data were analyzed using GraphPad Prism 7.0 software (La Jolla, CA). The Student's t test was used for two-group comparison. A value of $p < 0.05$ was considered

statistically significantly different. All results were presented as the means ± the standard error of the mean (SEM). Fisher's Exact Test was used to validate the IPA data of spleen of each canonical pathway.

2.4 Results

2.4.1 Immune profiles in HIV-1 infected humanized mice

NSG mice were irradiated at birth then were transplanted by intrahepatic injection with human CD34+ cord blood hematopoietic stem cells (hu-HSC) (116). Monthly whole blood flow cytometry showed that by 22 weeks mouse blood contained 30-60% human immunocytes. Following HIV-1_{ADA} infection at 10^4 50% tissue culture infection dose ($TCID_{50}$)/animal, assays for viral and immune profiles were performed in blood and tissues at days 0, 3, 5, 7, 14, 28, and 42. Replicates of 3 to 5 animals were tested at each of the time points before and after infection (at the time of sacrifice) **(Figure 2.1A)**.

Our flow cytometric gating strategy is illustrated in **Figure 2.2A**. Prior to HIV-1 infection, the percentages of human CD45+ cells in hu-HSC mouse blood ranged between 30 to 60% **(Figure 2.1B)**. A significant decline was seen by 42 days (10.9% ± 0.9), but not much decline was observed in the earlier time points **(Figure 2.1B)**. Percentages of human cells stayed consistent between HIV-1 infected and mock infected controls in hu-HSC spleen and bone marrow that ranged from 45 to 55% **(Figure 2.2B, C)**.

Progressive loss of CD4+ T cells in blood was observed in infected hu-HSC mice. The mean decreases in CD4+ T cells were 4.7% ± 5.1, 10.2% ± 2.2, 14.0% ± 0.8, 11.9% ± 1.6, 14.0% ± 2.9, and 18.8% ± 1.8, at days 3, 5, 7, 14, 28, and 42, respectively. In parallel, CD8+ T cell counts were increased by 4.6% ± 3.8, 9.7% ± 2.0, 10.6% ± 1.6, 9.1% ± 1.3,

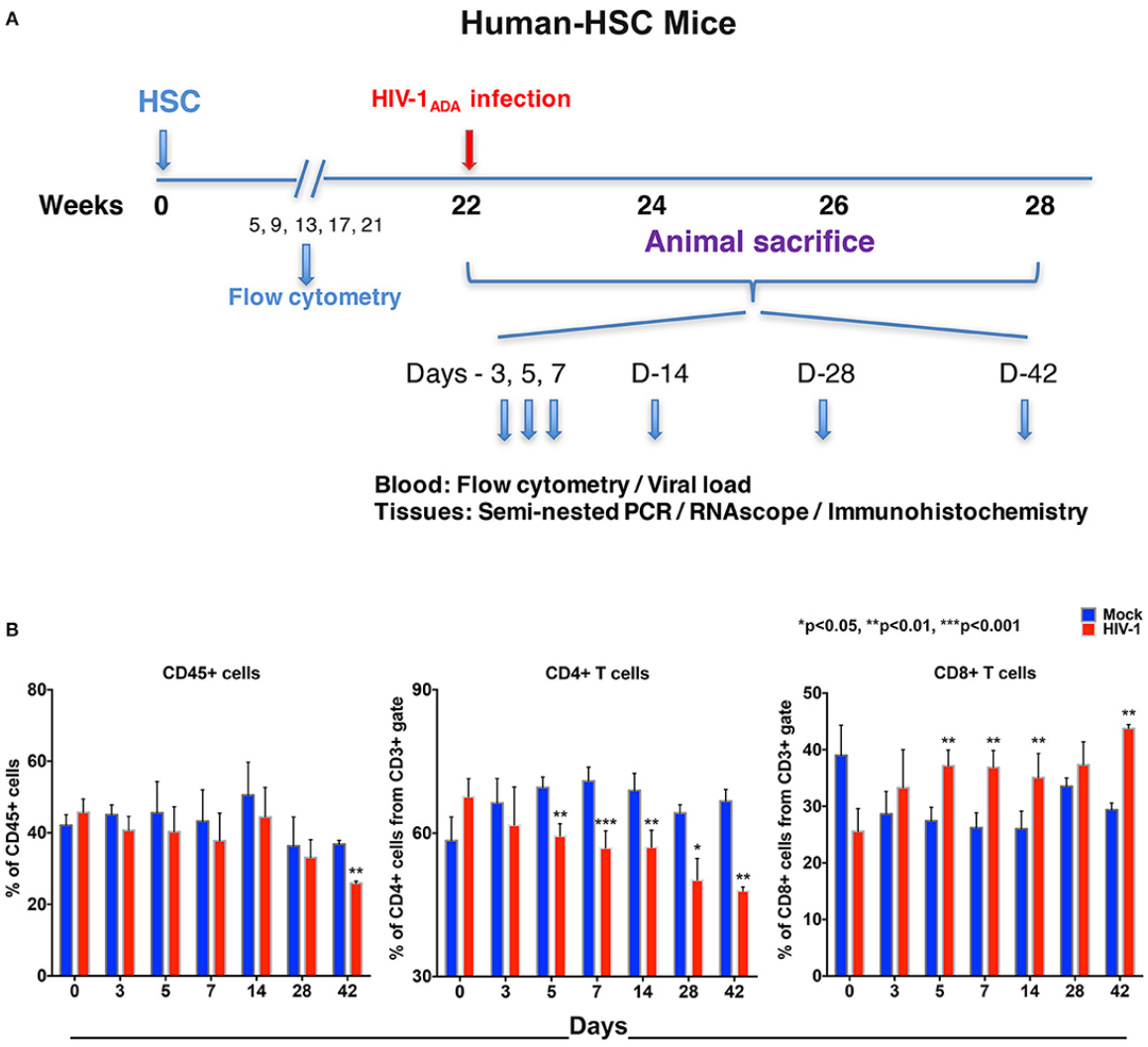

Figure 2. 1 Human lymphocyte responses following HIV-1 infection of hu-HSC mice.

(A) The illustrated experimental design for hu-HSC mice human cell reconstitution, HIV-1 infection, and serial animal sacrifice performed at days 0, 3, 5, 7, 14, 28, and 42. Animal numbers are N = 5, 5, 5, 5, 5, 3, and 3 at each of the time points. **(B)** Peripheral blood CD45+, CD4+, and CD8+ cell counts before/mock infection (blue) and after HIV-1 infection (red) for each of the time points by flow cytometry tests. Data are expressed as mean ± SEM and considered *, **, *** statistically different, at $p < 0.05$, $p < 0.01$, and $p < 0.001$.

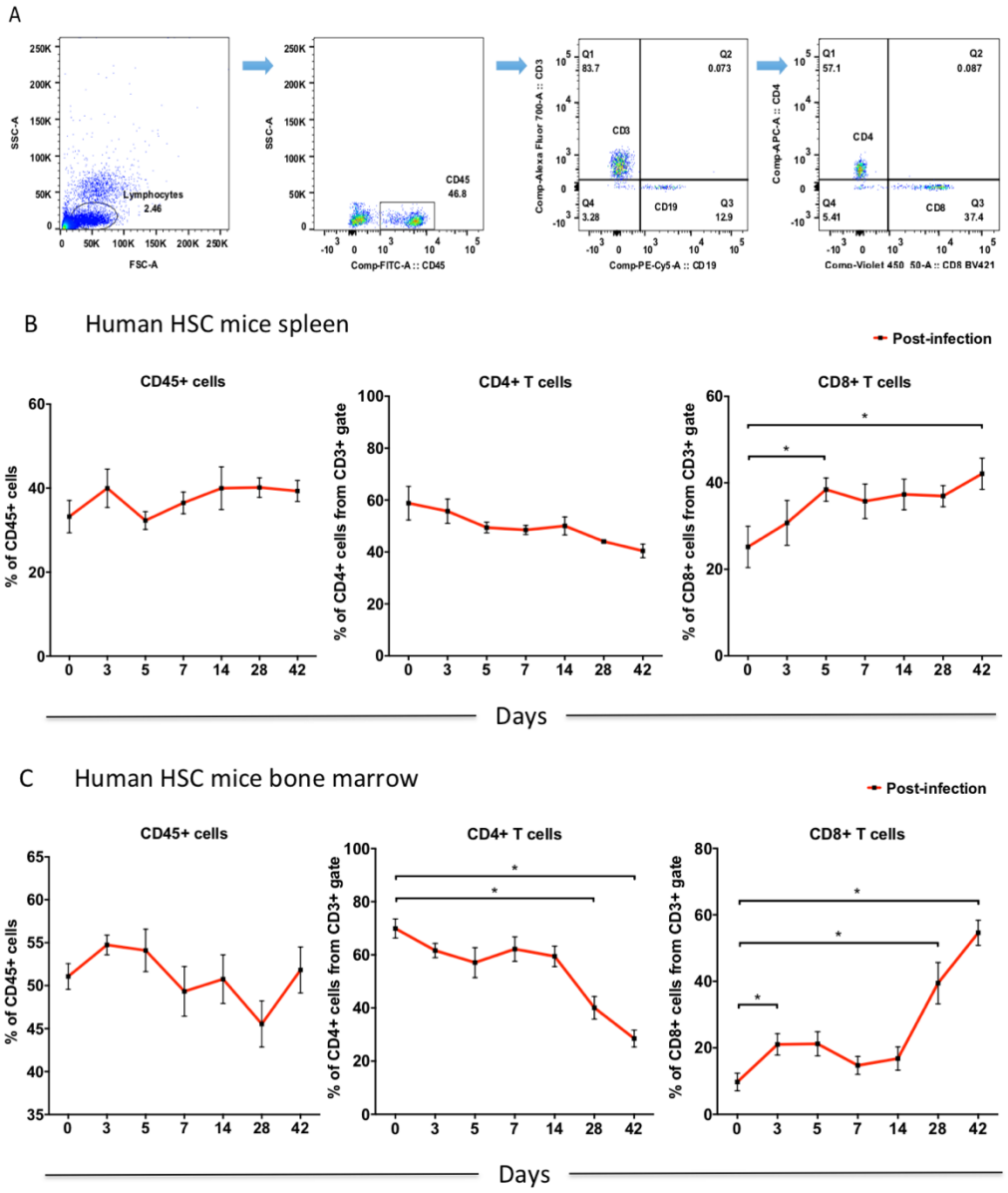
A
SSC-A
FSC-A
Lymphocytes
2.46
CD45
46.8
Comp-FITC-A :: CD45
Comp-Alexa Fluor 700-A :: CD3
Q1
83.7
Q2
0.073
CD3
CD19
Q4
3.28
Q3
12.9
Comp-PE-Cy5-A :: CD19
Comp-APC-A :: CD4
Q1
57.1
Q2
0.087
CD4
CD8
Q4
5.41
Q3
37.4
Comp-Violet 450 50-A :: CD8 BV421
B
Human HSC mice spleen
Post-infection
CD45+ cells
% of CD45+ cells
CD4+ T cells
% of CD4+ cells from CD3+ gate
CD8+ T cells
% of CD8+ cells from CD3+ gate
Days
C
Human HSC mice bone marrow
Post-infection
CD45+ cells
% of CD45+ cells
CD4+ T cells
% of CD4+ cells from CD3+ gate
CD8+ T cells
% of CD8+ cells from CD3+ gate
Days

Figure 2. 2 Human cells in spleen and bone marrow in infected hu-HSC mice.

(A) The gating strategy for this study is shown. In brief, human cells (hCD45+) were gated from total lymphocytes and subsequently separated into human T and B (hCD3+ and hCD19+) lymphocytes. Human CD4+ and CD8+ T cells were gated from hCD3+ cell populations. **(B)** Splenocytes and **(C)** bone marrow cells were acquired from hu-HSC mice at serial time points (days 0, 3, 5, 7, 14, 28, and 42) after HIV-1 infection and subjected to flow cytometric analyses. Numbers of human CD45+, CD4+, and CD8+ cells in both tissues are expressed as mean ± SEM. Values were statistically significant if $*p < 0.05$.

3.8% ± 2.6, and 14.4% ± 1.1, at respective time points **(Figure 2.1B)**. Splenocytes and bone marrow cells were collected at necropsy and showed parallel losses and increases in CD4+ and CD8+ T cells, respectively, in HIV-1 infected versus mock infected mice **(Figure 2.2B-C)**.

To compare virus-host interactions during early HIV-1 infection with immunologically "mature" hu-PBL mice, replicate evaluations were performed. Due to expected graft-versus-host disease in this model (124) testing was conducted up to 14 days. Adult NSG mice were engrafted with hu-PBL 10 days prior to HIV-1_{ADA} infection with up to 8 animals/time point evaluated at days 0, 3, 5, 7, and 14 **(Figure 2.3A)**. No significant changes of peripheral human CD45+ cell counts were observed in hu-PBL mice before and after infection. The values ranged from 25 to 45% of total immunocytes **(Figure 2.3B)**. The depletion of CD4+ T cells was robust in infected hu-PBL mice. These equaled 24.1% ± 4.6, 18.2% ± 3.0, 20.6% ± 2.6, and 37.4% ± 6.9, at days 3, 5, 7, and 14, respectively, following infection. In parallel, peripheral CD8+ T cell counts rose by 24.1% ± 4.3, 22.1% ± 3.8, 21.3% ± 3.9, and 40.5% ± 7.6, at equivalent time points **(Figure 2.3B)**. Taken together, the early and progressive impairment of human immune cells was observed during HIV-1 infection in both hu-HSC and hu-PBL mouse models, but more vigorously in hu-PBL than in hu-HSC mice.

2.4.2 Plasma viral loads in HIV-1 infected humanized mice

HIV-1 RNA appears before antiviral antibodies in blood at 10 to 14 days after viral exposure. To recapitulate these findings blood was collected from humanized mice and analyzed for viral loads by the COBAS Ampliprep V2.0 and Taqman-48 assay **(Figure 2.4)**. In hu-HSC mice, plasma HIV-1 RNA was detected in all animals with a mean of 5.0

± 3.4 x 10^4 copies/ml at 14 days after infection. At days 3, 5, and 7 after infection plasma viral loads were observed in 2/5 animals at or near to the detection limit of 400 copies/ml. Peak viremia was recorded at day 28 at a mean of 5.9 ± 3.4 x 10^5 copies/ml. At 42 days plasma viral load was at 6.6 ± 1.4 x 10^5 copies/ml **(Figure 2.4A)**.

In contrast, HIV-1 RNA was readily observed in all infected hu-PBL mice at day 3 with the mean of 4.7 ± 0.8 x 10^3 copies/ml. A 2-log increase in viral copies were observed at days 5 and 7 with means of 5.4 ± 2.6 x 10^5 and 8.0 ± 3.5 x 10^7 copies/ml, respectively. At day 14, plasma viral load was 8.3 ± 4.8 x 10^7 copies/ml **(Figure 2.4B)**.

2.4.3 Tissue compartments in HIV-1 infected humanized mice

HIV-1 infection is established in target tissues before viremia can be detected (125). To determine the early distribution of HIV-1 infection in tissues, gut, spleen, lung, liver, brain, and kidney were procured then evaluated after animal sacrifices **(Figure 2.1A** and **2.3A)**. Tissue HIV-1 DNA and RNA were quantified by ultrasensitive semi-nested real-time qPCR (121). In general, tissue viral levels were higher in longer infected hu-HSC and hu-PBL mice. In addition, tissue viral DNA and RNA corresponded to what was detected in plasma in both animal models **(Figure 2.5A-B** and **2.6A-B)**.

In hu-HSC mice, HIV-1 DNA and RNA were detected at low levels within 3 days after viral challenge, from spleen, lung, and liver in 1/5 animals **(Figure 2.5C-D)**. The same tissues examined at days 5 and 7 showed infection in 2/5 animals while HIV-1 remained undetected in other tested tissues. In the animals infected for 14 days, viral DNA and RNA were observed in 3/5 gut, spleen, lung, and kidney tissues, and 2/5 liver samples **(Figure 2.5C-D)**. However, HIV-1 was not detected in hu-HSC mouse brain until day 28. At 28 and 42 days, virus was readily observed throughout all tested tissues from all infected

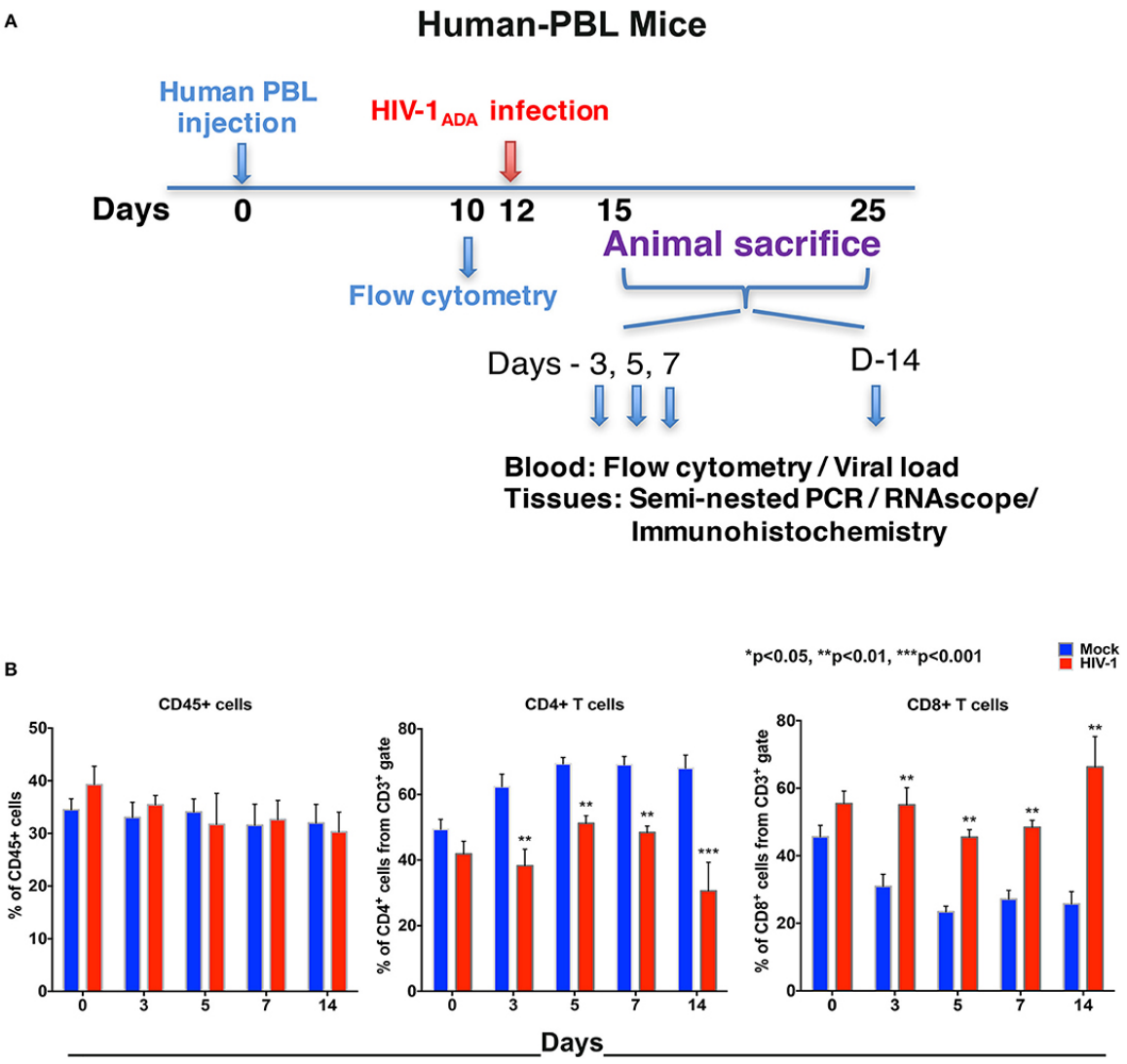

Figure 2. 3 Human lymphocyte responses following HIV-1 infection of hu-PBL mice.

(**A**) The illustrated experimental design for hu-PBL mice human cell reconstitution, HIV-1 infection, and serial animal sacrifice performed at days 0, 3, 5, 7, and 14. Animal number are N = 4, 6, 5, 5, and 8 at each of the time points, respectively. (**B**) Peripheral blood CD45+, CD4+, and CD8+ cell counts before/mock infection (blue) and after HIV-1 infection (red) for each of the time points by flow cytometry tests. Data are expressed as mean ± SEM and considered **, *** statistically significant, at $p < 0.01$ and $p < 0.001$.

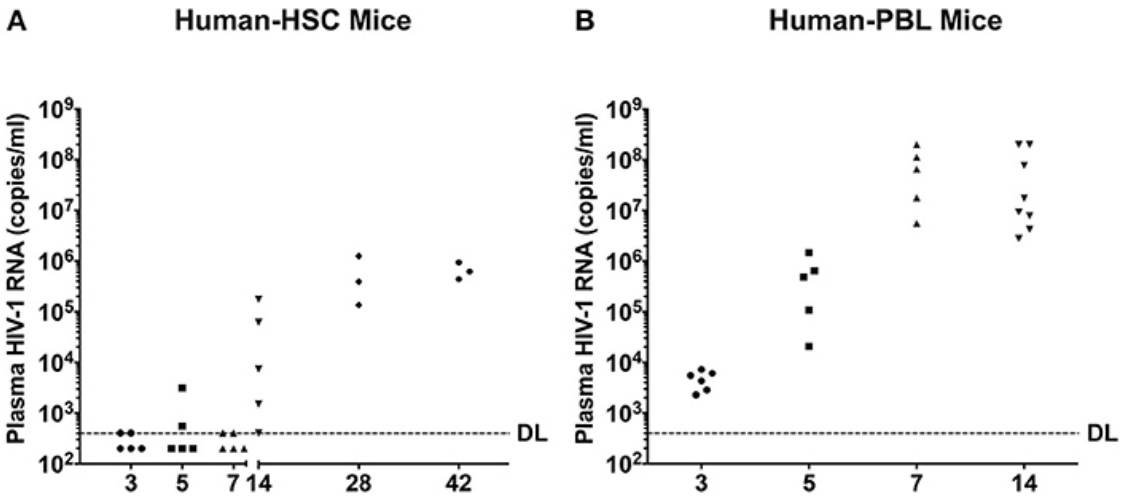

Figure 2. 4 Peripheral viral loads during the course of HIV-1 infection.

Plasma samples were collected following animal sacrifice from HIV-1 infected **(A)** hu-HSC and **(B)** hu-PBL mice. Fifty microliters of mouse sera were collected then diluted to 1 ml with sterile filtered healthy human sera enabling a detection limit (DL) of 400 HIV-1 RNA copies/ml that is illustrated by the dashed line. Each dot represents an individual animal. The mean HIV-1 copy value from each group of animals was labeled.

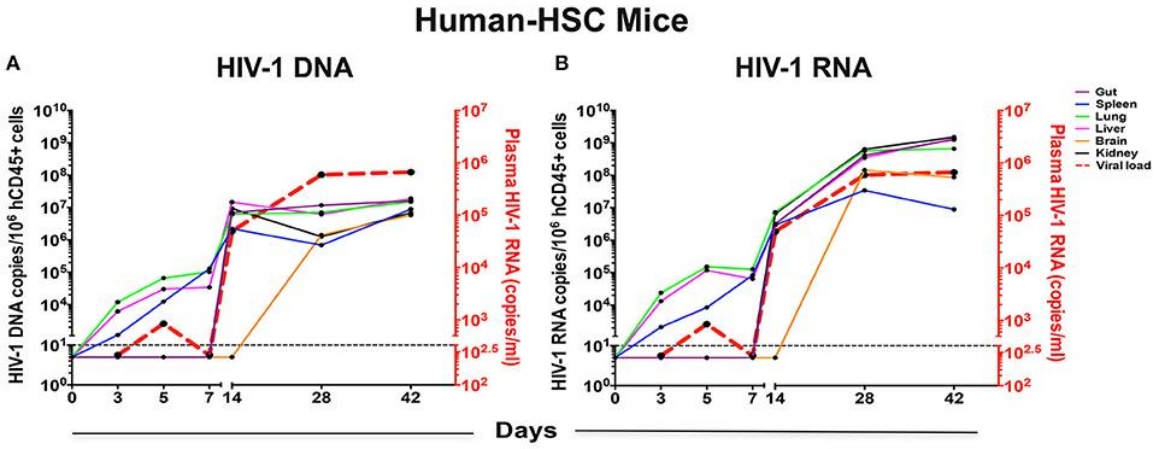

Figure 2. 5 Viral tissue compartments in HIV-1 infected hu-HSC mice.

Gut, spleen, lung, liver, brain, and kidney tissues were collected at necropsy at times indicated from HIV-1 infected hu-HSC mice, followed by assay of viral DNA and RNA by qPCR. The kinetics of **(A)** HIV-1 DNA and **(B)** HIV-1 RNA in each tissue are shown by colored straight lines assigning viral copies/10^6 hCD45+ cells (left Y axis) vs. time (X axis). The temporal relationship of viral load (acquired from **Figure 2.4A**) was plotted in red dashed line (right Y axis). Data are expressed as the means. **(C)** HIV-1 DNA and **(D)** HIV-1 RNA in tissues at single time point were listed with each dot representing an individual animal. Values below the horizontal line indicated that viral DNA and RNA were below the DL.

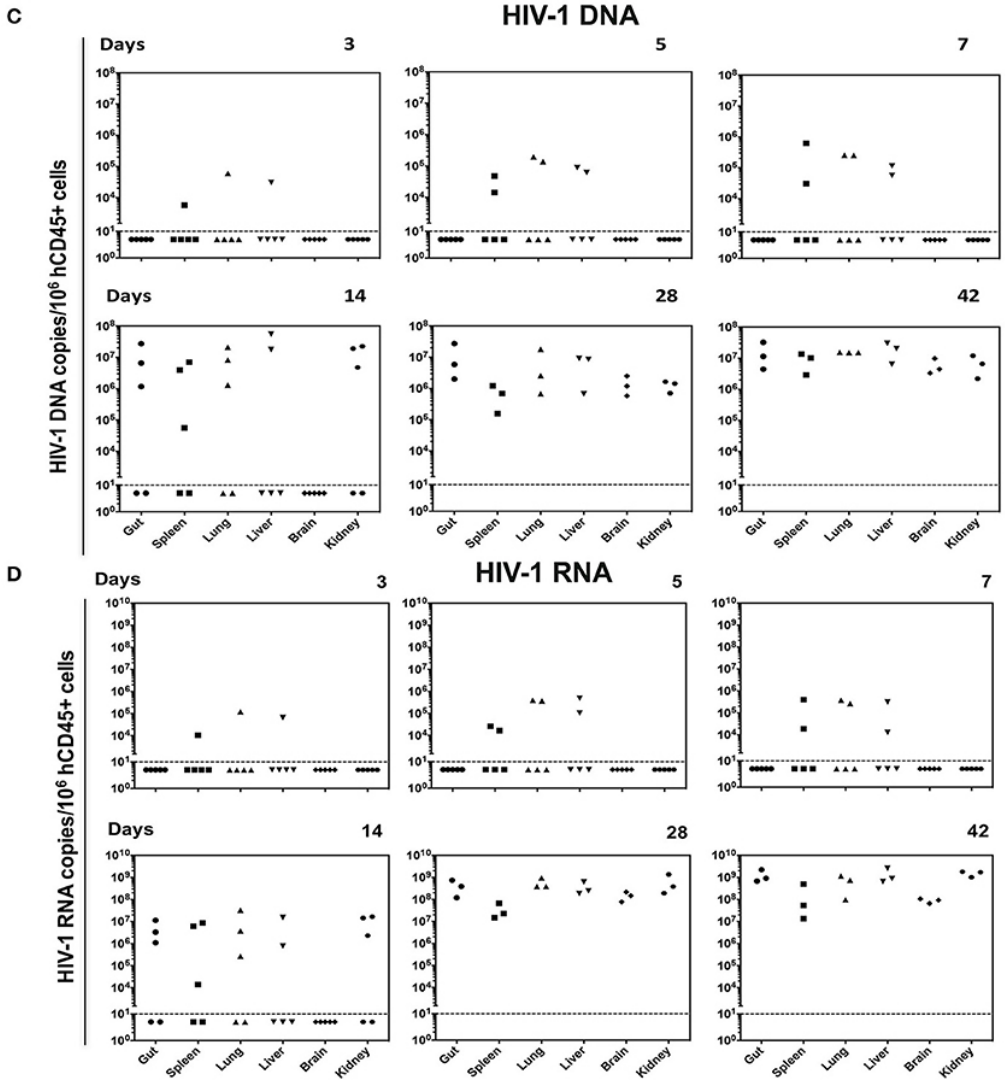

Figure 2. 5 Viral tissue compartments in HIV-1 infected hu-HSC mice.

Gut, spleen, lung, liver, brain, and kidney tissues were collected at necropsy at times indicated from HIV-1 infected hu-HSC mice, followed by assay of viral DNA and RNA by qPCR. The kinetics of **(A)** HIV-1 DNA and **(B)** HIV-1 RNA in each tissue are shown by colored straight lines assigning viral copies/10^6 hCD45+ cells (left Y axis) vs. time (X axis). The temporal relationship of viral load (acquired from **Figure 2.4A**) was plotted in red dashed line (right Y axis). Data are expressed as the means. **(C)** HIV-1 DNA and **(D)** HIV-1 RNA in tissues at single time point were listed with each dot representing an individual animal. Values below the horizontal line indicated that viral DNA and RNA were below the DL.

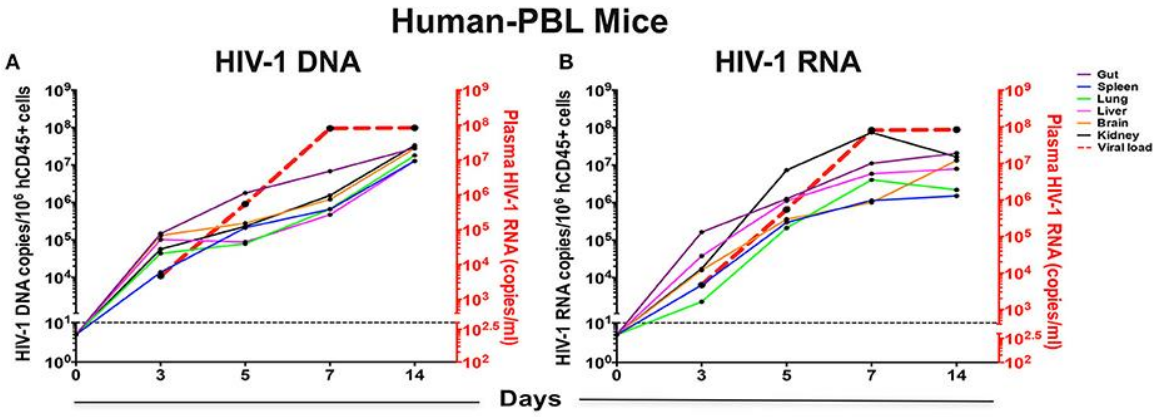

Figure 2. 6 Viral tissue compartments in HIV-1 infected hu-PBL mice.

Gut, spleen, lung, liver, brain, and kidney tissues were collected at necropsy at times indicated from HIV-1 infected hu-PBL mice, followed by assay of viral DNA and RNA by real-time qPCR. The kinetics of (**A**) HIV-1 DNA and (**B**) HIV-1 RNA in each tissue are shown by colored straight lines assigning viral copies/10^6 hCD45+ cells (left Y-axis) vs. time (X axis). The temporal relationship of viral load (acquired from Figure 2.4B) was plotted in red dashed line (right Y axis). Data are expressed as the means. (**C**) HIV-1 DNA and (**D**) HIV-1 RNA in tissues at single time point were listed with each dot representing an individual animal. Values below the horizontal line indicated that viral DNA and RNA were below the limit of detection.

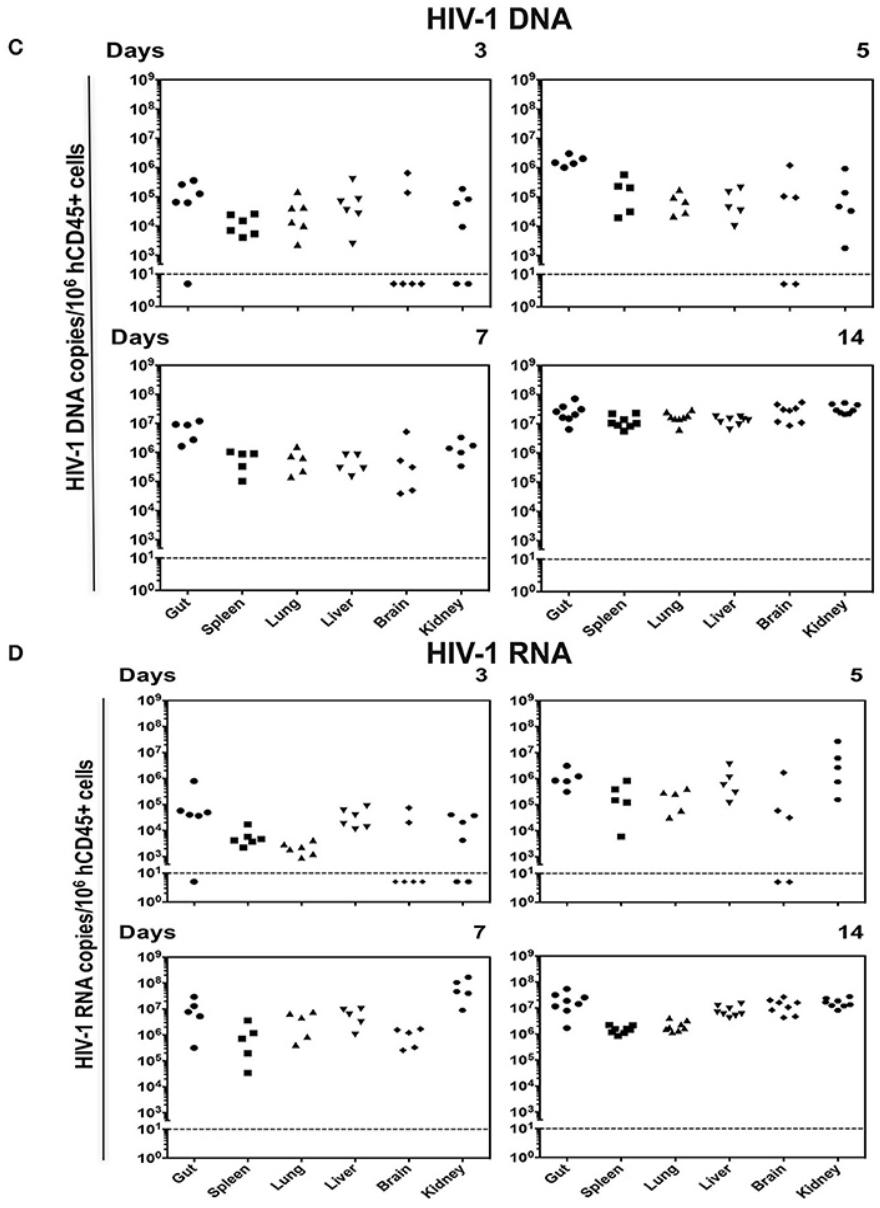
C
HIV-1 DNA
Days
3
5
7
14
HIV-1 DNA copies/10^6 hCD45+ cells
Gut
Spleen
Lung
Liver
Brain
Kidney
D
HIV-1 RNA
HIV-1 RNA copies/10^6 hCD45+ cells

Figure 2. 6 Viral tissue compartments in HIV-1 infected hu-PBL mice.

Gut, spleen, lung, liver, brain, and kidney tissues were collected at necropsy at times indicated from HIV-1 infected hu-PBL mice, followed by assay of viral DNA and RNA by real-time qPCR. The kinetics of (**A**) HIV-1 DNA and (**B**) HIV-1 RNA in each tissue are shown by colored straight lines assigning viral copies/10^6 hCD45+ cells (left Y-axis) vs. time (X axis). The temporal relationship of viral load (acquired from Figure 2.4B) was plotted in red dashed line (right Y axis). Data are expressed as the means. (**C**) HIV-1 DNA and (**D**) HIV-1 RNA in tissues at single time point were listed with each dot representing an individual animal. Values below the horizontal line indicated that viral DNA and RNA were below the limit of detection.

animals **(Figure 2.5C-D)**.

HIV-1 was detected earlier and at higher levels in hu-PBL versus hu-HSC mouse tissues at all time points **(Figure 2.6C-D)**. Viral DNA and RNA were seen by day 3 in 81% (29/36) gut, spleen, lung, liver, brain, and kidney tissues examined. At day 5, 93% (28/30) infected tissue were HIV nucleic acid positive. Notably, 67% (6/9) brain tissue samples from days 3 and 5 showed absent virus that supported later seeding for this tissue compartment. In the animals infected for 7 and 14 days virus was readily observed in all tissues **(Figure 2.6C-D)**. HIV-1 DNA levels in gut were higher than that in all other tissues and supported the notion that gut serves as a prominent virus tissue compartment **(Figure 2.6A)**. Altogether, these data suggested that both peripheral and tissue HIV-1 compartments were rapidly established in hu-HSC (day-14) and hu-PBL (day-3) mouse models, but much faster in hu-PBL than in hu-HSC mice.

2.4.4 Confirmatory tests of viral gene expression in infected humanized mice

To confirm tissue compartmentalization in early HIV-1 infected humanized mice, spleen sections were obtained then tested by RNAscope that can detect up to 1-2 copies of viral RNA (representative images shown in **Figure 2.7**). An antisense HIV-1 Clade B probe was employed which covers nearly entire viral genome (except LTR region). To this end, spleen HIV-1 RNA was shown as a single or cluster of brown dots, at the earliest stage of infection in both mouse models. In hu-HSC mice, HIV-1 RNA was visualized within 3 days of infection, which reaffirmed the rapid set-up of viral tissue compartment. As infection proceeded, virus spread as shown in multiple clusters of brown dots within each tissue section. By day 42, viral burden was much more prominent with invaded cells aggregated throughout the observed field of interest **(Figure 2.7A)**. In hu-PBL mice, HIV-

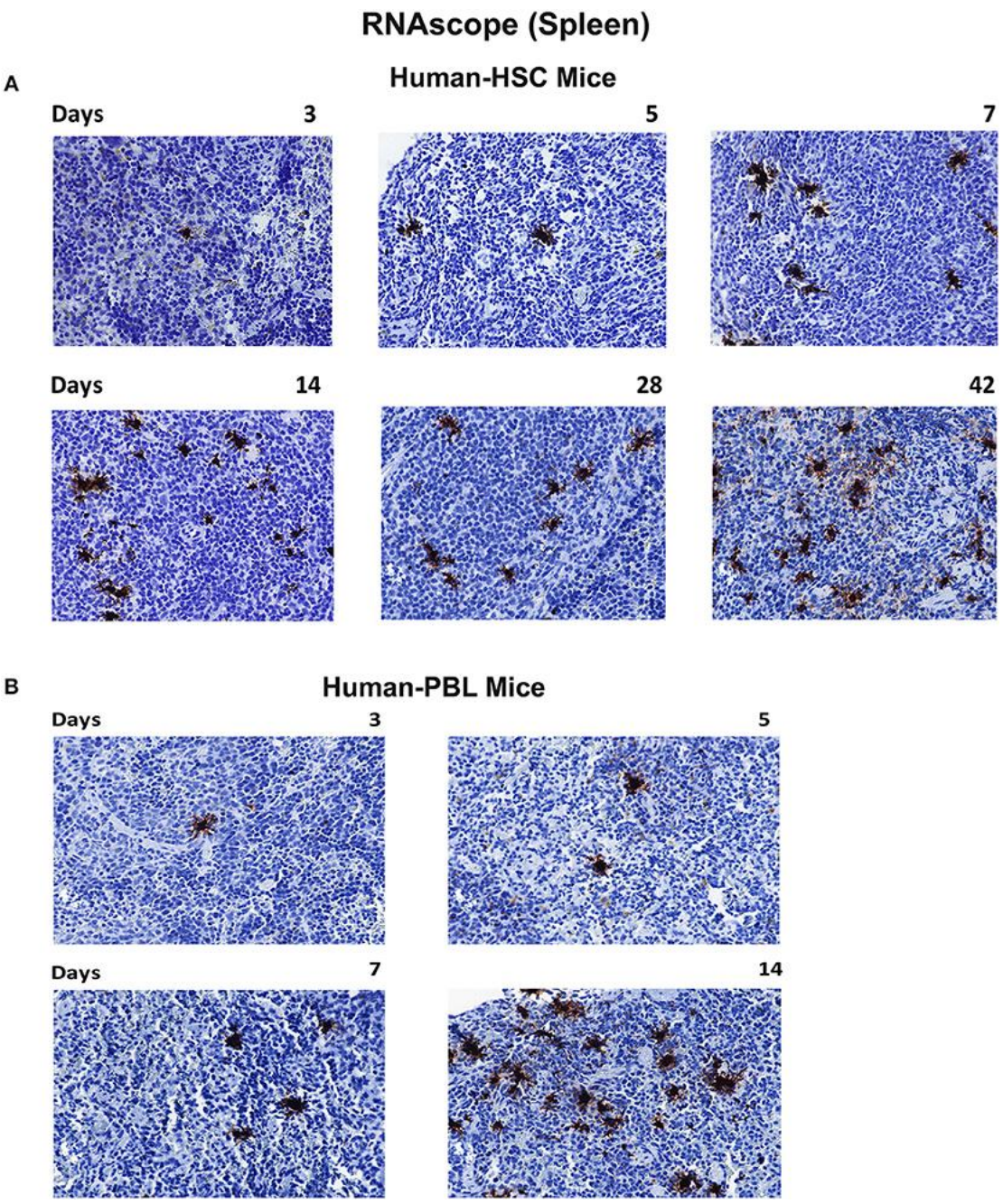

Figure 2. 7 Viral RNA tissue expression in infected humanized mice.

Spleen tissues of hu-HSC **(A)** and hu-PBL **(B)** mice were collected with formalin fixed and paraffin embedded at necropsy. Five micrometer thick slices were prepared for RNAscope assays. Representative images from each group were shown with HIV-1 RNA labeled as single or cluster of brown dots. Images were taken at 40 x objective magnifications.

1 RNA was observed in all infected animal spleens at each time point. Viral RNA levels were comparable or higher in hu-PBL than hu-HSC mice at equivalent time courses **(Figure 2.7B)**.

2.4.5 Viral protein expression in infected humanized mice

HIV-1p24 is a capsid component that is among the earliest expressed viral proteins. To assess its presence in infected tissues we employed immunohistochemistry assays to trace HIV-1p24 along with human HLA-DR staining. Representative photomicrographs were taken from each tissue sample stained with both antibodies **(Figure 2.8)**. In hu-HSC mice, while HLA-DR+ cells were easily seen in the observation field, HIV-1p24 cells, however, were observed only in 1/5 animal spleens infected for 5 or 7 days. No infected cells were seen at 3 days. By day 14, 3/5 animals were HIV-1p24 positive. These 3 animals were the same ones where virus was detected by viral qPCR and RNAscope tests **(Figure 2.5** and **2.7)**. At 28 and 42 days, HIV-1p24 stained cells were demonstrated in all infected animals **(Figure 2.8A)**. In hu-HSC lymph nodes, HIV-1p24 antigens were detected starting at 14 days after infection and increased over time **(Figure 2.8A)**.

In hu-PBL mice, HIV-1p24 antigens were captured in all infected animal spleens and lymph nodes during serial necropsies while human HLA-DR+ cells were well reconstituted **(Figure 2.8B)**. Levels of HIV-1 p24 and nucleic acids in spleen measured by immunostaining and qPCR and RNAscope tests paralleled one another **(Figures 2.6** and **2.7B)**. During the equivalent infection windows, tissue HIV-1p24 expansion was more aggressive in hu-PBL than that in hu-HSC mice **(Figure 2.8B)**. These data together confirmed that the quickly established HIV-1 infection in both models were replication-competent and virus spread more aggressively in hu-PBL than in hu-HSC mice.

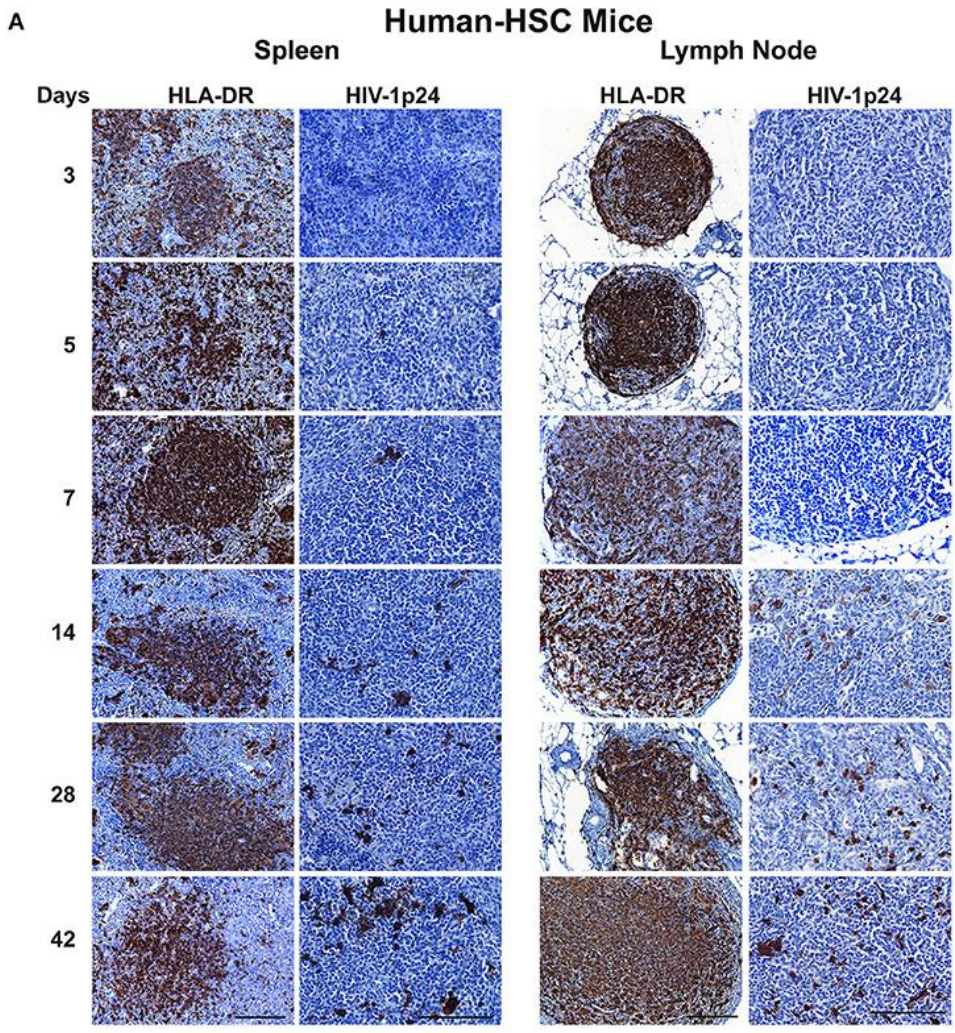

Figure 2. 8 HIV-1p24 expression in infected humanized mice.

Spleen and lymph node samples were collected from **(A)** hu-HSC and **(B)** hu-PBL mice at necropsy then formalin fixed and paraffin embedded. Five micrometer thick sections were cut then stained with human HLA-DR and HIV-1p24 antibodies. Representative images from each group were selected and pictures were captured for both markers (shown as brown dots) from individual animals. Human HLA-DR images were taken at 20 x objective magnifications and HIV-1p24 images were captured at 40 x objective magnifications.

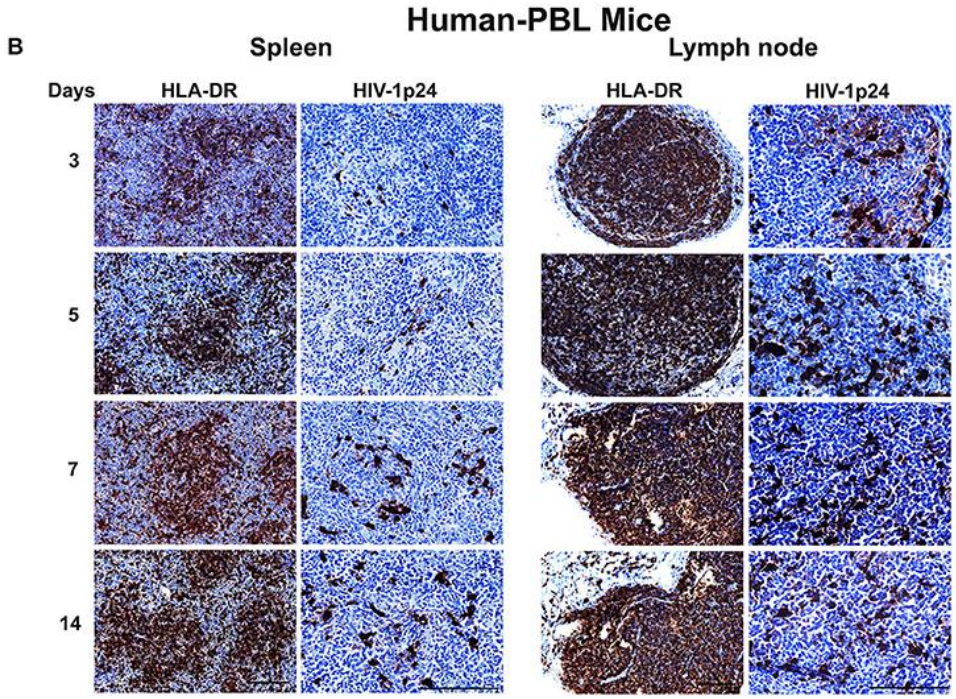

Figure 2. 8 HIV-1p24 expression in infected humanized mice.

Spleen and lymph node samples were collected from **(A)** hu-HSC and **(B)** hu-PBL mice at necropsy then formalin fixed and paraffin embedded. Five micrometer thick sections were cut then stained with human HLA-DR and HIV-1p24 antibodies. Representative images from each group were selected and pictures were captured for both markers (shown as brown dots) from individual animals. Human HLA-DR images were taken at 20 x objective magnifications and HIV-1p24 images were captured at 40 x objective magnifications.

2.4.6 Host immunity in humanized mouse models

Different strategies of humanization shape unique cellular integrations in humanized mice. Previous studies observed that the engrafted human T cells in hu-PBL mice expressed a predominated memory/activated (CD45RO) phenotype that supports HIV-1 infection (126) while in hu-HSC mice approximately 50% of human T cells are naive (CD45RA) that are less susceptible to HIV-1 infection (121). Therefore, viral infection is usually more aggressive in hu-PBL mice than that in hu-HSC mice (41). In the current study, we also observed a similar pattern during early HIV-1 infection where virus was seeded at accelerated rates in hu- PBL than in HSC mice. To further characterize and compare the intrinsic host environment in both mouse models that may affect HIV-1 infection, we adopted naïve hu-HSC and hu-PBL mice (n=3/group) with comparable human cell reconstitutions **(Table 2.1)**. In these animals, immune-linked host gene expression was tested. Total RNA was isolated from individual animal spleen and a total of 84 gene expressions were evaluated. Overall, increases in gene expressions paralleled adaptive immune activation and were most prominent in hu- PBL versus HSC mice **(Figure 2.9 and Table 2.2)**. Upregulated T cell genes were readily observed affecting cell activation (e.g. CD2, CD3, CD4, CD8, FOXP3, and LAG3), proliferation (e.g. CD28, IL2, IL1β, IL18, and TNFSF14), and differentiation (e.g. CD27, CD80, CD86, and IL15). Two major co-receptors for HIV-1 entry, CCR5 and CXCR4, were also found to be upregulated in hu-PBL compared to HSC mice. The elevated B cell activation and proliferation markers included CD27, CD40, CD80, CD81, IL2, and IL10. To investigate how these differentially expressed molecules may impact the host environment, we subjected the genes with fold changes above 2 (81/84) to Ingenuity Pathway Analysis (IPA). These tests

Table 2. 1 Human cell engraftment in individual humanized mice (for IPA analyses)

Peripheral human cells (%)	**Humanized mouse model**					
	Hu-HSC (#)			Hu-PBL (#)		
	3631	3641	3655	A1	A2	A3
CD45	45.6	63.3	53.8	52.2	49.1	70.2
CD3	70.9	66.4	85.9	97.1	96.3	96.9
CD4	70.3	71.1	75.8	49.8	43.6	32.2
CD8	24.0	22.5	21.2	38.5	40.3	53.3

A

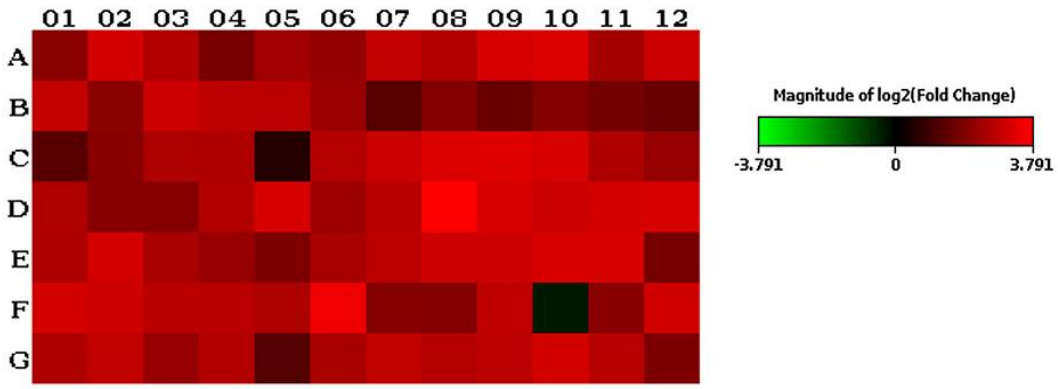

Layout	01	02	03	04	05	06	07	08	09	10	11	12
A	ADA 2.06	AICDA 3.11	APC 2.61	BCL2 1.77	BLM 2.39	BLNK 2.17	CCL3 2.82	CCR1 2.62	CCR2 3.15	CCR3 3.24	CCR4 2.43	CCR5 3.04
B	CD1D 2.88	CD2 2.05	CD27 3.00	CD274 2.77	CD276 2.76	CD28 2.25	CD3D 1.29	CD3E 1.90	CD3G 1.50	CD4 1.89	CD40 1.70	CD40LG 1.53
C	CD47 1.28	CD5 2.01	CD7 2.52	CD80 2.55	CD81 0.54	CD86 2.66	CD8A 2.99	CD8B 3.24	CSF2 3.27	CX3CL1 3.18	CXCR3 2.54	CXCR4 2.24
D	CXCR5 2.52	DPP4 2.00	EGR1 1.95	FAS 2.63	FASLG 3.17	FOXP3 2.32	ICOSLG 2.70	IFNG 3.79	IL10 3.18	IL11 2.98	IL12A 3.11	IL12B 3.18
E	IL12RB1 2.56	IL12RB2 3.13	IL13 2.51	IL15 2.24	IL18 1.86	IL18R1 2.49	IL1B 2.77	IL2 3.04	IL2RA 3.00	IL3 3.17	IL4 3.20	IL4R 1.74
F	IL5 3.12	IL6 2.99	IL7 2.74	CXCL8 2.72	IRF4 2.52	LAG3 3.54	LCK 1.93	MAP3K7 1.89	MICB 2.79	MS4A1 -0.34	NCK1 2.02	NOS2 3.07
G	PTPRC 2.56	RAG1 2.82	RIPK2 2.24	SOCS1 2.61	TGFB1 1.25	TLR1 2.50	TLR2 2.85	TLR4 2.66	TLR6 2.76	TLR9 3.13	TNFSF14 2.72	VAV1 1.85

Figure 2. 9 Expression of human immune activation markers in humanized mice.

Total RNA was isolated from uninfected humanized mouse spleens and analyzed for the expression of markers for human immune activation. A total of 84 genes were evaluated and compared between the two animal models. (**A**) Heatmap depicted the differentially expressed genes (for 1–12) associated with immune activation in hu- PBL compared against HSC mice (for A–G). The log2 fold change of the individual gene is listed in the bottom panel. (**B**) Differentially expressed genes with log2 fold change of ≥3 are outlined that are expressed in hu-PBL spleens over what was found in HSC mice. A complete gene list can be found in Table 2.2.

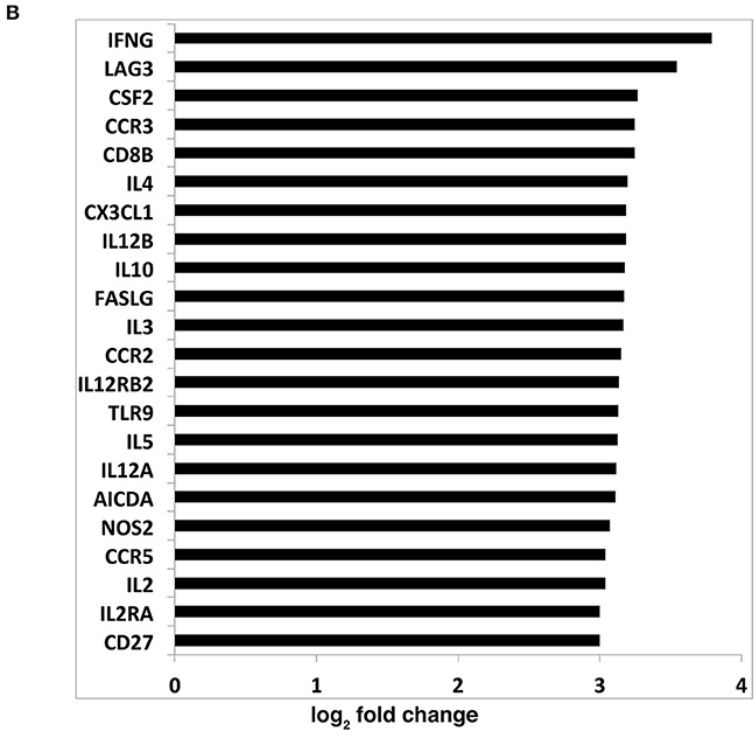

Figure 2. 9 Expression of human immune activation markers in humanized mice.

Total RNA was isolated from uninfected humanized mouse spleens and analyzed for the expression of markers for human immune activation. A total of 84 genes were evaluated and compared between the two animal models. (**A**) Heatmap depicted the differentially expressed genes (for 1–12) associated with immune activation in hu- PBL compared against HSC mice (for A–G). The log2 fold change of the individual gene is listed in the bottom panel. (**B**) Differentially expressed genes with log2 fold change of ≥3 are outlined that are expressed in hu-PBL spleens over what was found in HSC mice. A complete gene list can be found in Table 2.2.

Table 2. 2 Changes of human gene expressions in hu-PBL compared to hu-HSC mice

Gene Symbol	Gene Description	Fold Change
IFNG	Interferon, gamma	13.85
LAG3	Lymphocyte-activation gene 3	11.67
CSF2	Colony stimulating factor 2 (granulocyte-macrophage)	9.63
CD8B	CD8b molecule	9.48
CCR3	Chemokine (C-C motif) receptor 3	9.48
IL4	Interleukin 4	9.16
IL12B	Interleukin 12B (natural killer cell stimulatory factor 2)	9.09
CX3CL1	Chemokine (C-X3-C motif) ligand 1	9.09
IL10	Interleukin 10	9.05
FASLG	Fas ligand (TNF superfamily, member 6)	9.01
IL3	Interleukin 3 (colony-stimulating factor, multiple)	8.97
CCR2	Chemokine (C-C motif) receptor 2	8.88
IL12RB2	Interleukin 12 receptor, beta 2	8.78
TLR9	Toll-like receptor 9	8.76
IL5	Interleukin 5 (colony-stimulating factor, eosinophil)	8.72
IL12A	Interleukin 12A (natural killer cell stimulatory factor 1)	8.66
AICDA	Activation-induced cytidine deaminase	8.62
NOS2	Nitric oxide synthase 2, inducible	8.41
CCR5	Chemokine (C-C motif) receptor 5	8.23
IL2	Interleukin 2	8.21

IL2RA	Interleukin 2 receptor, alpha	8.01
CD27	CD27 molecule	7.99
IL6	Interleukin 6 (interferon, beta 2)	7.93
CD8A	CD8a molecule	7.93
IL11	Interleukin 11	7.9
CD1D	CD1d molecule	7.35
TLR2	Toll-like receptor 2	7.2
CCL3	Chemokine (C-C motif) ligand 3	7.08
RAG1	Recombination activating gene 1	7.07
MICB	MHC class I polypeptide-related sequence B	6.94
IL1B	Interleukin 1, beta	6.84
CD274	CD274 molecule	6.8
CD276	CD276 molecule	6.78
TLR6	Toll-like receptor 6	6.76
IL7	Interleukin 7	6.7
CXCL8	Interleukin 8	6.61
TNFSF14	Tumor necrosis factor (ligand) superfamily, member 14	6.58
ICOSLG	Inducible T-cell co-stimulator ligand	6.5
TLR4	Toll-like receptor 4	6.31
CD86	CD86 molecule	6.3
FAS	Fas (TNF receptor superfamily, member 6)	6.2
CCR1	Chemokine (C-C motif) receptor 1	6.14
SOCS1	Suppressor of cytokine signaling 1	6.12

APC	Adenomatous polyposis coli	6.12
PTPRC	Protein tyrosine phosphatase, receptor type, C	5.89
IL12RB1	Interleukin 12 receptor, beta 1	5.89
CD80	CD80 molecule	5.85
CXCR3	Chemokine (C-X-C motif) receptor 3	5.83
CXCR5	Chemokine (C-X-C motif) receptor 5	5.75
CD7	CD7 molecule	5.75
IRF4	Interferon regulatory factor 4	5.74
IL13	Interleukin 13	5.68
TLR1	Toll-like receptor 1	5.65
IL18R1	Interleukin 18 receptor 1	5.62
CCR4	Chemokine (C-C motif) receptor 4	5.39
BLM	Bloom syndrome, RecQ helicase-like	5.23
FOXP3	Forkhead box P3	4.99
CD28	CD28 molecule	4.76
RIPK2	Receptor-interacting serine-threonine kinase 2	4.73
CXCR4	Chemokine (C-X-C motif) receptor 4	4.73
IL15	Interleukin 15	4.71
BLNK	B-cell linker	4.51
ADA	Adenosine deaminase	4.17
CD2	CD2 molecule	4.13
NCK1	NCK adaptor protein 1	4.05
CD5	CD5 molecule	4.03

DPP4	Dipeptidyl-peptidase 4	3.99
EGR1	Early growth response 1	3.86
LCK	Lymphocyte-specific protein tyrosine kinase	3.81
CD3E	CD3e molecule, epsilon (CD3-TCR complex)	3.72
MAP3K7	Mitogen-activated protein kinase kinase kinase 7	3.71
CD4	CD4 molecule	3.71
IL18	Interleukin 18 (interferon-gamma-inducing factor)	3.62
VAV1	Vav 1 guanine nucleotide exchange factor	3.61
BCL2	B-cell CLL/lymphoma 2	3.42
IL4R	Interleukin 4 receptor	3.34
CD40	CD40 molecule, TNF receptor superfamily member 5	3.24
CD40LG	CD40 ligand	2.89
CD3G	CD3g molecule, gamma (CD3-TCR complex)	2.83
CD3D	CD3d molecule, delta (CD3-TCR complex)	2.44
CD47	CD47 molecule	2.43
TGFB1	Transforming growth factor, beta 1	2.38
CD81	CD81 molecule	1.45
MS4A1	Membrane-spanning 4-domains, subfamily A, member 1	-1.27

revealed that the top canonical pathways affected in hu-PBL over HSC mice were (1) Th1 and Th2 activation pathway (p=4.62E-56); (2) innate and adaptive immunocyte communications (p=3.03E-47); (3) Th2 (p=5.58E-43); (4) Th1 (p=2.14E-42) and (5) T-helper cell differentiation (p=1.76E-39, **Figure 2.10A)**. All five pathways are engaged in T cell regulation. Downstream Effects Analysis was performed to assess regulatory hierarchy. A total of 500 gene-related diseases or functions each with a minimum of 10 molecules related were predicted and top 10 functions were listed (**Table 2.3**). The differential genetic network in the hu-PBL mice was most significantly correlated with the activation of lymphatic systems with 80% (65/81) of the input genes involved and 83% (54/65) led to systemic activation responses **(Figure 2.10B)**. A spectrum of inflammation-associated genes was also upregulated in hu-PBL as compared to hu-HSC mice, including both pro-inflammatory (e.g. IL1, IL17, IFNγ, TNFα, CXCL3, and CXCL8) and anti-inflammatory (e.g. IL4, IL6, IL10, IL12, IL13, and TNFβ) molecules **(Figure 2.9 and Table 2.2)**. IPA analysis confirmed that this genetic pattern was associated with inflammatory responses with 67% (54/81) of the input genes involved and 81% (44/54) linked to cell activation pathways **(Table 2.3** and **Figure 2.11)**. Taken together, these data support the notion that an established immune activated and inflammatory tissue environment facilitates HIV-1 infection and dissemination.

2.5 Discussion

Early ART intervention restricts the HIV-1 reservoir size (127-129) and may achieve long-term viral remission in select infected individuals (50, 130). However, all patients inevitably experience viral relapse even when treatment is started as early as 14 days after

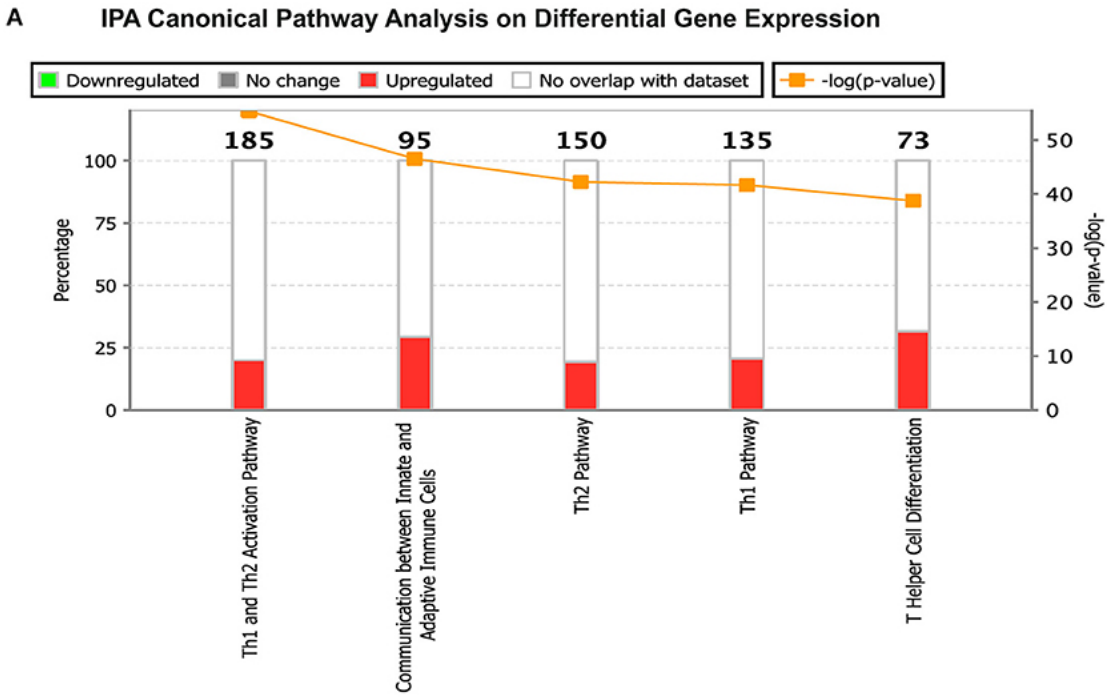

Figure 2. 10 Gene expression patterns analysis by IPA in humanized mice.

(A) Canonical pathway gene analyses. The stacked bar chart demonstrates the percentage of upregulated (red) and downregulated (green), as well as non-overlapped (white) genes from the prestored genebank in IPA (numbers listed at the top of each bar). The right y-axis displays the –log of p-Value calculated by Fisher's Exact Test illustrates the significance of each canonical pathway. **(B)** Downstream biological effects prediction. The most relevant downstream effect predicted by IPA was lymphoid activation. A set of 65 genes that were differentially expressed between hu-PBL and hu-HSC mice co-regulate this pathway. The putative function was located in the center while the related regulator listed at the periphery. The type of interaction is indicated by red (prediction of activation), blue (prediction of inhibition), yellow (inconsistent), and gray (related, not predicted).

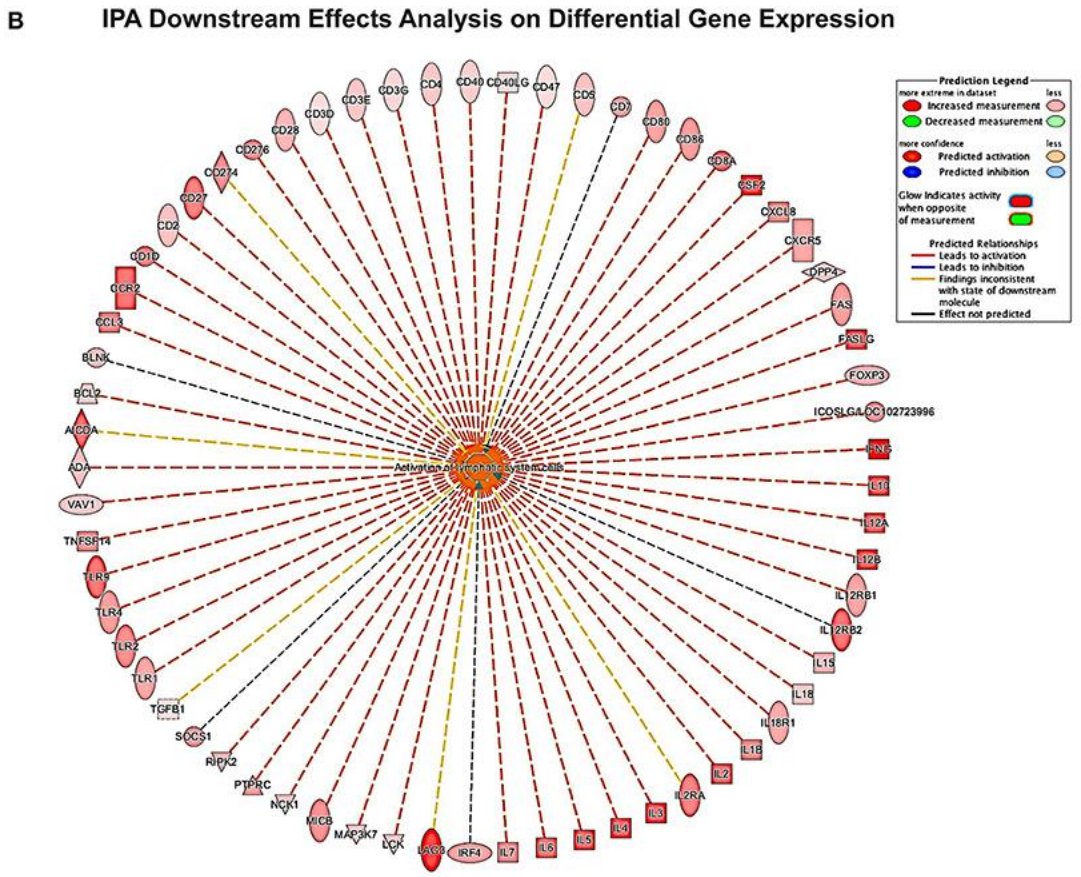

Figure 2. 10 Gene expression patterns analysis by IPA in humanized mice.

(A) Canonical pathway gene analyses. The stacked bar chart demonstrates the percentage of upregulated (red) and downregulated (green), as well as non-overlapped (white) genes from the prestored genebank in IPA (numbers listed at the top of each bar). The right y-axis displays the –log of p-Value calculated by Fisher's Exact Test illustrates the significance of each canonical pathway. **(B)** Downstream biological effects prediction. The most relevant downstream effect predicted by IPA was lymphoid activation. A set of 65 genes that were differentially expressed between hu-PBL and hu-HSC mice co-regulate this pathway. The putative function was located in the center while the related regulator listed at the periphery. The type of interaction is indicated by red (prediction of activation), blue (prediction of inhibition), yellow (inconsistent), and gray (related, not predicted).

Table 2. 3 p-value ranking of top 10 Disease and Bio-Functions by IPA on differential gene expression between hu-PBL and hu-HSC mice

Categories	Diseases or Functions Annotation	p-Value	Activation z-score	Molecules related (#)
Cell-To-Cell Signaling and Interaction	Activation of lymphatic system cells	4.22E-86	6.324	65
Cell-To-Cell Signaling and Interaction, Hematological System Development and Function, Immune Cell Trafficking, Inflammatory Response	Activation of mononuclear leukocytes	3.94E-85	6.308	65
Cell-To-Cell Signaling and Interaction, Hematological System Development and Function, Immune Cell Trafficking, Inflammatory Response	Activation of lymphocytes	1.67E-84	6.255	64
Cell-To-Cell Signaling and Interaction, Hematological System Development and Function, Immune Cell Trafficking, Inflammatory Response	Activation of leukocytes	1.46E-83	6.523	70
Cell-To-Cell Signaling and Interaction	Activation of cells	8.43E-76	6.837	72
Hematological System Development and Function, Tissue Morphology	Quantity of mononuclear leukocytes	4.43E-74	4.681	67

Cellular Development, Cellular Growth and Proliferation, Hematological System Development and Function, Hematopoiesis, Lymphoid Tissue Structure and Development, Tissue	Differentiation of mononuclear leukocytes	1.48E-73	7.253	66
Hematological System Development and Function, Tissue Morphology	Quantity of leukocytes	2.38E-73	4.435	70
Cellular Development, Cellular Growth and Proliferation, Hematological System Development and Function, Hematopoiesis, Lymphoid Tissue Structure and Development, Tissue	Leukopoiesis	3.59E-73	7.542	68
Cellular Development, Cellular Growth and Proliferation, Hematological System Development and Function, Hematopoiesis, Lymphoid Tissue Structure and Development, Tissue	Hematopoiesis of mononuclear leukocytes	1.02E-71	7.192	65
. . .	. . .	. . .	. . .	. . .
Inflammatory Response	Inflammatory response	3.01E-49	4.939	54

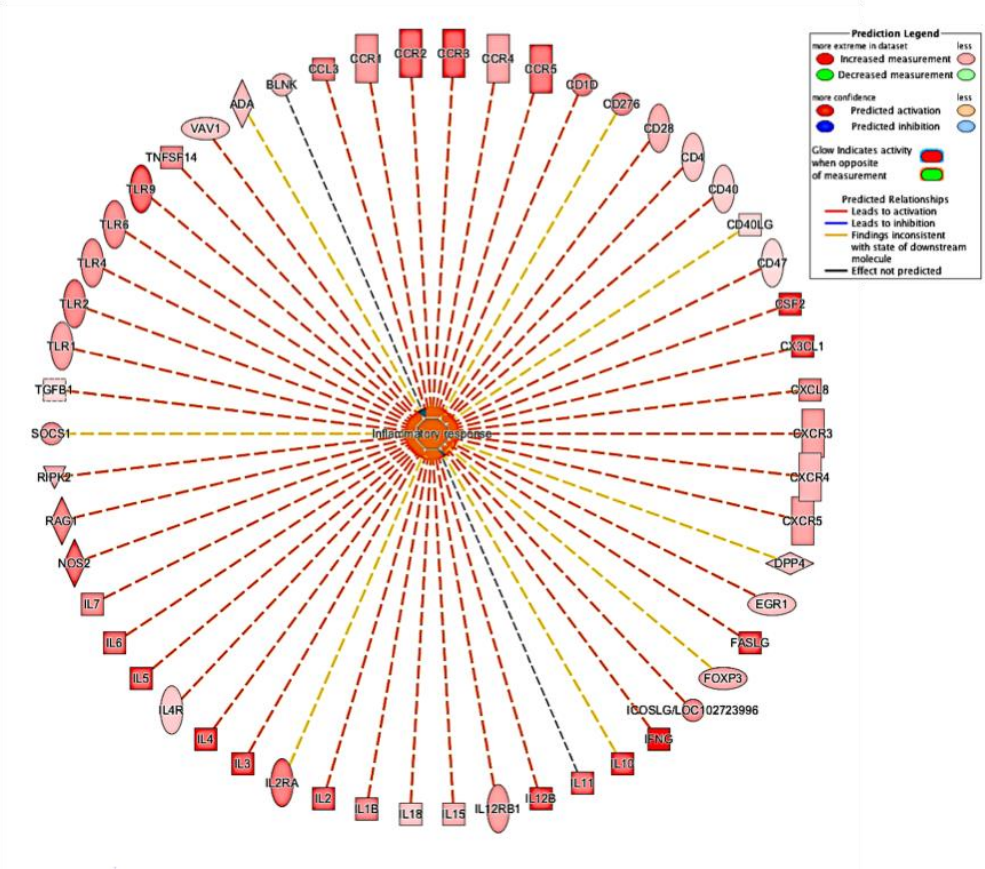

Figure 2. 11 The prediction of biological processes according to changed expression of humanized mouse genes by IPA was associated with inflammatory response.

Total spleen RNA was isolated from hu-HSC and hu-PBL mice and probed using RT^2 Profiler PCR Array for T & B cell activation analysis. Hu-HSC mice were chosen as control group while hu-PBL mice as test group. The fold changes of human genetic expression (hu-PBL / hu-HSC) were determined by SABioscience RT^2 Profiler PCR Array Data Analysis software, version 3.5. IPA was applied for predicting the biological function based on the pattern of differentially expressed genes in the dataset. Inflammatory was one of the most significantly affected pathway co-regulated by a set of 54 genes that were differentially expressed between hu-PBL and hu-HSC mice. The putative function was located in the center while the related regulators listed at the periphery. The type of interaction is indicated by red (prediction of activation), blue (prediction of inhibition), yellow (findings inconsistent), and gray (known to be related, but effect not predicted).

infection (111). It is thus important to determine viral compartmentalization in cells and tissues. Nonetheless, it is not possible to accurately answer this question in an infected human. Therefore, in the current study we traced HIV-1 peripheral and tissue dissemination after infection in humanized mice used to reflect the temporal dynamics of tissue infection. The major advancements of this study were direct comparisons between hu- HSC and PBL mice using a dual tropic HIV-1 strain (HIV-1_{ADA}) in study (131). Multiple time points after HIV-1 infection to reflect a complete picture of early viral dynamics as well as host immune responses. By comparing the viral-host kinetics, we were able to identify the host factors that affect early events of HIV-1 infection. Limitations in accessing human samples to correlate immune responses with levels of viral growth were achieved through the use of humanized mice.

Herein, two well studied chimeric humanized mouse models were used in this report with divergent biologic and immune characteristics. Hu-HSC mice were made after engrafting human CD34+ HSC into new born NSG mice (132). After cell differentiation and maturation, mice are reconstituted with multiple lineages of human immune cells. The cellular type and composition in hu-HSC mice are more similar to human (T and B cells and monocyte-macrophages) with a life expectancy of more than a year. Hu-PBL mice are produced by implanting human peripheral blood lymphocytes into the adult NSG mice. This leads to dominant human lymphocyte reconstitution of up to 95 % T cells within 2-3 days (133). However, as a result of GvHD, the life span of the viral immune responses in these animals can only be measured for a single month. Results from both models allowed us not only able to trace early HIV-1 infection, but investigate how host environments may affect viral-host outcomes (134).

Effector memory CD4+ T cells are the primary targets of HIV-1 and their depletion parallels the development of the acquired immune deficiency syndrome (125). CD4+ T cell

loss is observed within months of HIV-1 infection from both peripheral blood and lymphoid tissues (135). In the current study, we observed modest CD4+ T depletion in blood of hu-HSC mice as early as 3 days after infection that progressed over time. A similar trend was also observed in infected splenocytes and bone marrow. Altogether, such results indicate that human immune function is impaired at the earliest stage of infection (136). CD8+ T cell percentages were elevated in parallel to CD4+ T cell losses. In hu-PBL mice, peripheral CD4+ T cell depletion was more significant than what was observed in hu-HSC mice. This reflected a highly activated cell phenotype facilitating productive HIV-1 infection and cellular degradation.

Plasma HIV-1 RNA is first seen within three weeks after HIV-1 infection in humans (137, 138). Due to the difficulty of early HIV-1 screen in the clinic, a gap between initial viral exposure and estimated infection period is inevitable, which can be bridged using suitable animal models. In the current study, peripheral viral load was detected in 40% (2/5) of hu-HSC animals by days 3, 5, and 7 after infection each and 100% by day 14. It implied that peripheral viral replication might be established earlier than what is usually observed in humans given the possibility that highly sensitive techniques may further improve detection limit. In hu-PBL mice peripheral viral load was fully expressed in all monitored animals within 3 days of infection with a peak viremia seen at day 7. The data clearly support the notion that viral replication is linked to immune activation.

Tissue HIV-1 DNA and RNA was first detected by semi-nested qPCR at 3 days after infection in hu-HSC mouse spleen, lung, and liver, demonstrating that infection was established and disseminated to multiple tissues rapidly while plasma viral load is extremely low or undetectable. Interestingly, at 5 and 7 days after infection, viral nuclear

acids were recovered from each of these tissues in 2/5 animals and supported the fact that all three tissue compartments were seeded by virus at the earliest stage of infection. The observation of HIV-1 RNA and HIV-1p24 antigen on the corresponded spleen sections supported that the detected virus completed its life cycle and demonstrating that spleen could serve as a major anatomical infectious site (139). In addition, infected cells were highly enriched within lymphoid follicles. This is due to the known higher numbers of reconstituted human cells in follicles and supports its role in early tissue infection. As the germinal centers are poorly developed in humanized mice, their role in viral compartmentalization requires further study in defining it as a sanctuary site during ART (140). At 14 days after HIV-1 infection, virus was easily seen in spleen, lung, liver, gut and kidney. Tissue viral DNA and RNA levels were dramatically increased compared to the early time points, accordant with plasma HIV-1 RNA. One can speculate that multiple peripheral and tissue sanctuaries have been established at early points after viral infection, which may illustrate the hurdles that need be overcome to achieve viral eradication (111). These observations highlight hu-HSC mice as a model for the earliest stages of HIV-1 infection. The observations now made also support our prior works investigating cellular and tissue replication patterns seen during chronic infections (121). In these works virus was identified in bone marrow, spleen, lung, gut, brain, kidney and liver tissues as well as in CD34+ progenitors, monocyte-macrophages, dendritic cells, and CD4+ stem cell memory, naïve memory, central memory, effector memory and regulatory T cells. All were identified after 5 to 14 weeks of viral infection.

Lymph nodes are major tissue compartments that harbor HIV-1 (141). In the current study, we did not detect HIV-1p24 in hu-HSC mouse lymph nodes until 14 days after

infection. This reflected, in measure, the underdeveloped lymph nodes in immune deficient animals (142). While gut-associated lymphoid tissue or GALT is one of the earliest observed infected tissue during acute HIV-1 infection (20) we also were not able to detect HIV-1 infection in hu-HSC mouse GALT until day 14. This was later than what was observed from spleen, lung, and liver. These data reflect the relatively low humanization operative in hu-HSC mouse GALT (143). This limitation restricts studies of viral transmission (144). However, even considering the limitations of the model infection of GALT showed high levels of infection at later time points. The low reconstitution of human immune cells may also explain delayed HIV-1 infection in hu-HSC mouse brains. A recent study reported that within early infected individuals (median 15 days), HIV-1 RNA was observed in cerebrospinal fluid from 83%, 15/18 infected subjects, with the earliest detection by 8 days (138). However, according to variant humanized mouse models studied, HIV-1 seeding in the central nervous system was generally much more delayed (43, 118, 145). This discordance demonstrates some of the limitation of our current humanized mouse models. Of interest to the current studies are our prior experiences in using hu-HSC mice that showed sustained bone marrow viral burden (121, 146). Although bone marrow HIV-1 infection was not measured in the current study, the progressive decline of CD4+ T cells indicated that active viral replication was rapidly established in the hu-HSC mouse bone marrow. Notably and distinct from hu-HSC mice, HIV-1 was seeded into tissue compartments more rapidly in hu-PBL mice. At 3 days post-infection, HIV-1 DNA and RNA were readily detected across a wide range of tested tissues, including brains. HIV-1p24 was also observed in the 3-day infected lymph node sections. Viral levels were higher in hu-PBL mice at the same time courses compared to that in hu-HSC mice. Altogether,

these results strengthen the notion that the host microenvironment is closely linked to early HIV-1 tissue replication.

Previous studies by others showed that low levels of T cell activation and proliferation lead to reduced HIV-1 susceptibility (147, 148). Nevertheless, comorbid factors such as sexually transmitted infectious diseases substantially increased the risks of HIV-1 acquisition and transmission as well as affecting viral load. All are known to be associated with inflammation and immune activation (149-151). Our data support the idea that immune activation markers predict viral susceptibility in mouse models of human disease. Comparisons in host tissue environments were made at the transcriptional level in both models. These data support the idea that immune activation that occurs prior to infection could predict early HIV-1 infection dynamics in these animal models. In addition, a wide range of inflammation-associated genes was also found to be upregulated in hu-PBL compared to HSC mice. While pro-inflammatory conditions facilitate viral acquisition and promote T cell activation (152), anti-inflammatory factors serve to maintain systemic homeostasis. Noteworthy, a recent report demonstrated that a systemic proinflammatory signature was established by as early as 24 hours after SIV infection of rhesus macaques (114). It will be interesting to evaluate how early inflammasome activated in HIV-1 infection affects early viral dynamics. We posit that immune-activation and inflammation explains early HIV-1 infection, rapid viral dissemination and accelerated CD4+ T cell loss in the hu-HSC mice.

Recently we demonstrated that hu-HSC mice infected with HIV-1_{NL4-3} strain (153) expressed high levels of HIV-1 replication in peripheral blood, gut, spleen, lung, liver, brain, kidney, lymph node and bone marrow. These results illustrated that viral factors also

affect the formation of HIV-1 infection in tissue compartments. In addition, a recent report found that after acute intravaginal challenge of HIV-1_{BaL} on humanized Rag1KO.IL2RγcKO.NOD mice expressing HLA class II (DR4) molecule (DRAG) mice (118), virus was detected at certain tissues by day 4 while brain was lastly infected until day 21. This also suggested that different infection routes and genetic background should be considered in reflecting what would be operative in an infected human host. While we understand that the intraperitoneal route used to establish viral infection does not reflect what is operative during natural infection routes such as mucosal transmission. However, we performed this route to ensure infection was operative in 100% of challenged animals and was able to explore viral compartmentalization during the evolution of persistent viral infection. The deployment of humanized mouse models allows researchers to determine how, where and at what levels virus gains a foothold in tissue sites and prior to any or all therapeutic strategies. Indeed, based on this work, our group has shown that combinations of long acting slow effective release antiretroviral therapy and CRISPR-Cas9 for viral excision led to permanent HIV-1 elimination in up to one third of infected humanized mice (109) and supports the use of this model in viral eradication schemes.

2.6 Conclusions

In conclusion, by using humanized mouse models, our study identified a wide range of tissue compartments and their temporal and spatial dynamics during early HIV-1 infection. The four major findings from this study are summarized as *First,* HIV-1 infection was identified in multiple tissue compartments as early as 3 days post-infection using highly sensitive detection techniques in two different humanized animal models. *Second*

HIV-1 was detected in all tissue by day 14 in hu-HSC mice. *Third,* tissue viral replication patterns were linked to markers of immune activation and immunity for each animal model that included T cell maturation and inflammation. *Fourth,* spleen, lung, and liver were among the earliest infected tissues and sustained heavy viral burden throughout the monitoring period as shown in proviral DNA amplifications. It is noteworthy that the tissue types listed above do not cover all the human anatomical viral sanctuaries. Others tissues that require analyses in humanized mice include but not limited by thymus, male and female reproductive tract, skin, and adipose tissue (18, 154). Even accepting the limitation of both models and underdevelopment of secondary lymphoid tissues this information will instruct us on the guideline of early ART intervention and development of tissue-specific ART. It has been an intriguing question whether a window exists for 'HIV-1 cure', if ART is administrated soon after viral exposure to maximize the restriction of viral replication followed by combinational strategies targeting the residual proviral DNA. Using humanized mouse model under controlled conditions, we will be able to answer this question, which will benefit the translation of clinical investigation.

Chapter 3 Combination of LASER ART and CRISPR-Cas9 Eliminates HIV-1 in Humanized Mice

3.1 Abstract

Human immunodeficiency virus (HIV-1) eradication can be achieved by complete elimination of viral reservoirs from host cell and tissue sanctuaries. Success of HIV-1 eradication can be affirmed through the absence of viral rebound after cessation of antiretroviral therapy (ART). Here we demonstrate, for the first time, that sequential treatment of HIV-1 infected humanized mice with long-acting slow-effective release ART (LASER ART) followed by viral CRISPR-Cas9 excision achieved viral eradication in up to a third of infected dual treated humanized mice. In these HIV-1 eradicated mice, ultrasensitive nested and digital droplet PCR and RNAscope assays did not detect virus in blood, spleen, lung, kidney, liver, gut-associated lymphoid tissue, and brain. Excision of proviral HIV-1 DNA fragments spanning the LTRs and the Gag gene by CRISPR-Cas9 was seen in the absence of off-target effects and viral rebound following ART cessation and CD4+ T cell restoration. Adoptive transfer of lymphoid cells, from dual-treated virus-free animals, to uninfected humanized mice or by direct co-cultivation with mitogen stimulated lymphocytes failed to recover infectious progeny virus. In contrast, replication competent HIV-1 was readily detected in all infected animals treated with ART or CRISPR-Cas9 alone. Thus, sequential LASER ART and CRISPR-Cas9 therapies administered to HIV-1 infected humanized mice provide the first proof-of-concept that viral sterilization is possible.

3.2 Introduction

According to UNAIDS, by 2018 more than 37.9 million people worldwide were living with the human immunodeficiency virus type one (HIV-1) and 1.7 million people

were newly infected. Among infected individuals, 23.3 million (62%) people had access to antiretroviral therapy (ART). While ART restricts various steps of the hiv-1 life cycle, including cellular entrance, reverse transcription, genome integration, and viral assembly, it fails to eliminate integrated HIV-1 proviral DNA (155, 156). Even though majority of proviral DNA that recombines into host genome is defective, some replication-competent HIV-1 DNA maintains latent infection in cellular and tissue reservoirs and ready to be reactivated upon ART interruption and causes HIV-1 resurgence (157). HIV-1 reservoirs have become the major obstacle to viral cure, alongside a combination of factors including inadequate ART to viral reservoirs, less efficient cytotoxic lymphocyte killing, rapid viral spread and mutations. By far, successful HIV-1 eradication has only been achieved in two cases who experienced aggressive chemotherapy and bone marrow transplantation from donors with CCR5 mutation (47, 48). The success in these individuals likely resulted from the clearance of majority if not all of HIV-1 reservoirs and with newly transplanted cells that are intrinsically resistant to viral infection. However, this procedure is very dangerous and cannot be extended as a regular therapy for millions of HIV-1 infected individuals. Other current cure strategies that covered latency reversal agents, broadly neutralizing antibody, therapeutic vaccine, chimeric antigen receptor T cells and immune enhancers have not been able to achieve long-term suppression in patients after stopping ART (52, 53, 158-160). To address this dilemma, we conducted a proof-of-concept study using state-of-art long-acting nanoformulation of ART and CRISPR-Cas9 gene editing technology to pursue HIV-1 eradication from humanized mouse model. The long-acting highly hydrophobic lipophilic antiretroviral prodrugs were named long-acting slow-effective release ART (LASER ART). These LASER ARTs demonstrated enhanced drug half-life,

cellular up-take and retention, penetration across cell and tissue barriers and improved control against ongoing viral infection (44, 161-164). While HIV-1 replication was effectively inhibited, CRISPR-Cas9 was employed to excise integrated viral copies. CRISPR-Cas9 technology has grown rapidly and shown promise in treatment of multiple genetic diseases including cancer, blindness, muscular dystrophy, and HIV-1/AIDS. Indeed, CRISPR-Cas9 that was designed to specifically target conserved HIV-1 sequences have successfully excised HIV-1 fragments from the host genome in cell cultures and in tissues from small animal models of HIV-1 infection (107, 165-169). To this end, we tested whether or not a combination of LASER ART and CRISPR-Cas9 treatments would work "in synergy" for viral elimination. Using HIV-1 infected humanized mice, we demonstrated that a complete viral eradication was achieved in a subset of animals that received LASER ART and CRISPR-Cas9 dual treatment. Viral elimination was exhaustively scrutinized by nested and digital PCR, RNAscope, and in vitro and in vivo viral outgrowth assay using seronegative healthy donor PBMCs and naïve humanized mice, respectively. While HIV-1 was not detected in all these tests from 'cured' animals, virus was observed in all other HIV-1 infected humanized mice that received LASER ART or CRISPR-Cas9 treatment alone. We demonstrate that HIV-1 can be eradicated using this combinational strategy of LASER ART and CRISPR-Cas9.

3.3 Materials and Methods

3.3.1 Generation and HIV-1 infection of humanizded mice

NSG mice were obtained from the Jackson Laboratories, Bar Harbor, ME and bred under specific pathogen-free conditions at the University of Nebraska Medical Center

(UNMC). Human CD34+ HSC were enriched from human cord blood or fetal liver cells using immune-magnetic beads (Miltenyi Biotec Inc., Auburn, CA, USA). Cells were intrahepatic injected into newborn NSG mice after irradiation at 1 Gy using a RS-2000 X-Ray Irradiator (Rad Source Technologies, Buford, GA). Human cell reconstitution was evaluated by flow cytometry (120, 170). At the age of 18 weeks, humanized mice with comparable human cell levels were intraperitoneally infected with HIV-1_{NL4-3} or HIV-1_{ADA} (43, 171) at 10^4 $TCID_{50}$/ml. Plasma viral RNA levels (copies/ml) were analyzed using the automated COBAS Ampliprep System V2.0/Taqman-48 system (Roche Molecular Diagnostics, Basel, Switzerland) (120, 171). For this assay, 100 µl of mouse serum was diluted to 1 ml with sterile filtered normal human serum. The detection limit of the assay is 200 viral RNA copies/ml.

3.3.2 Synthesis of nanoformulated antiretroviral drugs

Dolutegravir (DTG), lamivudine (3TC), and abacavir (ABC) were generously provided by ViiV Healthcare, Research Triangle Park, NC. Rilpivirine (RPV) was purchased from Hangzhou Bingo Chemical Co., Ltd, Hangzhou, China. Parent antiretroviral drugs DTG, 3TC, and ABC were myristoylated into prodrugs and named as MDTG, M3TC, and MABC. These three prodrugs were encased into poloxamer 407 (P407) and RPV was encased into poloxamer 338 (P338) in native form. All drugs were formulated into nanosuspensions using high pressure homogenization as previously described (44, 161, 162). Final drug concentrations for injection were determined by HPLC-UV/Vis and UPLC-MS/MS and intramuscularly injected to humanized mice.

3.3.3 Antibodies for flow cytometry

Humanized mice were bled through submandibular vein longitudinally to track human cell levels. Animal blood was collected using ethylenediaminetetraacetic acid (EDTA)-coated tubes or by cardiac puncture at animal sacrifice. Flow cytometry staining employed a five-color panel to label human CD45, CD3, CD4, CD8, and CD19 markers using FITC-conjugated mouse anti-human CD45 (555482), Alexa Fluor 700-conjugated mouse anti-human CD3 (557943), APC-conjugated mouse anti-human CD4 (555349), BV421-conjugated mouse anti-human CD8 (562428), and PE-Cy5-conjugated mouse antihuman CD19 (555414) antibodies; all antibodies were purchased from BD Biosciences, San Jose, CA. Antibodies. Flow cytometry tests were operated using LSR-II FACS analyzer (BD Biosciences) and analyzed by a FlowJo (BD Immunocytometry Systems, Mountain View, CA, USA).

3.3.4 Tissue HIV-1 analysis by semi-nested qPCR

Humanized mouse tissues (spleen, bone marrow, lung, gut, liver, kidney, and brain) were collected at sacrifice and total HIV-1 DNA and RNA were extracted using a Qiagen Kit (Qiagen, Hilden, Germany) according to the manufacturer's instructions. Total HIV-1 DNA isolated from ACH2 cell line which contains one HIV-1 DNA copy per cell was serially diluted and used as standard control. Human CD45 gene were used as human cell marker for normalization (Thermo-Fisher Scientific). HIV-1 RNA was first reverse transcribed into cDNA using SuperScript III (Invitrogen, MA, USA) at 42 °C for 60 min. HIV-1 cDNA and total DNA were subjected to semi-nested qPCR and ddPCR assays for quantification as previously described (43). The first round of PCR was performed on a conventional PCR machine (T100 Thermal Cycler, Biorad, CA, USA) in 25 μl of PCR

reaction mix containing 500 ng of template and 50 ng each of both primers annealing to HIV-1 gag region; the reaction conditions are as follows: 94 °C for 3 min, followed by 15 cycles of 94 °C for 30 s, 55 °C for 30 s, and 72 °C for 1 min. The product of the first PCR was subsequently used as a template in the second semi-nested real-time PCR amplification performed on the ABI Step One Plus real-time PCR machine (Applied Biosystems, Foster City CA, USA) using TaqMan detection probe and primers (172). Two µl of the first PCR product was diluted to 50 µl with PCR master mix containing two primers at 0.2 µM each and 0.2 µM TaqMan dual-labeled fluorescent probe. Real-time PCR settings were as follows: 50 °C for 2 min, then 95 °C for 10 min, followed by 40 cycles of 95 °C for 15 s and 60 °C for 1 min. The amplicon sizes are 221 bp for the first round of PCR and 83 bp for the second round (real-time) PCR. DNA extracted from ACH2 cells containing one integrated copy of HIV-1 per cell was used as standard in serial 10-fold dilutions with HIV copy numbers ranging from 10^1 to 10^5 DNA copies/reaction (43, 173). Semi-nested real-time RT-PCR on HIV-1 RNA was performed as described (43, 173).

3.3.5 Detection of tissue HIV-1 nucleic acids by ddPCR

ddPCR was performed based on the water–oil emulsion droplet technology, using the ddPCR™ Supermix for Probes reagents in the QX200™ Droplet Digital™ PCR system (Bio-Rad Laboratories, Hercules, CA, USA). For quantification of HIV-1 DNA, the eluted cellular DNA was PCR amplified (43, 173, 174) targeting the HIV-1 gag gene using the outlined primers targeting HIV-1 gag gene (Forward-5'-TCAGCCCAGAAGTAATACCCATGT-3' and Reverse-5'-CACTGTGTTTAGC ATGGTGTTT-3') and a TaqMan probe (5’ FAM-ATTATCAGA AGGAGCCACCCCACAAGA-3’ IBFQ). A total of 100-200 ng DNA from each tissue

was used as a template for ddPCR amplifications with the same thermal cycling conditions used for real-time q-PCR detection. Data acquisition and analysis were done using QX200 droplet reader and QuantaSoft™ software provided with the instrument.

3.3.6 Viral recovery by in vitro viral outgrowth assay

Human PBMCs were collected from HIV-1,2 seronegative donors and cultured with PHA and IL-2 containing 10% RPMI (128, 175, 176). Humanized mouse splenocytes and BM were isolated and separately co-cultured with PBMCs at concentrations of (1:5). Eight days later, cells were collected and HIV-1 RNA and DNA were extracted for downstream qPCR analysis as described above.

3.3.7 Viral recovery by in vivo viral outgrowth assay

Humanized mouse splenocytes and BM cells were collected at sacrifice and homogenized and counted using TC-20 automated cell counter (Bio-Rad). A total of 8-10 x 10^6 either splenocytes or BM were adoptively transferred into naïve humanized mice intraperitoneally. Recipient animals were maintained for 4 weeks before sacrifice and tissue and peripheral HIV-1 levels were evaluated as described above.

3.3.8 Study Approval

All experimental protocols that use laboratory animals were approved by the UNMC Institutional Animal Care and Use Committee ensuring the ethical care and use of laboratory animals in experimental research. All animal studies were performed in compliance with UNMC institutional policies and NIH guidelines for laboratory animal housing and care. Human blood cells were isolated by leukapheresis from HIV-1/2 and hepatitis seronegative donors and were deemed exempt from approval by the Institutional

Review Board of the University of Nebraska Medical Center. Human CD34+ hematopoietic stem cells were isolated from umbilical cord blood and are exempt from UNMC IRB approval.

3.3.9 Statistics

Data were analyzed using GraphPad Prism 7.0 software (La Jolla, CA, USA) and presented as the mean ± the standard error of the mean (SEM). Experiments were performed using a minimum of three biologically distinct replicates. For comparisons of two groups, Student's t test (two-tailed) was used. Tissue drug levels, HIV-1 RT activity, HIV-1p24 antigen staining, T cell populations, viral RNA and DNA, and viral load were analyzed by one-way ANOVA with Bonferroni correction for multiple-comparisons. For studies with multiple time points, two-way factorial ANOVA and Bonferroni's post-hoc tests for multiple comparisons were performed. Animal studies included a minimum of six animals per group. Extreme outliers beyond the 99% confidence interval of the mean and 3-fold greater than the SEM were excluded. Significant differences were determined at $P < 0.05$.

3.4 Results

3.4.1 Viral and immune profiles of HIV-1 infected LASER ART and CRISPR-Cas9 treated humanized mice

Hematopoietic stem cells (HSC) reconstituted NOD.Cg-Prkdc^{scid} Il2rgt^{m1Wjl}/SzJ (NSG) mice exhibiting matured T cells that are broadly susceptible to HIV-1 infections has served a suitable model to investigate long terms viral infections and viral reservoir (45, 120, 169, 172, 177-180). To establish this model for our studies, after irradiation of NSG

mice at birth, animals were engrafted with human CD34+ HSC isolated from cord blood by intrahepatic injection. The presence of human immunocytes in blood was evaluated by flow cytometry for times up to 20 weeks. After humanization was confirmed, animals were infected with HIV-1 (NL4-3 or ADA) at 10^4 tissue culture infection $dose_{50}$ ($TCID_{50}$)/animal. In the initial experiment, 29 humanized mice were infected with HIV-1_{NL4-3} for two weeks **(Figure 3.1A).** Moderate CD4+ T cell depletion was observed **(Figure 3.1B)** and plasma HIV-1 RNA was established at a median of 2.2 x 10^5 copies/ml **(Figure 3.1C).** Then animals were randomly distributed into four groups as followed: the first group (n = 6) was HIV-1 positive control, the second group (n = 6) received a single intravenous (IV) injection of AAV_9-CRISPR-Cas9 at 10^{12} GC (genome copy); the third group (n = 10) were administered LASER ART containing 45 mg/kg parent drug equivalents of NRPV and MDTG, and 40 mg/kg parent drug equivalents of M3TC and MABC nanoparticles by intramuscular injection, the fourth group (n = 7) received LASER ART followed by AAV_9-CRISPR-Cas9. At eight weeks after the last injection of LASER ART which equaled to five weeks post the administration of AAV_9-CRISPR-Cas9, animals were sacrificed to evaluate the dynamic changes of immune and viral profiles **(Figure 3.1A)**. In groups 1 and 2 where LASER ART was not administered, peripheral CD4+ T cells dropped dramatically to < 6% and 15 ± 6%, respectively. In contrast, when LASER ART was present with or without CRISPR-Cas9 as shown in groups 3 and 4, peripheral CD4+ T cells were preserved at 68 ± 15% and 90 ± 7%, respectively **(Figure 3.1B).** Humanized mice in groups 1 and 2 remained highly infected throughout the study. In group 3, although plasma viral load was significantly decreased to undetectable level after LASER ART administration but all 10 animals experienced viral rebound after treatment interruption as observed in the clinic. In

group 4 where animals received dual treatment, 5 out of 7 animals experienced viral rebound after treatment was discontinued but 2 animals remained undetected at animal sacrifice **(Figure 3.1C).** Consistent human cell levels as shown by human CD45+ **(Figure 3.1D)** and CD3+ T cells **(Figure 3.1E)** was monitored throughout the study.

3.4.2 HIV-1 elimination from dual-treated humanized mouse tissue compartments

HIV-1 DNA and RNA were extracted from animal tissues (spleen, BM, gut, brain, liver, kidney, and lung) from all 4 groups. Viral levels were first determined by semi-nested real-time qPCR **(Figure 3.2A and B).** Tissue HIV-1 DNA and RNA replication were significantly lower in dual-treated animals compared to animals without treatment, or animals receiving treatment of either LASER ART or CRISPR-Cas9 alone. In animals M4346 and M4349, HIV-1 DNA and RNA were not detected in all the tissues tested **(Figure 3.2A and B, as shown in red square).** Absence of HIV-1 replication in M4346 and M4349 was also confirmed using droplet digital PCR (ddPCR). While HIV-1 DNA was not detected in these 2 animals within all tested tissues, HIV-1 DNA was observed in all other animals **(Figure 3.3A and B).** Humanized mouse splenocytes and BM were further cocultured with phytohemaglutinin/interleukin-2 (PHA/IL-2)-stimulated peripheral blood mononuclear cells (PBMCs) for 2 weeks to recovery HIV-1 from latent reservoirs. Cells were collected at end point and tested for cell-associated HIV-1 DNA and RNA. HIV-1 was not recovered from cells of M4346 and M4349 but readily recovered from all other tested animals **(Figure 3.3C and D).**

3.4.5 Cross validation for HIV-1 eradication using LASER ART and CRISPR-Cas9

To validate HIV-1 eradication by this combinational strategy using LASER ART

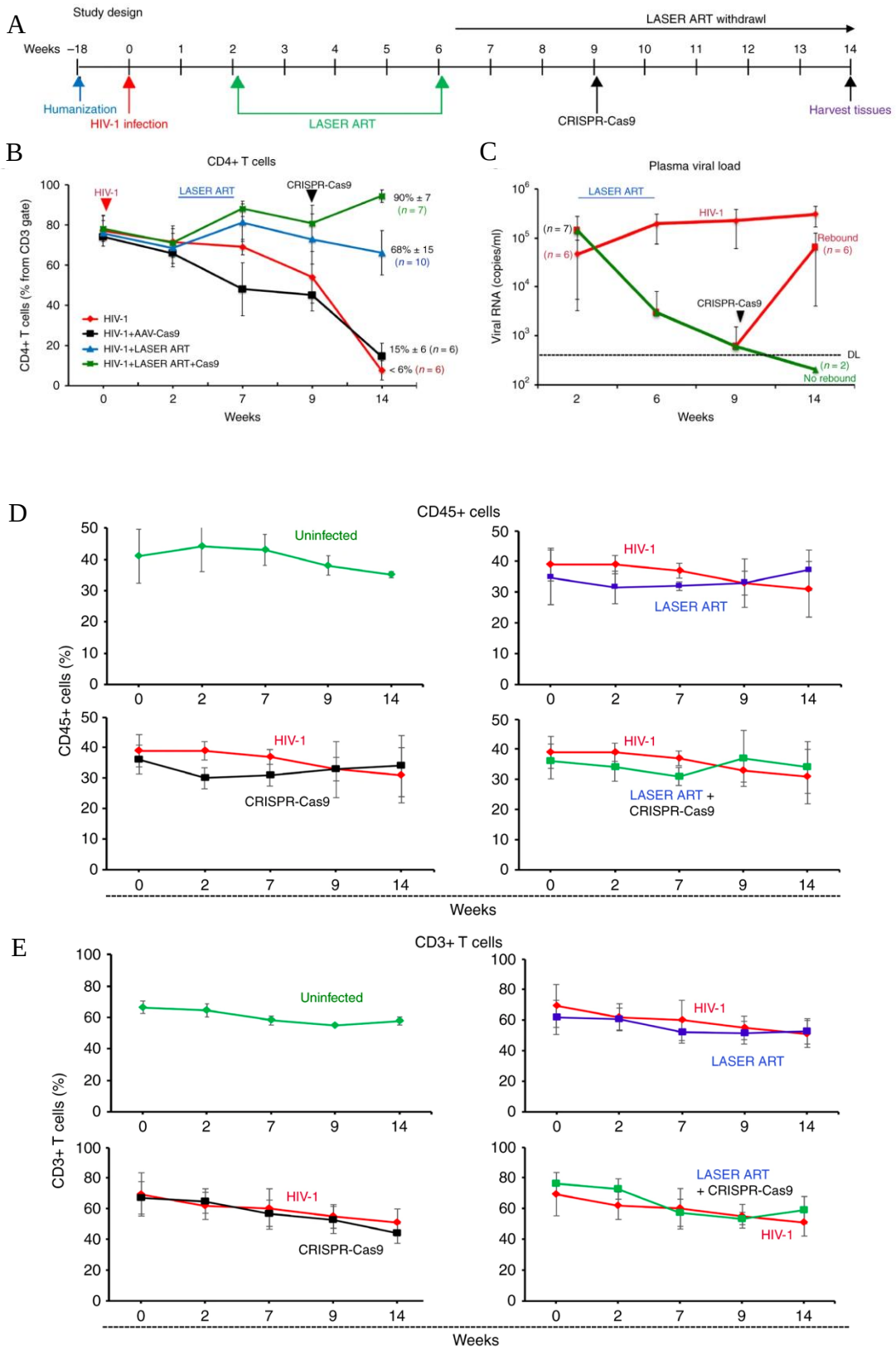
A
Study design
LASER ART withdrawl
Weeks −18 0 1 2 3 4 5 6 7 8 9 10 11 12 13 14
Humanization
HIV-1 infection
LASER ART
CRISPR-Cas9
Harvest tissues
B
CD4+ T cells
CD4+ T cells (% from CD3 gate)
HIV-1
LASER ART
CRISPR-Cas9
90% ± 7 (n = 7)
68% ± 15 (n = 10)
15% ± 6 (n = 6)
< 6% (n = 6)
HIV-1
HIV-1+AAV-Cas9
HIV-1+LASER ART
HIV-1+LASER ART+Cas9
Weeks
C
Plasma viral load
Viral RNA (copies/ml)
LASER ART
HIV-1
(n = 7)
(n = 6)
Rebound (n = 6)
CRISPR-Cas9
DL
(n = 2)
No rebound
Weeks
D
CD45+ cells
CD45+ cells (%)
Uninfected
HIV-1
LASER ART
HIV-1
CRISPR-Cas9
HIV-1
LASER ART + CRISPR-Cas9
Weeks
E
CD3+ T cells
CD3+ T cells (%)
Uninfected
HIV-1
LASER ART
HIV-1
CRISPR-Cas9
LASER ART + CRISPR-Cas9
HIV-1
Weeks

Figure 3. 1 Humanization and plasma viral load of HIV-1 infected and treated humanized mice.

The study scheme is shown in **(A)** where humanized mice were infected with 10^4 $TCID_{50}$ of HIV-1_{NL4-3} followed without treatment or with treatments of either LASER ART or CRISPR-Cas9 alone or both. Peripheral human CD4+ T cells **(B)**, CD45+ cells **(D)**, and CD3+ cells **(E)** were monitored by flow cytometry throughout the study. **(C)** Plasma viral load was determined by the COBAS Ampliprep-Taqman-48 V2.0 assay with a sensitivity of 200 copies/ml.

A

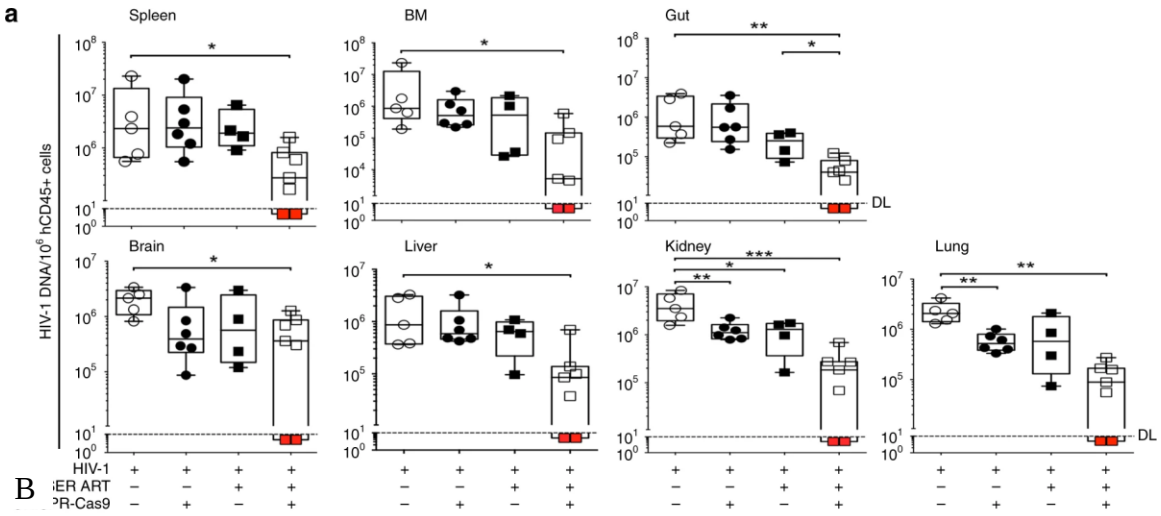
a
Spleen
BM
Gut
Brain
Liver
Kidney
Lung
HIV-1 DNA/10^6 hCD45+ cells
DL
HIV-1
LASER ART
CRISPR-Cas9

B

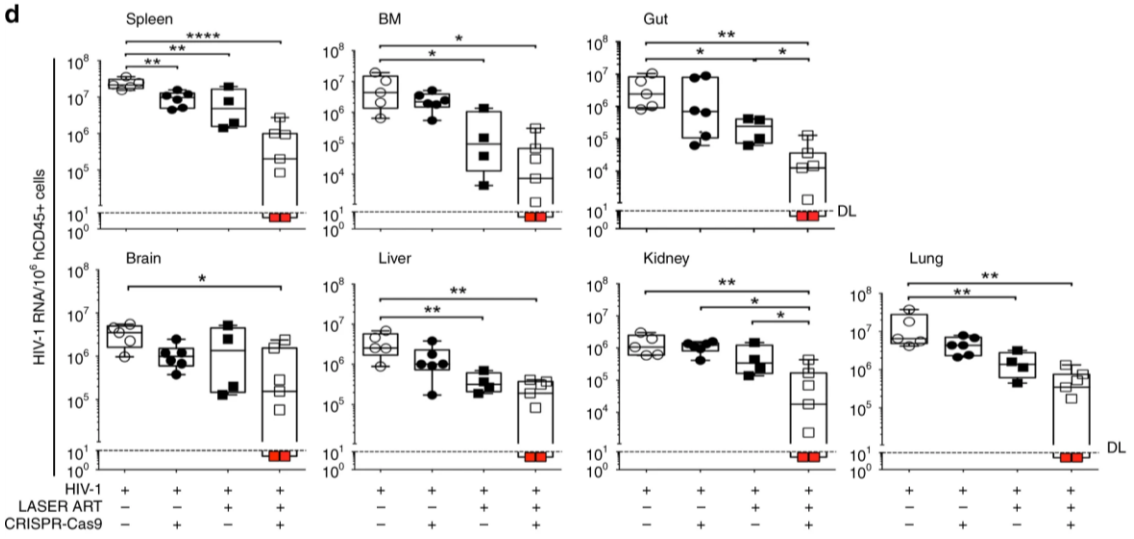
d
Spleen
BM
Gut
Brain
Liver
Kidney
Lung
HIV-1 RNA/10^6 hCD45+ cells
DL
HIV-1
LASER ART
CRISPR-Cas9

Figure 3. 2 Tissue HIV-1 DNA and RNA in HIV-1 infected and treated humanized mice.

(A) HIV-1 DNA and **(B)** HIV-1 RNA were extracted from humanized mouse spleen, bone marrow, gut, brain, liver, kidney, and lung and subjected to semi-nested qPCR assays. HIV-1 DNA and RNA levels of individual animal were listed and expressed as total HIV-1 DNA **(A)** and HIV-1 RNA **(B)** copies/10^6 human CD45+ cells. Two animals from dual treatment group, M4346 and M4349 showed absence of HIV-1 DNA and RNA in all the tissues (shown as red squares below the detection limit of 10 viral copies). One-way ANOVA and Bonferroni's post-hoc tests were used to compare multiple groups. *$P < 0.05$, **$P < 0.01$, ***$P < 0.001$, ****$P < 0.0001$.

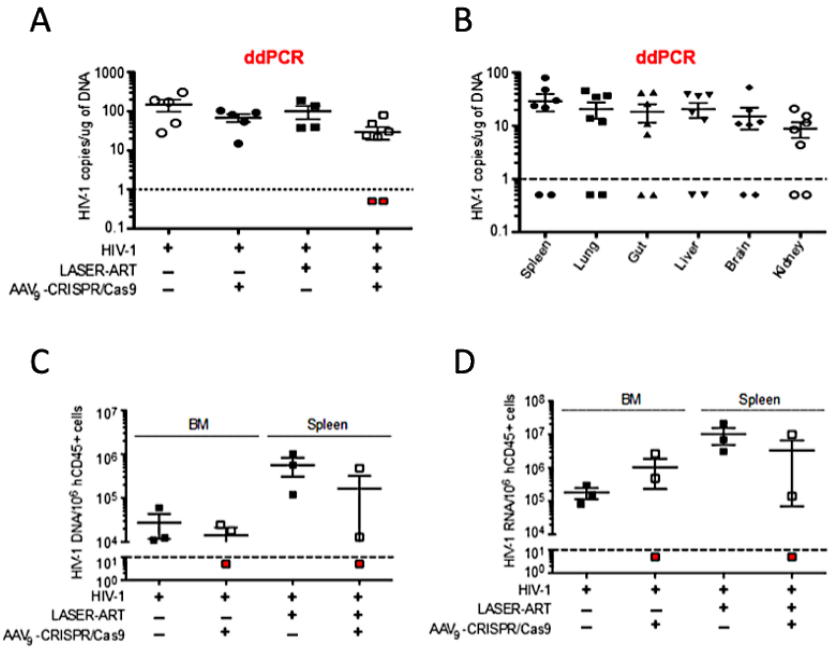

Figure 3. 3 Confirmation of HIV-1 absence from sterilized humanized mice by ddPCR and *in vitro* viral outgrowth assay.

ddPCR was applied to detect low level of HIV-1 DNA in spleen of humanized mice of all 4 groups **(A)** and various organs of the dual-treated animals **(B)**. M4346 and M4349 showed no sign of HIV-1 replication presented as dots below the detection limit of 2 viral copies. Data were expressed as the mean ± SEM. Bone marrow (BM) cells and splenocytes were isolated from humanized mice from different groups and co-cultivated with PHA/IL-2 stimulated human PBMCs. Cells were harvested after 14 days of co-culture and analyzed for cell-associated HIV-1 DNA **(C)** and HIV-1 RNA **(D).** Virus failed to be recovered from M4349 (M4346 was not tested due to sample unavailability) but able to be recovered from all other tested animals. Data are expressed as viral copies/10^6 human CD45+ cells and presented as the mean ± SEM.

and CRISPR-Cas9, we conducted a replicate study using a macrophage tropic viral strain (HIV-1_{ADA}) infected humanized mice **(Figure 3.4A).** Animals were infected with 10^4 $TCID_{50}$ of HIV-1_{ADA} for two weeks when plasma HIV-1 RNA was readily detected at a median level of 8.4 x10^4 copies/ml **(Figure 3.4C).** Peripheral CD4+ T cells did not show significant change at this point **(Figure 3.4B).** Infected animals were randomly divided into two groups, the HIV-1 control group (n = 4) and the dual-treatment group receiving sequential administration of LASER ART and CRISPR-Cas9 (n = 6). Animals were monitored for 9 weeks after cessation of LASER ART which equaled to 8 weeks after single injection of CRISPR-Cas9 before sacrifice. Continuous viral replication was observed in untreated animals alongside with decreased peripheral CD4+ T cell level to 48.3 ± 4.5%. In contrast, peripheral CD4+ T cells were well preserved in dual-treated animals at 71.3 ± 3.5%. Notably, 3/6 animals that received LASER ART and CRISPR-Cas9 demonstrated no viral rebound **(Figure 3.4C).** Tissue HIV-1 amplification was determined by semi-nested qPCR **(Figure 3.4D).** Notably, out of 3 animals that were negative in the peripheral only 2 animals remained negative across multiple tissues while 1 animal presented active tissue viral replication. This emphasized the important role of tissue HIV-1 sanctuary even under efficient treatment.

To further confirm a complete HIV-1 elimination from humanized mice. We applied in vivo viral outgrowth assay (VOA) by adoptively transferring animal splenocytes and BM cells from all 4 groups into naïve humanized mice. This murine-based VOA has been proved to be more sensitive than cell culture-based VOA on evaluating HIV-1 latency (181). To this end, splenocytes and BM from 2 animals from HIV-1 control groups, 1 animal from LASER ART alone group, and 5 animals from dual treatment group (including

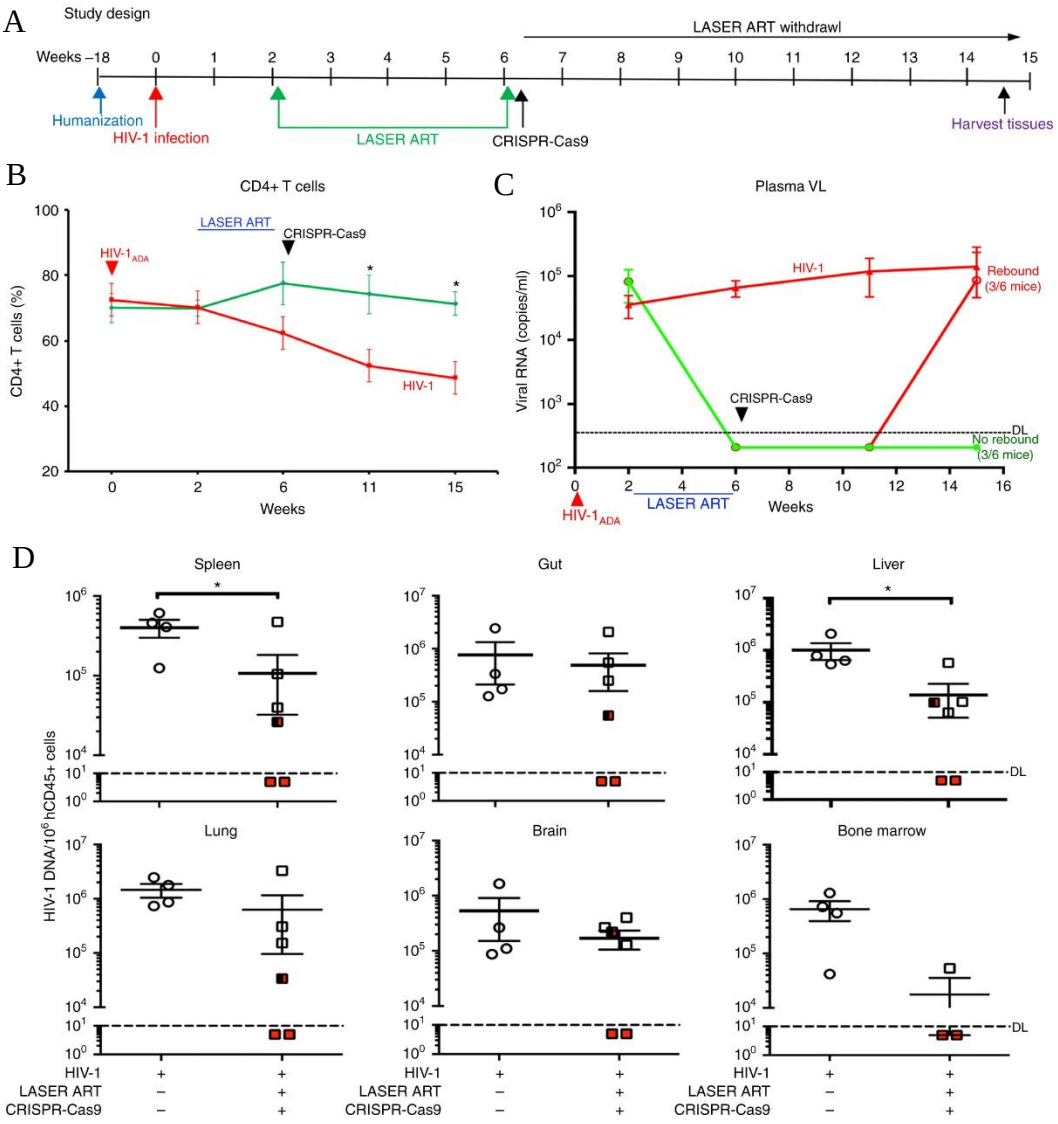
A
Study design
LASER ART withdrawl
Weeks –18 0 1 2 3 4 5 6 7 8 9 10 11 12 13 14 15
Humanization
HIV-1 infection
LASER ART
CRISPR-Cas9
Harvest tissues
B
CD4+ T cells
LASER ART
CRISPR-Cas9
HIV-1ADA
CD4+ T cells (%)
HIV-1
Weeks
C
Plasma VL
HIV-1
Rebound (3/6 mice)
CRISPR-Cas9
DL
No rebound (3/6 mice)
Viral RNA (copies/ml)
HIV-1ADA
LASER ART
Weeks
D
Spleen
Gut
Liver
Lung
Brain
Bone marrow
HIV-1 DNA/10^6 hCD45+ cells
DL
HIV-1
LASER ART
CRISPR-Cas9

Figure 3. 4 Validation of HIV-1 elimination in humanized mice treated with LASER ART and CRISPR-Cas9.

(A) Replication study was designed. **(B)** Peripheral human CD4+ T cells and **(C)** plasma viral loads were monitored throughout the study. Plasma HIV-1 RNA in dual-treated animals was suppressed to undetectable levels after LASER ART was initiated. After treatment interruption, 3 animals experienced viral rebound (green to red) and 3 remained negative (green). **(D)** Tissue HIV-1 DNA was determined by semi-nested qPCR assays and data were expressed as total HIV-1 DNA copies/10^6 human CD45+ cells. In dual-treated animals, M3319 and M3336 remained tissue viral negative consistent with negative plasma viral load (shown in red squares). In M3324 which presented negative plasma viral load, tissue HIV-1 replication was positive (shown in half-red-half-black square). Data were expressed as mean ± SEM with the detection limit at 10 viral copies.

2 potential ‘cured’ animals) were engrafted into 16 uninfected humanized mice (8 for splenocytes transplant and 8 for BM transplant). Recipient animals were maintained for 30 days to observe HIV-1 recovery. Two BM recipients died at study end while the rest remained healthy. Animals that received splenocytes or BM from M3319 and M3336 failed to recover HIV-1 according to viral assessment from both peripheral and tissue systems. In contrast, HIV-1 was detected in animals engrafted from all other donors including M3324 **(Figure 3.5).** This result demonstrated that HIV-1 was completed eradicated from M3319 and M3336.

3.4.6 Improved efficacy of HIV-1 sterilization through sequential LASER ART and dual AAV9-CRISPR-Cas9 treatments of infected humanized mice

The β-chemokine receptor type 5 (CCR5) is a major coreceptor that mediates macrophage-tropic HIV-1 entry of immune cells (182, 183). About 1% of European possess a 32-base-pair deletion in the CCR5 coding region (CCR5Δ32) that render them resistance to CCR5-tropic HIV-1 infection (184, 185). More importantly, to date, the only two cases of HIV-1 cure were achieved through allogeneic stem cell transplantation from CCR5Δ32 donors (47, 48). While bone marrow transplantation is highly risky and cannot be introduced as a regular therapy, genomic edition of CCR5 has therefore become a promising strategy for HIV-1 eradication. The first clinical trial employed zinc finger nucleases (ZFNs) to modify CCR5 on autologous CD4+ T cells and refused them back to patients. The study proved the safety of this procedure and modified CD4+ T cells showed resistance to viral infection and sustained for a long period of time in participants (103). *In vitro* modification of primary T cells, hematopoietic stem cells (HSCs), or induced pluripotent stem cells (iPSCs) by ZFNs or CRISPR-Cas9 showed successful CCR5

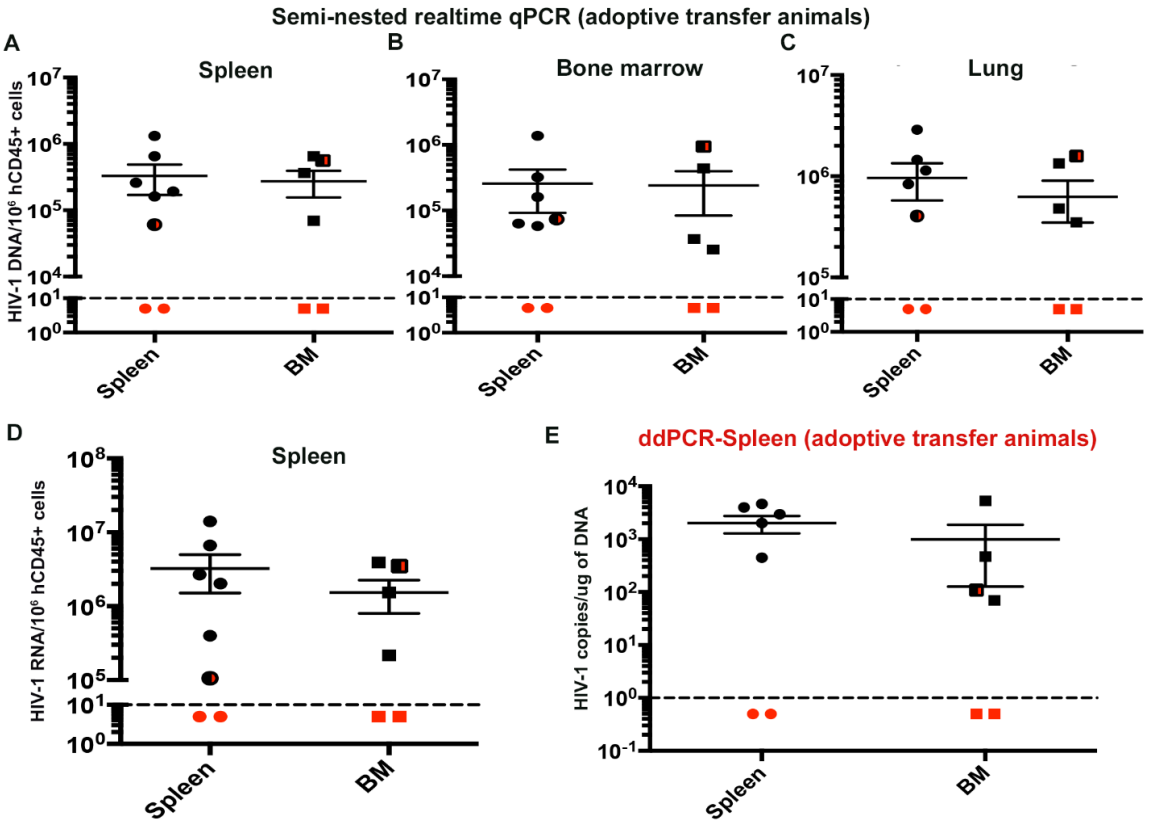
Semi-nested realtime qPCR (adoptive transfer animals)
A
Spleen
B
Bone marrow
C
Lung
HIV-1 DNA/10⁶ hCD45+ cells
Spleen
BM
D
Spleen
HIV-1 RNA/10⁶ hCD45+ cells
E
ddPCR-Spleen (adoptive transfer animals)
HIV-1 copies/ug of DNA

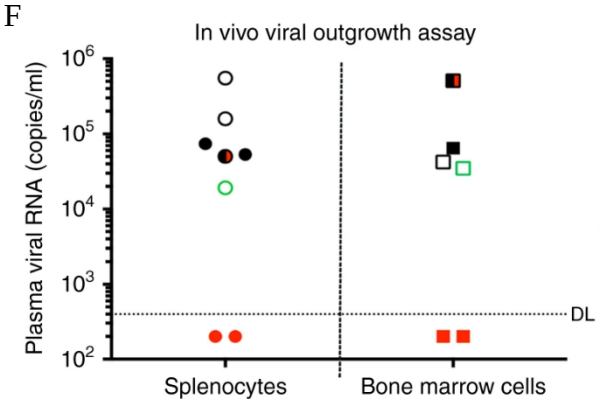
F
In vivo viral outgrowth assay
Plasma viral RNA (copies/ml)
DL
Splenocytes
Bone marrow cells

Figure 3. 5 Confirmation of HIV-1 elimination from humanized mice using muring-based viral outgrowth assay.

At animal sacrifice, splenocytes and BM cells were isolated from donor animals from HIV-1 control, LASER ART alone, and dual-treatment groups. Splenocytes and BM were separately adoptive transferred into naïve humanized mice for viral recovery. The recipient animals were sacrificed at 30 days after engraftment with viral levels measured for HIV-1 DNA in **(A)** spleen, **(B)** BM, and **(C)** lung, and **(D)** HIV-1 RNA in spleen using semi-nested qPCR with the detection limit of 10 viral copies. **(E)** Recipient spleen HIV-1 DNA was also evaluated using ddPCR with the detection limit of 2 viral copies. **(F)** Plasma HIV-1 RNA was analyzed using COBAS Ampliprep-Taqman-48 V2.0 assay with a sensitivity of 200 copies/ml. In all the tests, virus was not detected in recipient animals engrafted from M3319 and M3336 as shown in red square. HIV-1 can be detected in all other recipient animals adoptively transferred from other donors including M3324 that showed negative plasma viral load but positive tissues viral replication (as shown in half-red-half-black square). The green dots in **(F)** indicates plasma viral load of recipients engrafted from the LASER ART alone donor.

disruption and conferred HIV-1 resistance in humanized mice (104, 105, 186). By far, direct administration of CRISPR-Cas9 targeting CCR5 *in vivo* has not been tested. To this end, we evaluated a sequential LASER and dual CRISPR-Cas9 system (one targets HIV-1 LTR and Gag and the other targets human CCR5) in eradication of HIV-1 from infected humanized mice. Similar to previous study design, we deployed a total of 28 hu-HSC reconstituted NSG mice and infected them with 10^4 $TCID_{50}$ of $HIV\text{-}1_{ADA}$ for two weeks **(Figure 3.6A).** At this point, there was no significant change of peripheral CD4+ T-cells **(Figure 3.6B).** Plasma VL was readily established in all animals at a mean 1.8 x 10^4 HIV-1 RNA copies/ml **(Figure 3.6C).** Animals were then randomly distributed into four groups. The first group (n = 7) of mice were left untreated (HIV-1 control), the second group (n = 7) received dual intravenous (IV) injection of CRISPR-Cas9 (one AAV_6-CRISPR-Cas9 targeting CCR5 and the other AAV_9-CRISPR-Cas9 targeting HIV-1 LTR and Gag), both at 10^{12} GC (genome copy) units, with a volume of 50 µl each; the third group (n = 4) were administered LASER ART as previously that consisted of 45 mg/kg parent drug equivalents of NRP and myristoylated DTG, and 40 mg/kg parent drug equivalents of myristoylated 3TC and ABC nanoparticles by intramuscular (IM) injection. A fourth group (n = 10) received LASER ART followed by two CRISPR-Cas9 injections. After LASER ART was initiated, plasma VL was rapidly decreased until undetectable levels in animals from groups 3 and 4. Plasma VL continued to elevate from groups 1 and 2 animals **(Figure 3.6C).** Correspondingly, peripheral CD4+ T cells remained protected in animals from groups 3 and 4 but decreased in groups 1 and 2 **(Figure 3.6B).** Six weeks following the last administration of LASER ART and four weeks after the second CRISPR-Cas9 treatment, HIV-1 rebounded in 1 out of 10 dual-treated animals but remained negative

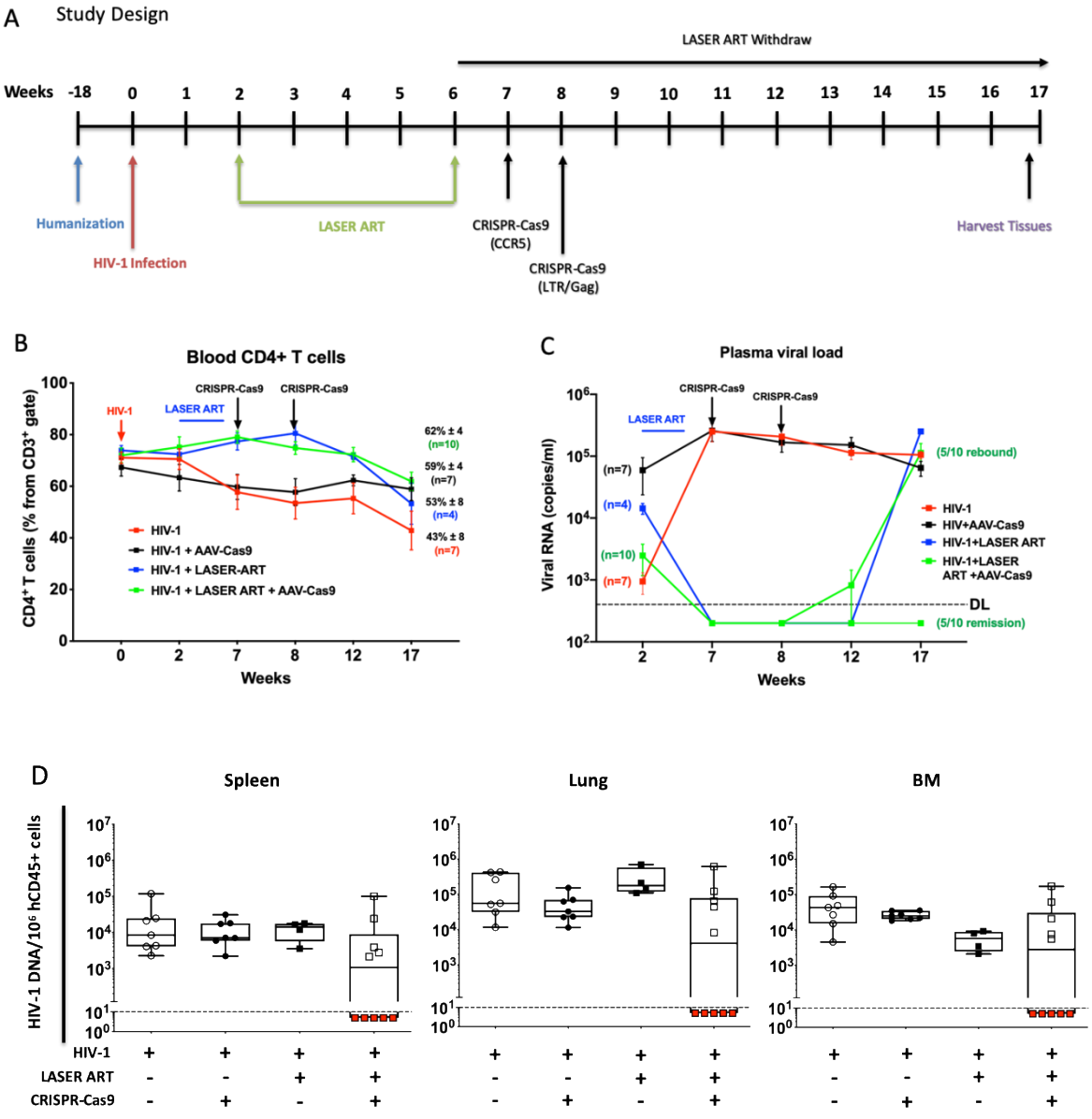
A
Study Design
LASER ART Withdraw
Weeks -18 0 1 2 3 4 5 6 7 8 9 10 11 12 13 14 15 16 17
Humanization
HIV-1 Infection
LASER ART
CRISPR-Cas9 (CCR5)
CRISPR-Cas9 (LTR/Gag)
Harvest Tissues
B
Blood CD4+ T cells
CD4+ T cells (% from CD3+ gate)
HIV-1
LASER ART
CRISPR-Cas9
CRISPR-Cas9
62% ± 4 (n=10)
59% ± 4 (n=7)
53% ± 8 (n=4)
43% ± 8 (n=7)
HIV-1
HIV-1 + AAV-Cas9
HIV-1 + LASER-ART
HIV-1 + LASER ART + AAV-Cas9
Weeks
C
Plasma viral load
Viral RNA (copies/ml)
LASER ART
CRISPR-Cas9
CRISPR-Cas9
(n=7)
(n=4)
(n=10)
(n=7)
(5/10 rebound)
HIV-1
HIV+AAV-Cas9
HIV-1+LASER ART
HIV-1+LASER ART +AAV-Cas9
DL
(5/10 remission)
Weeks
D
Spleen
Lung
BM
HIV-1 DNA/10^6 hCD45+ cells
HIV-1
LASER ART
CRISPR-Cas9

Figure 3. 6 Plasma viral load, peripheral CD4+ T cells, and tissue HIV-1 DNA in infected and treated humanized mice.

Mice were infected with 10^4 $TCID_{50}$ of $HIV\text{-}1_{ADA}$ followed by treatments with LASER ART, dual CRISPR-Cas9 or both. **(A)** The study scheme shows the times of infection and treatments. After confirmation of viral infection, 28 infected humanized mice were subdivided into four groups. The first group (n = 7, red) were left untreated (control); the second group (n = 7, black) received two individual intravenous (IV) dose of CRISPR-Cas9 targeting human CCR5 and HIV-1 LTR/Gaga (10^{12} units each), respectively, at seven and eight weeks after viral infection, respectively; the third group (n = 4, blue) were administered LASER ART (NMDTG and NRPV at 45 mg/kg and NMABC and NM3TC at 40 mg/mg) by intramuscular (IM) injection two weeks after viral infection, the fourth (n = 10, green) were given LASER ART (as in group 3) followed with 2 IV injection CRISPR-Cas9 (as in group 2). At 17 weeks after infection, which was equivalent to 10 weeks after LASER ART intervention and 9 weeks after second dose of CRISPR-Cas9, animals were sacrificed to evaluate viral rebound. **(B)** Dynamic changes of peripheral human CD4+ T cells from all the animals were measured by flow cytometry. **(C)** Dynamic changes of plasma VL from all the animals were determined by the COBAS Ampliprep-Taqman-48 V2.0 assay with a sensitivity of 200 copies/ml once adjusted to the plasma dilution factor. Viral RNA rebound was observed at the study end in all 4 LASER ART alone treated animals. In dual treated animals HIV-1 rebound was observed in 5 out of 10 animals but not from the other 5 animals. **(D)** HIV-1 DNA from spleen, lung, and BM of all the animals were evaluated by ultrasensitive semi-nested real-time qPCR assays. The individual dot represents each of the animals from four groups. The data are expressed as total HIV-1 DNA copies/10^6 human CD45+ cells. In dual treated animals, HIV-1 DNA was below the detection limit in 5 out of 10 animals (shown by the red squares below the dashed lines), which was considered sterilization of virus.

in the rest of dual-treated animals and all 4 animals receiving LASER ART alone. Eleven weeks after LASER ART interruption, another 4 dual-treated animals making it a total 5 out of 10 (50%) animals viral rebound was observed while the other 5 out of 10 (50%) remained undetected. In contrast, all 4 animals that were treated with LASER ART alone experienced viral rebound. Animals remained readily infected in group 1 and 2 **(Figure 3.6C).** As HIV-1 came back, peripheral CD4+ T cells continued to drop in all the groups with a mean level of 43% ± 8, 59% ± 4, 53% ± 8, and 62% ± 4 at sacrifice from group 1 to4, respectively **(Figure 3.6B).** Viral clearance was further determined in animal tissues tested (spleen, lung, and BM), HIV-1 DNA was absent in the 5 animals that showed negative plasma VL but was detected in all other animals **(Figure 3.6D).** Further confirmation of HIV-1 eradication from these animals is ongoing including viral assessment from other tissue types (brain, gut, liver, kidney, and lymph nodes) as well as viral recovery using humanized mice based viral outgrowth assay as previously described.

3.5 Discussion

Although considerable progress has been made during the thirty-six years of HIV-1 research, this once lethal pathogen can be well managed under effective ART while an HIV-1 ‘cure’ has not been realized. The major barrier to HIV-1 eradication lies on the broad cellular and tissue viral reservoirs that are resistant to ART and other immune surveillance. It is commonly accepted that a complete HIV-1 cure cannot be achieved until all viral reservoirs are cleared. Researchers have employed different strategies targeting HIV-1 latency including early ART intervention, latency reversal agents, immune enhancers, broadly neutralizing antibodies. However, thus far, successful HIV-1

eradication has only been realized in 2 patients who received aggressive bone marrow transplant. The difficulties of eliminating HIV-1 reservoirs are attributed to multiple factors including lack of proper animal models, insufficient ART penetration, inadequate latency reverse, incompetent CTL function, inability of targeting integrated proviral DNA, and viral mutation. To partially overcome these challenges, we first adopted human CD34+ HSC-reconstituted mice where both myeloid and lymphoid lineages human immune cells can be established (43, 116, 120, 132, 171-173, 187-189). Indeed, our lab as well as other labs have applied these mice models to study HIV-1 pathogenesis, immunology, therapy, and eradication that significantly extend our understanding of this disease (43-45, 116, 173, 190). The longevity of these humanized mice with consistent human cell levels allow longitudinal studies of viral and host interaction and evaluate the effects of therapeutic intervention in a long life span (44, 45, 161, 162, 164, 191-193). Therefore, in the current study we employed this mouse model to investigate a combinational strategy for potential HIV-1 eradication (44, 45, 161, 164, 192, 194, 195). In addition, from previous study, we identified acute HIV-1 infection pattern in this mouse model and demonstrated that by 2 weeks HIV-1 infection is readily established in both peripheral and tissue system (196). Based on this discovery, we elected day 14 as the time point to start ART intervention.

The second factor that may lead to the success of HIV-1 elimination in the present study is LASER ART. Compared to conventional ART, LASER ART was designed to improve hydrophobicity and lipophilicity that can establish drug depots in tissue-residing macrophages to enhance drug sustention and tissue penetration (163, 164, 189, 197-202). In this manner, LASER ART has shown superior tissue concentrations and inhibition of HIV-1 replication in a longer period of time compared to conventional ART. This will

further limit the size of HIV-1 reservoir which provides optimal setting for subsequent proviral excision (116, 164, 190). Next, gene editing was employed to overcome the major limitation of LASER ART that none of current ART targets integrated HIV-1 genome in the host. To this end, we selected CRISPR-Cas9 and employed a dual-gRNA system that target conserved HIV-1 LTR and Gag sequences. In this manner, Cas9 endonuclease is able to cleave the entire viral genome from host genome. Indeed, from both cell culture and animal model of HIV-1 infection, the entire removal of viral sequence was achieved while viral production was mitigated (165, 168). Notably, CRISPR-Cas9 alone was not able to eliminate HIV-1 infection which may result from outnumbered virus and less efficient delivery method. This can be compensated by LASER ART which limits required targets and therefore works in synergy with CRISPR-Cas9 to eliminate HIV-1 infection.

In the current report, we proved that HIV-1 eradication is possible using a combinational strategy of sequential administration of LASER ART and CRISPR-Cas9. This was achieved and successfully repeated in two independent studies. Interestingly, from both experiments, HIV-1 was eliminated from up to one third of animals that received dual treatment. A complete viral sterilization was exhaustively tested by long-term treatment interruption, plasma viral load, sensitive semi-nested qPCR, ddPCR, RNAscope, and *in vitro* and *in vivo* VOA. Notably, in one animal that showed negative plasma viral load, tissue HIV-1 tests were positive and subsequent adoptive transfer demonstrated that the virus were replication-competent. This emphasizes tissue HIV-1 replication could be more resistant to treatment and contribute to viral rebound after ART is discontinued. This may explain the failure of viral control in patients that stopped ART even when peripheral HIV-1 was below the detection limit.

In summary, for the first time, we achieved a complete HIV-1 eradication from infected animal model which was likely attributed to a combination of factors evolving a suitable animal model, low viral set points, enhanced ART (LASER ART) with better viral control and latency target, and precise excision of viral sequence by CRISPR-Cas9. We posit that this could be a pathway leading to eventual HIV-1 eradication. Every modification on each component of this strategy may further improve the viral 'cure rate'. We believe this proof-of-concept study will open new doors to HIV-1 eradication.

Chapter 4 Amplification of Replication Competent HIV-1 by Adoptive Transfer of Human Cells from Tissues of Infected Humanized mice

4.1 Abstract

Detection of latent human immunodeficiency virus type one (HIV-1) in infectious viral reservoirs during antiretroviral therapy (ART) is a requirement for viral elimination. Such detection schemes require sensitive assays that require induction of replication competent virus in infectious tissue compartments. While viral outgrowth assays have, in part, filled such a need they are insensitive and often fail to detect low-levels of replication competent virus. To overcome this limitation, we used naïve humanized mice transplanted with hematopoietic stem cells (hu-HSC) as recipients for adoptive transfer of infected human donor cells. Viral recovery was then measured from transfers of HIV-1 infected humanized mouse splenocytes and bone marrow cells infected in vivo and treated with or without ART and ART and CRISPR/Cas9. The latter of which resulted in a subset of virus sterilized "cured" animals. In each but the "cured" mice replication competent HIV-1 was readily detected in all recipient animals. We demonstrate here that adoptive transfer of cells between humanized mice is a sensitive assay system to interrogate replication competent HIV-1.

4.2 Introduction

Antiretroviral therapy (ART) has transformed human immunodeficiency virus type one (HIV-1) infection from a life-threatening disease into a life-long chronic condition. Though ART maintains viral suppression and preserves immune function it demands strict regimen adherence with associated stigmas, costs and inherent drug toxicities. Therefore, complete HIV-1 sterilization is the best means to end the epidemic (157). Now after almost 40 years since the discovery of HIV-1, viral cure has been reported in only two cases (48,

116). The major barrier to achieve more wide spread "cure" rests in the ability of HIV-1 to sustain latency. Throughout the course of disease and during treatment, a small cell population, $1/10^6$ resting CD4+ T cells contains replication-competent dormant HIV-1 DNA that after activation leads to full blown viral growth (203). While active research efforts have pursued elimination strategies for this HIV-1 latent reservoir there are few sensitive, precise and practical methods to measure the size, location and distribution of such viral compartments (176, 204-206). For the most part viral detection requires viral nucleic acid amplification or cell co-cultures (207, 208). While the former readily amplify virus, the test fails to differentiate intact from defective provirus (209). In this way it commonly overestimates the size of the viral reservoir. Thus, even considering sensitivity limitations, cell co-culture assays. based on quantitative viral outgrowth (qVOA) remain the gold standard for measures of latent HIV-1 (210). While the qVOA detects < 1% of total proviruses induced after activation, additional virus in infectious reservoirs may only be awaken by repetitive stimulations (67, 211). Therefore, qVOA underestimate the true viral reservoir size. This has led to the use of animal adoptive transfers for viral recovery. Since naturally HIV-1 exclusively infects humans and chimpanzees, immunodeficient mice have been used as alternative to recover replication competent virus (43-45, 196, 212) and coined as a "mouse viral outgrowth assay (mVOA). The assay was used previously to quantify HIV-1 reservoirs from viral suppressed donors (181, 213, 214). After transplant with million(s) of human unfractionated peripheral blood mononuclear cells or CD4+ T cells, HIV-1 can be successfully recovered. In the current report we employed human CD34+ cord blood HSC-reconstituted NOD.Cg-Prkdc^{scid}IL2rg^{tm1Wjl}/SzJ mice as donors for adoptive transfer. Interestingly, in donors where animals showed undetectable peripheral

viral load (VL), tissue HIV-1 was readily detected. This humanized mouse-to-mouse VOA assays demonstrate that adoptive transfer between humanized mice can thus be used to interrogate HIV-1 in models of human disease.

4.3 Materials and Methods

4.3.1 Generation, HIV-1 infection and treatment of humanized mice

NSG mice were purchased from the Jackson Laboratory (Bar Harbor, ME) and bred under pathogen-free conditions in compliance with ethical guidelines required by the National Institutes of Health and the University of Nebraska Medical Center. All experimental protocols were approved by the University of Nebraska Medical Center Institutional Animal Care and Use Committee. All animal studies were performed according to UNMC institutional policies and the National Institutes of Health guidelines.

Human CD34+ HSCs were enriched from umbilical cord blood using immunomagnetic beads according to manufacturer instructions (CD34+ selection kit, Miltenyi Biotec Inc., Auburn, CA). Hu-HSC mice were generated by intrahepatic injection of human CD34+ HSCs into new-born NSG pups that received 1Gy of irradiation (RS 2000 X-ray Irradiator, Rad Source Technologies, Buford, GA,) (120, 188). Human cell reconstitution was monitored monthly for 5-6 months by flow cytometry (**Figure 4.1A**) (116). At 20 to 24 weeks of age, hu-HSC mice following affirmation of human cell reconstitution were intraperitoneally infected with HIV-1_{NL4-3} (215) or HIV-1_{ADA} (216). Both viruses were administered at 10^4 tissue culture infection $dose_{50}$ ($TCID_{50}$)/animal (see **Table 4.1**). Viral infection was confirmed at week 2 by peripheral HIV-1 RNA assays (automated COBAS Ampliprep System V2.0/Taqman-48 system, Roche Molecular

Diagnostics, Basel, Switzerland) according to the manufacturer's instructions. Hu-HSC mice were then randomly distributed into 4 groups (109). Group 1, HIV-1 infectious control; Group 2, HIV-1 and a single intravenous injection of AAV_9-CRISPR/Cas9 (165); Group 3, HIV-1 plus intramuscular administration of dolutegravir (DTG), rilpivirine (RPV), lamivudine (3TC), and abacavir (ABC) as a long acting slow effective release ART regimen (44, 109, 161, 162) and Group 4, HIV-1 and sequential LASER ART and AAV_9-CRISPR-Cas9. At 8 weeks after a final CRISPR-Cas9 injection or 9 weeks after LASER ART ceased (109), donor hu-HSC mice were sacrificed and analyzed for immune profiles and viral infection. Splenocytes and bone marrow (BM) cells were isolated from donor animals and assessed for cell viability by trypan blue and live/dead stains. The TC-20 automated cell counter (Bio-Rad, Hercules, CA) assayed viable cells were subsequently resuspended in cold sterile phosphate buffered saline (PBS) (GE healthcare life sciences, Logan, UT) then used without delay for adoptive transfer.

4.3.2 Adoptive transfer

Naïve recipient hu-HSC mice with sustained levels of human cell reconstitution were selected for allograft as previously reported (132, 172, 196). Adoptive transfers were made by intraperitoneal injection of donor splenocytes or BM cells into recipient animals (**Table 4.2**). To preclude loss of human cell numbers in virus suppressed animals' mixtures of mouse and human cells were isolated together from donor humanized mice. One month after engraftment, recipient mice were sacrificed and examined for viral presence.

4.3.3 Flow cytometry

Peripheral blood was collected from facial vein for routine monitoring or cardiac puncture at animal sacrifice. Blood was collected in ethylenediaminetetraacetic acid (EDTA)-coated tubes and incubated with pan-human monoclonal antibodies to CD45, CD3, CD19, CD4, and CD8 (BD Pharmingen, San Diego, CA). Flow cytometry was operated on BD LSRII (BD Immunocytometry Systems, Mountain View, CA) system and data were analyzed using FlowJo software (BD Pharmingen, San Diego, CA).

4.3.4 Tissue nucleic acid extraction and viral quantification

Animal tissues (brain, lung, liver, spleen, BM, gut and kidney) were collected and homogenized by Qiagen Tissue Lyser II (QIAGEN, Hilden, Germany). Total cellular DNA and RNA were extracted using Qiagen All Prep DNA/RNA Mini Kit (QIAGEN, Hilden, Germany). Tissue HIV-1 RNA was reverse transcribed to complementary DNA using Thermo-Fisher Scientific Verso cDNA Synthesis Kit (Invitrogen, MA). HIV-1 DNA and RNA were quantified by semi-nested real-time PCR as previously described (121). HIV-1 DNA isolated from serial dilutions of ACH-2 cell line was adopted as standard positive control. The detection limit is below 10 viral copies. Human CD45 (Hs0036534_g1) and mouse GAPDH (Mm99999915_g1) sequences were applied as reference genes from Thermo-Fisher Scientific.

4.3.5 Immunohistochemistry

Tissue samples were collected and fixed with 4% paraformaldehyde for 24h then processed followed by paraffin embedding. Five-micron thick tissue sections were collected and immuno-stained with mouse monoclonal antibodies against human HLA-

DQ/DP/DR (clone CR3/43, 1:100, DAKO, Carpinteria, CA) and HIV-1 p24 (1:10, DAKO, Carpinteria, CA). The polymer-based horse radish peroxidase (HRP) and 3,3′-Diaminobenzidine (DAB) DAKO EnVision system was used for staining development. The nuclei were counterstained with Mayer's hematoxylin (116). Images were acquired with a Nuance EX camera fixed to a Nikon Eclipse E800 microscope using Nuance software (Cambridge Research & Instrumentation, Woburn, MA). Human HLA-DR images were obtained at 20 x magnifications and HIV-1p24 images were captured at 40 x objective magnifications.

4.3.6 Statistical analyses

Data were analyzed using GraphPad Prism 8.0 software (La Jolla, CA) and results were presented as the means ± the standard error of the mean (SEM). The Student's t-test was used for two-group comparison (two-tailed) while a value of $p < 0.05$ was considered statistically significantly different. Association between 2 parameters was conducted using two-tailed Spearman's rank correlations.

4.4 Results

4.4.1 Characterization of donor hu-HSC mice

Eighteen donor humanized mice were used in this study which included 11 males and 7 females (**Table 4.1**). The median age at the completion of the allograft was 37 (34 to 45) weeks. Animals with sustained human cell reconstitution had a mean percentage of human leukocytes that included CD45+ cells of 25.8% ± 3.7, CD3+ cells of 81.8% ± 2.9, CD4+ cells of 58.8% ± 4.5, CD8+ cells of 35.3% ± 4.0 and CD19+ cells at 9.1% ± 2.4 (**Figure 4.1A-B**). The mean CD4/CD8 T cell ratios were 2.6 ± 0.7 (**Figure 4.1C**). No

Table 4. 1 Characteristics of Donor Humanized Mice

Animal ID (n=18)	Sex	Age (weeks)	Peripheral hCD45 (%)	HIV clade	Treatment	Plasma HIV RNA (copies/ml)
3136	F	44	28.3	NL4-3	LASER-ART	42800
3181	M	42	22.9	NL4-3	LASER-ART	632000
3182	M	42	22.1	NL4-3	LASER-ART	324000
3198	M	37	17.9	NL4-3	Dual	181000
3199	M	37	19.1	NL4-3	Dual	1860000
3201	F	37	48.0	NL4-3	Dual	44640
3319	M	36	27.0	ADA	Dual	TND
3322	M	36	20.6	ADA	Dual	400
3324	F	34	77.0	ADA	Dual	TND
3327	M	39	37.8	ADA	Dual	400
3328	M	39	12.9	ADA	LASER-ART	159000
3333	M	34	21.9	ADA	LASER-ART	110000
3336	M	34	13.9	ADA	Dual	TND
3353	M	34	23.0	ADA	Dual	400
3357	F	34	16.5	ADA	/	226000
3359	F	34	14.2	ADA	/	131000
3636	F	45	14.5	ADA	Dual	524000
3637	F	45	26.1	ADA	Dual	178000

Donor hu-HSC mouse ID and sex (F, female; M, male) were listed. Animals were infected with either HIV-1_{NL4-3} or HIV-1_{ADA}, followed with no treatment (/), long acting slow effective release antiretroviral therapy (LASER-ART), or LASER-ART plus CRISPR-Cas9 (Dual). Animals were sacrificed at 8 weeks after CRISPR-Cas9 injection, which equaled to 9 weeks after last dose of LASER-ART, together with untreated animals. Hu-HSC mouse age, peripheral human CD45+ (hCD45+) cell level, and plasma HIV-1 RNA count at sacrifice were summarized. TND, target not detected.

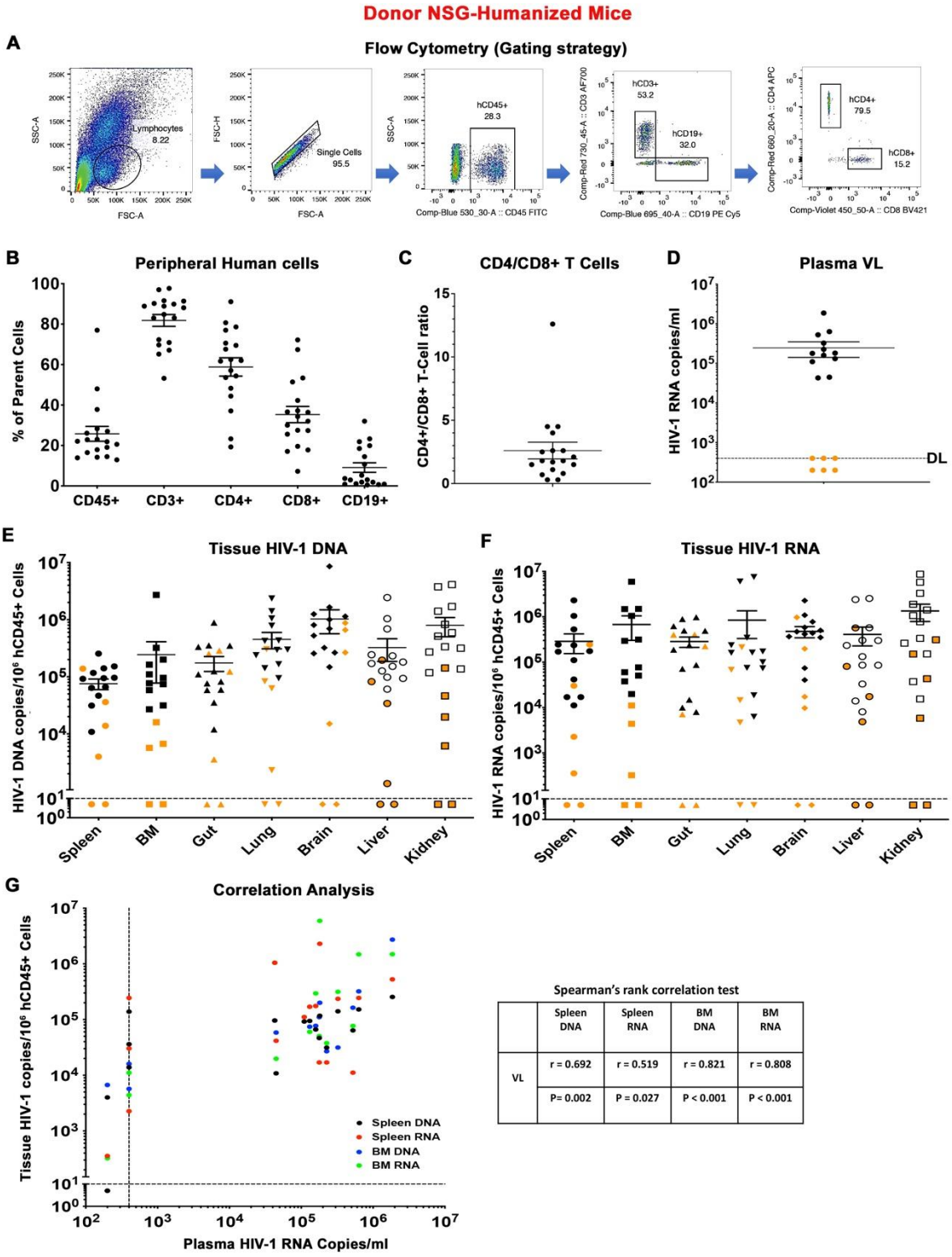

Spearman's rank correlation test

	Spleen DNA	Spleen RNA	BM DNA	BM RNA
VL	r = 0.692	r = 0.519	r = 0.821	r = 0.808
	P= 0.002	P = 0.027	P < 0.001	P < 0.001

Figure 4. 1 Descriptors of donor humanized mice.

(**A**) Flow cytometric gating strategy for human cell reconstitution in NSG-humanized mice. In brief, human cells (hCD45+) were gated from total lymphocytes and single cells and subsequently grouped into human T lymphocytes (hCD3+) and B lymphocytes (hCD19+). Human CD3+ cells were separated into human CD4+ (hCD4+) and CD8+ (hCD8+) T lymphocytes. Detailed immune and viral information of individual animal (n = 18) was presented as scatter dots covering (**B**) peripheral human CD45+, CD3+, CD4+, CD8+, and CD19+ cell levels, (**C**) CD4+/CD8+ T cell ratio, (**D**) plasma viral load (pVL), (**E**) tissue HIV-1 DNA and (**F**) tissue HIV-1 RNA distributed across spleen, BM, gut, lung, brain, liver, and kidney. Data are expressed as mean ± SEM. Orange dots in (**D**) indicated that pVL was at or below the detection limit of 400 HIV-1 RNA copies/ml. Orange dots in (**E**) and (**F**) shows tissue viral levels of animals with minimal or undetected pVL. The detection limit is below 10 HIV-1 copies as measured using semi-nested real time qPCR using HIV specific primers, (**G**) Spearman's rank correlation tests were conducted between humanized mice pVL and respective spleen DNA (black), spleen RNA (red), BM DNA (blue), and BM RNA (green). The Spearman correlation coefficient (r) and p value for each analysis were displayed.

significant differences were observed between male and female donors based on the level of human cell engraftment and CD4/CD8 T cell ratios (**Figure 4.2A-B**). The life span of human cells in humanized mice supports the feasibility of the small animal model for these long-term studies. The mean peripheral viral load of donor humanized mice was 2.5 ± 1.0 x 10^5 HIV-1 RNA copies/ml, out of which 3 animals demonstrated virus at and another 3 animals below the detection limit of detection (**Figure 4.1D**). Sex did not affect plasma viral level (**Figure 4.2C**). Tissue HIV-1 compartments were readily established in donor animals as observed by broad distribution of viral DNA and RNA in spleens, BM, gut-associated lymphoid tissue, lung, brain, liver and kidney (**Figure 4.1E-F**). Notably, of 6 animals that showed plasma viral load at or below the limit of detection only 2 were tissue virus negative. The other 4 animals carried low be readily detectable virus, emphasizing the essential role of virus in tissues serving as sanctuaries not readily observed in peripheral blood. Tissue viral burden did not show significant differences between male and female donors (**Figure 4.2D-E**). To determine the presence of replication-competent virus in tissues, single cell suspensions were isolated from spleen and BM, known reservoir sites in humanized mice. Recovered cells were then adoptively transferred to naïve reconstituted humanized mice to assess levels of viral recovery (**Figure 4.3**). Correlations between donor peripheral viral load and spleen and BM viral burden were recorded (**Figure 4.1G**). Overall, peripheral HIV-1 levels proved to be a viable indicator of tissue viral production. However, tissue virus was observed as the most sensitive and specific measure of virus.

4.4.2 Recipient hu-HSC mice

A total of 28 naïve humanized-NSG mice were employed as recipients (total recipient, TR). The current study used 18 animals that received splenocytes engraftment

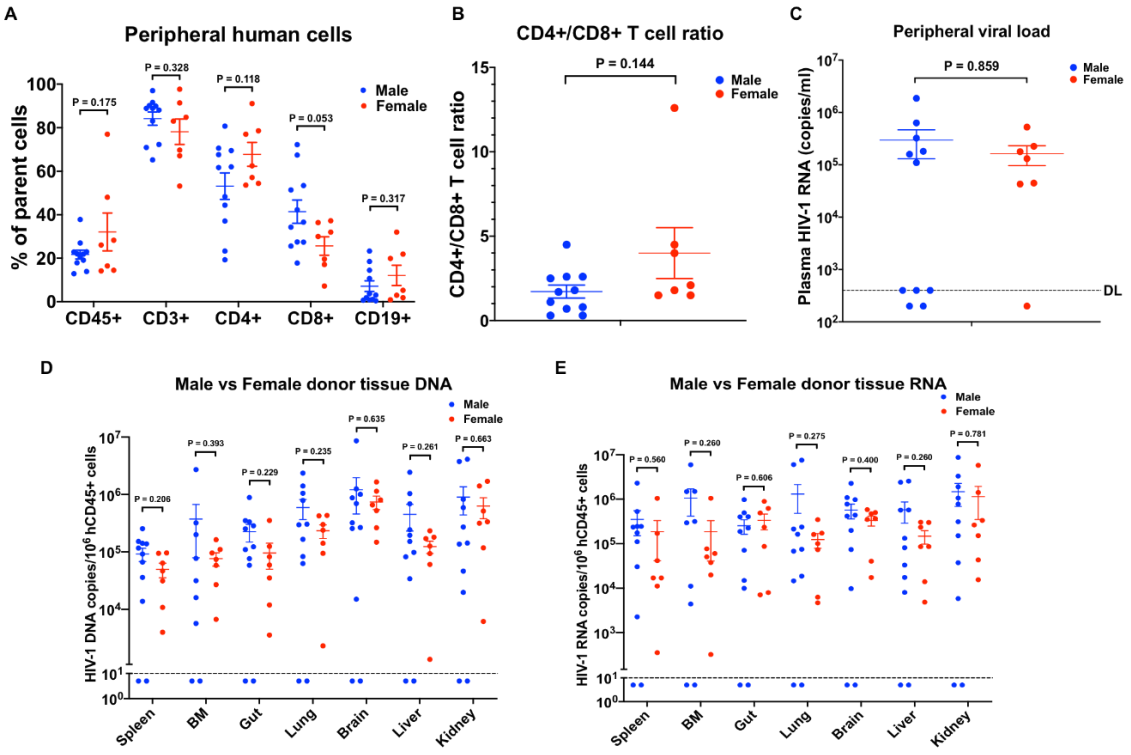

Figure 4. 2 Descriptions of donor humanized mice.

Detailed immune and viral profile of individual donor NSG-humanized mice (n = 18) was displayed as scatter dots according to sex. Male (n = 11, blue) and female (n = 7, red) donors were compared on (**A**) peripheral human CD45+, CD3+, CD4+, CD8+, and CD19+ cell levels, (**B**) CD4+/CD8+ T cell ratio, (**C**) plasma viral load (pVL), (**D**) tissue HIV-1 DNA and (**E**) tissue HIV-1 RNA distributed across spleen, BM, gut, lung, brain, liver, and kidney. Data are expressed as mean ± SEM. The detection limit (DL) of plasma VL is 400 HIV-1 RNA copies/ml. The detection limit of tissue viral analysis is below 10 HIV-1 copies as measure using real time semi-nested qPCR analysis.

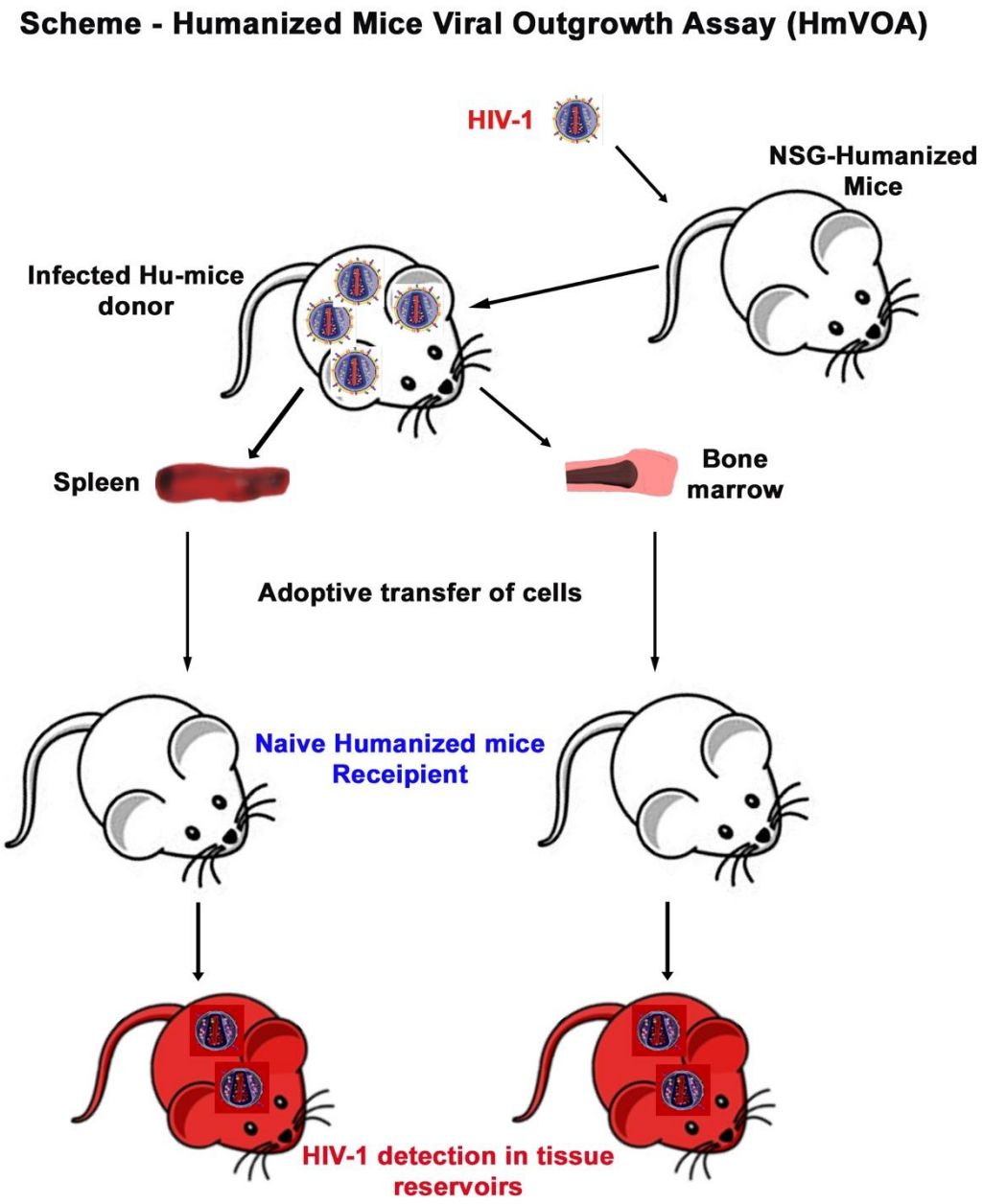

Figure 4. 3 Murine HIV-1 outgrowth assay.

A mixture of mouse and human cells were isolated from donor NSG-humanized mouse spleen or BM and immediately intraperitoneally injected into naïve hu-HSC mice as described in the scheme. Recipient animals were maintained for one month before sacrifice and evaluated for HIV-1 recovery.

(spleen recipient, SR) and 10 animals where BM cells were adoptive transferred (BM recipient, **Figure 4.3** and **Table 4.2**). The median age of TR at allograft was 30 (25~37) weeks with SR at 29.5 (25 to 37) weeks and BR at 30 (29 to 37) weeks. Baseline (pre-engraftment) humanization of individual TR, SR, and BR was shown in **Figure 4.4A-D** (blue dots) and summarized in **Table 4.3**. According to sample availability, donor splenocytes and BM cells contained a mixture of human- and mouse-originated cells. These were extracted and intraperitoneally injected into respective recipient animal. Human cell reconstitution levels across the donor tissues were consistent (**Figure 4.5**). The median viable engrafted cell count was 9.6 (5.1 to 19.8) million for SR and 8.7 (4.3 to 10.7) million for BR (**Table 4.2**). Engraftment was well tolerated by all recipient animals. Four weeks after adoptive transfer, recipient humanized mice were sacrificed and evaluated for HIV-1 recovery. Peripheral human CD45+, CD3+ T cells, and CD19+ B cells were not significantly changed in TR, SR, and BR before and after engraftment. Peripheral CD4+ T cells were significantly decreased in TR, SR, and BR at end point while CD8+ T cells significantly increased (**Figure 4.4A-C** and **Table 4.3**). CD4/CD8 T cell ratios, as a major indicator of immune function and long-term clinical outcomes (217), significantly declined in all recipients (**Figure 4.4D** and **Table 4.3**). HIV-1 was successfully recovered from the majority of allografted humanized mice including those adoptively transferred from donors exhibiting minimal infection (# 3322, 3324, 3327, and 3353), but not in the animals transplanted from ‘virus-free’ donors (# 3319 and 3336) (**Figure 4.4E** and **Table 4.1** and 4.2). There were no significant differences between SR and BR plasma VL (**Figure 4.4E** and **Table 4.3**). Peripheral viral replication was positively correlated with CD4+ T cell loss in TR (calculated as pre- minus post-engraftment CD4+ T cell levels) (**Figure 4.4F**). There

Table 4. 2 Characteristics of Recipient Humanized Mice

Donor ID (n=18)	Spleen recipient ID (n=18)	Sex	Age (weeks)	Peripheral hCD45 before AT (%)	AT live cell counts (million)	End point plasma HIV RNA (copies/ml)	BM recipient ID (n=10)	Sex	Age (weeks)	Peripheral hCD45 before AT (%)	AT live cell counts (million)	End point plasma HIV RNA (copies/ml)
3136	3361	F	25	62.8	16.0	455000	/	/	/	/	/	/
3181	3355	F	25	37.1	12.3	495000	/	/	/	/	/	/
3182	3360	F	25	53.5	14.7	640000	/	/	/	/	/	/
3198	3323	M	27	53.3	12.9	966000	/	/	/	/	/	/
3199	3347	F	25	61.8	12.0	92200	/	/	/	/	/	/
3201	3362	F	25	55.7	19.8	657000	/	/	/	/	/	/
3319	3432	F	31	34.3	6.5	TND	3425	F	30	34.9	7.0	TND
3322	3433	F	31	51.4	9.6	74200	/	/	/	/	/	/
3324	3404	M	29	49.7	12.7	50400	3406	F	29	15.2	10.4	508000
3327	3428	F	33	26.4	5.1	21400	3430	M	33	14.2	10.7	28400
3328	3354	F	37	15.2	6.1	37200	3351	M	37	15.5	10.0	4460
3333	3422	F	30	24.3	9.0	19200	3407	F	30	27.2	5.2	34800
3336	3434	F	31	47	6.5	TND	3388	F	34	18.6	6.0	TND
3353	3435	F	31	25.4	9.0	159000	3416	M	30	39.8	4.3	42400
3357	3409	F	31	24.1	9.5	552000	/	/	/	/	/	/
3359	3410	F	31	9.33	9.6	53400	3411	F	31	28.6	8.3	64800
3636	3912	M	29	30.9	8.9	590000	3913	M	29	35.4	9.8	466000
3637	3914	M	29	28.4	7.3	208000	3905	F	29	42	9.1	157000

The ID of individual recipient hu-HSC mouse and corresponding donor hu-HSC mouse was listed. According to sample availability, a total of 18 hu-HSC mice received splenocytes transplant and 10 hu-HSC mice acquired BM transplant. Sex (F, female; M, male), age, and peripheral human CD45+ (hCD45+) cell levels of recipient animals before adoptive transfer (AT) were summarized. A range of 4.3~19.8 million live cells were engrafted. Recipient hu-HSC mice were maintained for 4 weeks before sacrifice and end point plasma HIV-1 RNA counts were displayed. TND, target not detected.

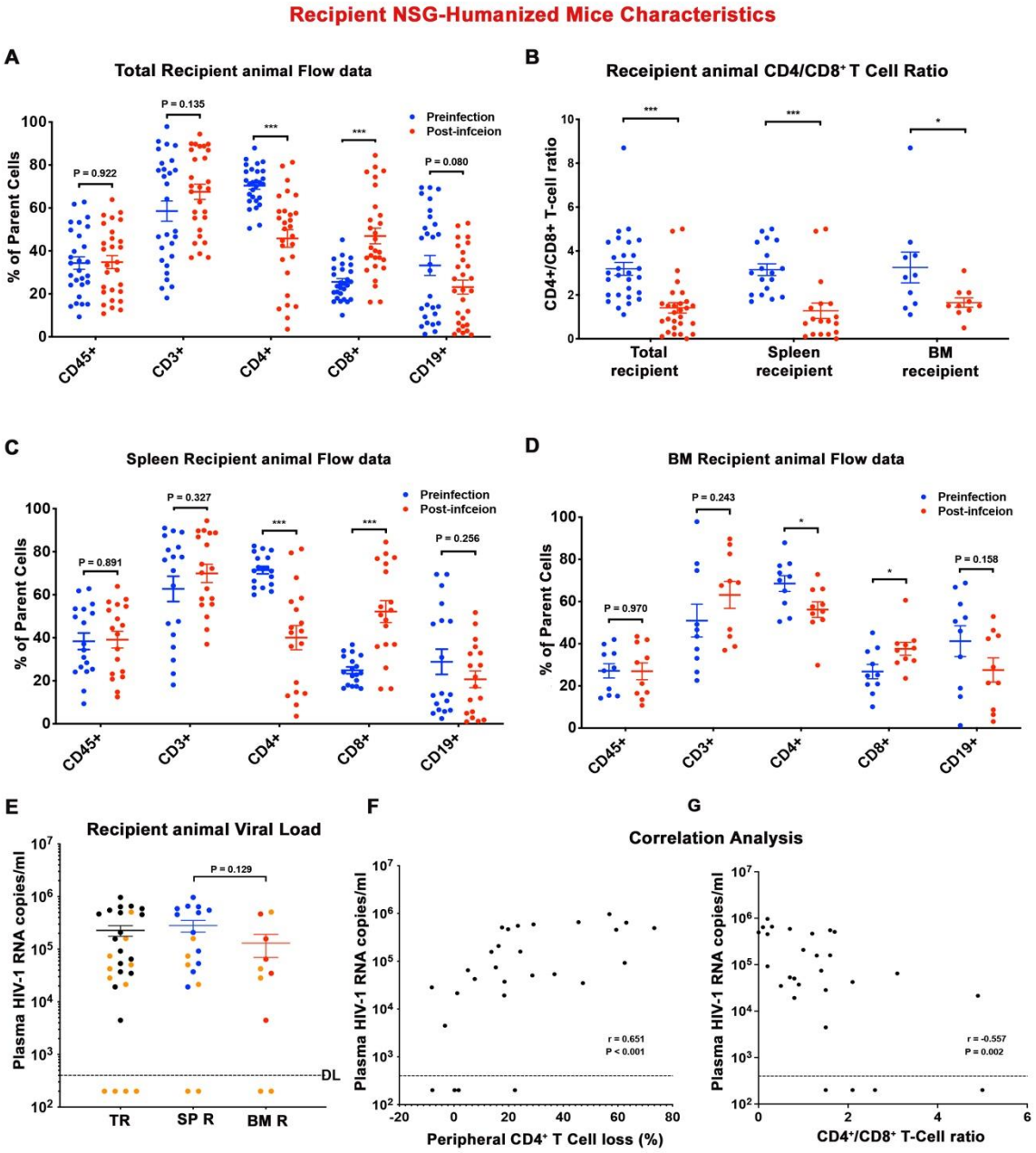
Recipient NSG-Humanized Mice Characteristics
A
Total Recipient animal Flow data
% of Parent Cells
Preinfection
Post-infceion
P = 0.922
P = 0.135
P = 0.080
CD45+
CD3+
CD4+
CD8+
CD19+
B
Receipient animal CD4/CD8+ T Cell Ratio
CD4+/CD8+ T-cell ratio
Total recipient
Spleen receipient
BM receipient
C
Spleen Recipient animal Flow data
P = 0.891
P = 0.327
P = 0.256
D
BM Recipient animal Flow data
P = 0.970
P = 0.243
P = 0.158
E
Recipient animal Viral Load
Plasma HIV-1 RNA copies/ml
P = 0.129
DL
TR
SP R
BM R
F
Peripheral CD4+ T Cell loss (%)
r = 0.651
P < 0.001
G
Correlation Analysis
CD4+/CD8+ T-Cell ratio
r = -0.557
P = 0.002

Figure 4. 4 Descriptors of recipient humanized mice.

Peripheral human cell levels (hCD45+, hCD3+, hCD4+, hCD8+, and hCD19+ cells) before (blue) and after (red) adoptive transfer were depicted for (A) total recipient (TR) humanized mice, and subgroups (C) spleen recipient (SR) and (D) bone marrow recipient (BR) humanized mice. (B) Scatter plots represented CD4+/CD8+ T cell ratio of individual TR, SR, and BR before (blue) and after (red) adoptive transfer. (E) Plasma viral load (pVL) of individual recipient humanized mouse at sacrifice was displayed for TR (black), SR (blue), and BR (red). Orange dots represented humanized mice receiving engraftment from donors with minimal or undetected plasma VL. The detection limit is < 400 HIV-1 RNA copies/ml. A Spearman's rank correlation test was conducted to investigate the association (F) between recipient humanized mouse plasma VL and respective peripheral CD4+ T cell loss and (G) between recipient humanized mouse plasma VL and respective end-point peripheral CD4+/CD8+ T cell ratio. The Spearman correlation coefficient (r) and p value for each analysis were displayed. In A-E, data are expressed as mean ± SEM and considered *, *** statistically significant, at $p<0.05$ and $p<0.001$.

Table 4. 3 Peripheral human cell reconstitution and plasma viral load of recipient humanized mice

		TR (n = 28)		SR (n = 18)		BR (n = 10)	
		Pre	Post	Pre	Post	Pre	Post
Peripheral human cells (%)	CD45	34.4 ± 2.9	34.8 ± 3.1	38.4 ± 3.9	39.1 ± 3.9	27.1 ± 3.4	26.9 ± 4.0
	CD3	58.5 ± 4.7	67.5 ± 3.5	62.7 ± 5.9	69.9 ± 4.2	51.0 ± 7.8	63.2 ± 6.4
	CD4	70.4 ± 1.7	45.8 ± 4.1	71.4 ± 1.7	40.0 ± 5.6	68.5 ± 3.8	56.2 ± 3.7
	CD8	25.6 ± 1.5	47.0 ± 3.7	24.9 ± 1.6	52.2 ± 5.1	26.8 ± 3.4	37.6 ± 3.1
	CD19	33.3 ± 4.6	23.1 ± 3.2	28.8 ± 5.9	20.7 ± 3.9	41.2 ± 7.3	27.5 ± 5.7
CD4/CD8		3.2 ± 0.3	1.4 ± 0.2	3.2 ± 0.3	1.3 ± 0.4	3.3 ± 0.7	1.7 ± 0.2
Plasma HIV-1 RNA ($x10^5$ copies/ml)		/	2.3 ± 0.5	/	2.8 ± 0.7	/	1.3 ± 0.6

TR, total recipient; SR, spleen recipient; BR, bone marrow recipient; Pre, pre-adoptive transfer; Post, post-adoptive transfer. Data are expressed as mean ± SEM.

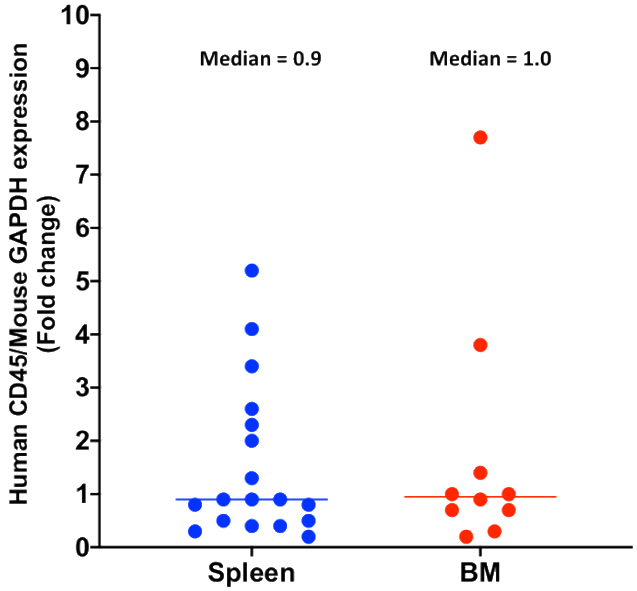

Figure 4. 5 Human cell reconstitution in donor humanized mouse spleens and BM.

Total DNA was isolated from donor spleen (blue) and BM (red) and subjected to real-time quantitative PCR analysis. Human CD45 was employed as human cell marker and mouse GAPDH as reference gene. Comparative ΔΔCT method was used. Data were shown as the median of fold change of individual human CD45/mouse GAPDH expression.

was a negative association between TR plasma VL and end point CD4/CD8+ T cell ratio (**Figure 4.4G**). We observed a positive correlation of plasma VL between donor and SR but not between donor and BR (**Figure 4.6**). Tissue HIV-1 infection as measured to look for viral DNA (**Fig. 4.7A** and **C**) and RNA (**Fig. 4.7B** and **D**) was readily established and disseminated amongst spleens, BM, guts, lungs, brains, livers, and kidneys in allografted humanized mice except those 4 animals obtaining engraftment from donors 3319 and 3336 (**Figure 4.7A-D**). We observed a positive correlation between the donor tissue proviral DNA amplification with that of recipient tissue nucleic acid amplification. There were not significant differences on tissue viral burdens (except gut-associated lymphoid tissue HIV-1 DNA) between SR and BR (**Figure 4.7A-D**). Tissue viral infection in recipients wasconfirmed by immunohistochemitry (**Figure 4.8**). Spleen and lymph node samples from SR and BR were stained for human HLA-DR and HIV-1p24 at the same region. Human HLA-DR signal (shown as brown dots) was readily detected in all recipients indicating proper humanization of the animals. While not being observed in recipients engrafted from sterilized donors 3319 and 3336 (data not shown), HIV-1p24 (shown as brown dots) was detected in both SR (**Figure 4.8A**) and BR (**Figure 4.8B**) that received engraftment from donors with undetectable or close-to-detection limit plasma VL. Viral replication was more prominent in lymph node than spleen from the same animal. Altogether, these data emphasize that replication-competent HIV-1 persists in tissue sanctuaries even under effective ART.

4.5 Discussion

A primary barrier to an HIV “cure” rests in the establishment of a stably integrated

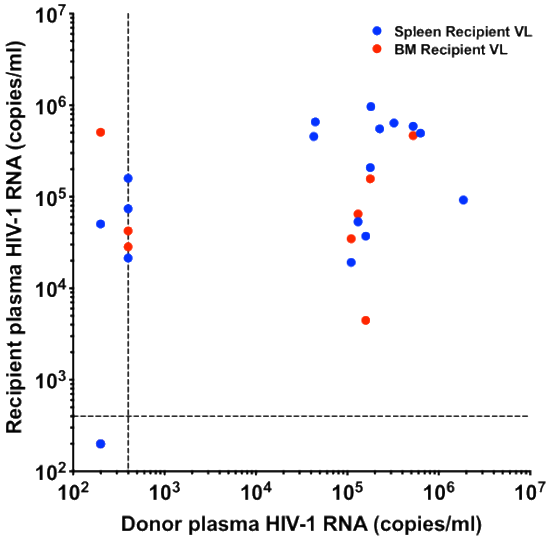

	Spleen Recipient VL (n=18)	BM Recipient VL (n=10)
Donor VL (n=18)	r = 0.623	r = 0.414
	P = 0.006	P = 0.232

Figure 4. 6 Correlations between donor and recipient mouse plasma VL.

Spearman's rank correlation tests were conducted to investigate associations between donor humanized mouse plasma VL and respective SR plasma VL (blue) and respective BR plasma VL (red). The Spearman correlation coefficient (r) and p value for each analysis were displayed. The detection limit of plasma VL is 400 HIV-1 RNA copies/ml.

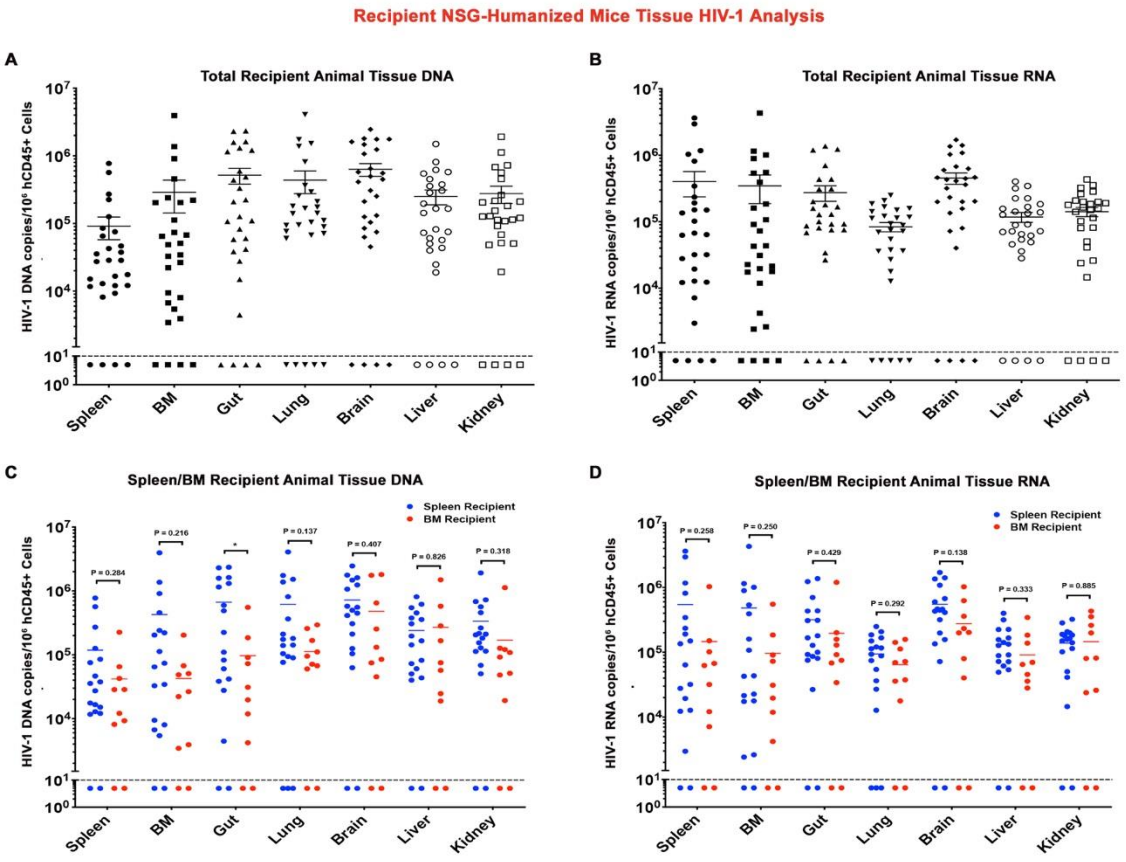

Figure 4. 7 Tissue HIV-1 DNA and RNA in recipient humanized mice.

(**A**) Tissue HIV-1 DNA and (**B**) tissue HIV-1 RNA in total recipient (TR) were established in spleen, BM, gut, lung, brain, liver, and kidney. (**C**) Tissue HIV-1 DNA and (**D**) tissue HIV-1 RNA in subgroups spleen recipient (SR) (blue) and bone marrow recipient (BR) (red) were displayed. The detection limit is below 10 HIV-1 copies as measured by real-time semi-nested qPCR assays. Data are expressed as mean ± SEM and considered *, *** statistically significant, at $p<0.05$ and $p<0.001$.

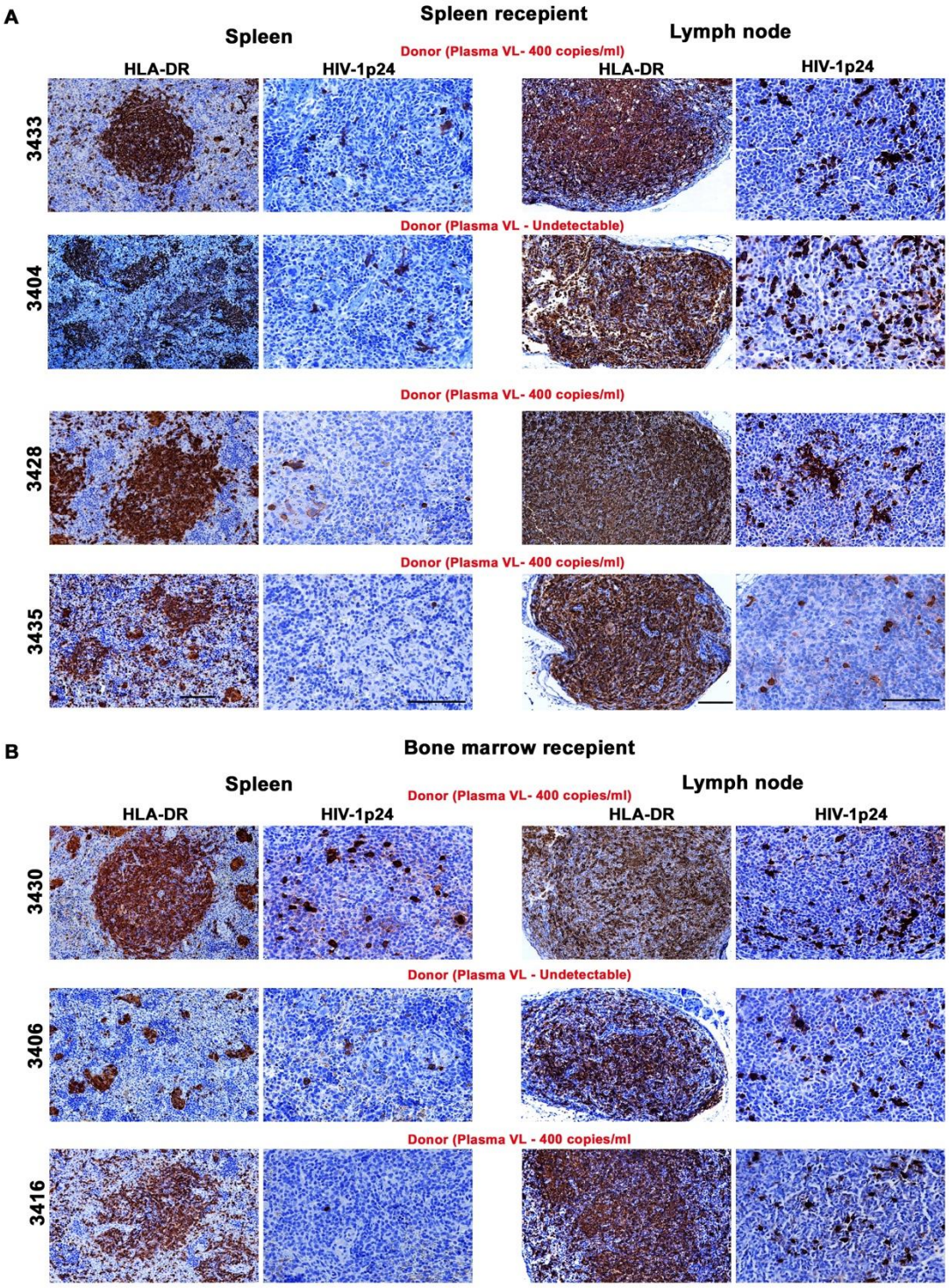
A
Spleen recepient
Spleen
Lymph node
Donor (Plasma VL- 400 copies/ml)
HLA-DR
HIV-1p24
HLA-DR
HIV-1p24
3433
Donor (Plasma VL - Undetectable)
3404
Donor (Plasma VL- 400 copies/ml)
3428
Donor (Plasma VL- 400 copies/ml)
3435
B
Bone marrow recepient
Spleen
Lymph node
Donor (Plasma VL- 400 copies/ml)
HLA-DR
HIV-1p24
HLA-DR
HIV-1p24
3430
Donor (Plasma VL - Undetectable)
3406
Donor (Plasma VL - 400 copies/ml)
3416

Figure 4. 8 Detection of HIV-1p24 in recipient humanized mouse tissues.

A representative photomicrographic analysis of spleen and lymph node samples from spleen and BM recipient humanized mice tissues adoptively transferred from either undetectable or close to detection limit (400 copies of HIV-1 RNA/ml) plasma viral load of donor mice. Spleen and lymph node tissues were collected from (**A**) Spleen recipient and (**B**) BM recipient mice at necropsy with formalin fixed and paraffin embedded for nest step. Five μM thick sections were cut and then stained with antibodies specific for human HLA-DR and HIV-1p24. Representative images from each group were selected and pictures were captured for both (shown as brown dots) from individual animals. The recipient mice numbers are presented on the left panel. The plasma viral load of the donor mice used for adoptive transfer of cells are presented on the top of each mice rows, suggesting the sensitivity of the method we adopted to detect tissue viral reservoirs when the plasma viremia is undetectable. Scale bar 10μM and 40 μM respectively for HLA-DR and HIV-1p24 analysis.

nonproductive infection that is termed viral latency. Elucidation of locale and extent of this viral reservoir is imperative if viral elimination is to be achieved. Current methods to quantitate latent HIV-1 infection relies principally on the use of nucleic acid polymerase chain reaction (PCR) and qVOA-based assays. While both are sensitive and specific both fall short in reflecting the absolute viral reservoir as it exists at extremely low levels (218, 219). The lack of assay sensitivity was seen from allogeneic hematopoietic stem cell transplant (HSCT) recipients who were found to be HIV-1 negative by conventional PCR and qVOA by tests of peripheral blood and rectal tissue biopsy for time periods of up to years before ART interruption (ATI). Unfortunately, both patients experienced viral resurgence (220). In the case of the "Mississippi baby", ART was initiated 30 hours after birth and while the baby remained virus free by PCR and qVOA tests before and after ATI virus rebounded after 27 months (50). From these studies it is argued that, ATI is the ultimate standard to justify HIV-1 cure. Both above cases emphasize that more sensitive assays are urgently required at the age of pursuing HIV-1 eradication. However, to date, studies that involved thousands of individuals undergoing ATI, only 2 cases were considered free of HIV-1 infection while others unexclusively experienced viral rebound (47, 48, 221). ATI endowed patients with unnecessary risks can be avoided if more sensitive assays for latency evaluation are developed.

An ideal model should have a shortened disease course for completion of therapeutic testing in a limited time and should possess immune cell markers that are readily translatable to humans. That encouraged the creation of immunodeficient rodents that accommodate human xenografts permitting study of diseases exclusively in human such as HIV-1. Mouse models have extended our understanding and prepared us with the

therapy for this once life-threatening disease. From the past 5 years, researchers employed these models to develop an in vivo VOA by engrafting blood samples from HIV-1 infected patient into either non-humanized or humanized mice (222). HIV-1 was successfully recovered from animals that received transplant from viral suppressed donors. In general, humanized mice are more sensitive on viral recovery than regular immunodeficient mice. There is a direct relationship between reservoir size and time to reawake. More importantly, mVOA was able to capture latent reservoirs that were not detected by qVOA (181, 213) revealing its better sensitivity on reservoir measurement.

Additionally, due to limited access of patient tissues, clinical determination of viral reservoirs, including mVOA, mostly relies on peripheral blood test while majority of latent cells hide in variant tissues (223). Humanized mice can overcome these challenges by enabling analysis of individual tissue types. The superior sensitivity of mVOA over qVOA likely attributes to a combination of factors including a physiological environment that favors the expansion and survival of donor cells, abundant HIV-1 susceptible cells (as in humanized mice) facilitating viral spread, and graft-versus-host (GvH) reaction that promotes the reversal of latent infected cells.

Currently, humanized mice VOA has been rarely studied due to lack of HIV-1 elimination strategies. In addition, finding viral sanctuaries from human tissues remains challenging, humanized mice can provide an alternative pathway for engrafting individual mouse tissues into naïve recipients to monitor viral resurgence. Recently our lab developed a combinatorial LASER ART and CRISPR/Cas9 strategy to pursue HIV-1 cure (109). After an 8 to 10 weeks period absence of ART, donor splenocytes and BM cells were adoptively transferred to naïve humanized mice. To maximally recover any replication

competent donor remaining virus, we adoptively transferred the maximum number of cells according to sample availability. Engraftment was well tolerated in all the recipients that were further kept for one month before sacrifice, which is generally sufficient for HIV-1 reservoirs to relapse (181, 213, 214). Animals receiving engraftment from the donors with higher plasma viremia (12/18) before allograft exhibited rigorous HIV-1 replication, indicating that similar to human samples, viral outgrowth from humanized mice-derived cells was permissive. In four animals (# 3322, 3324, 3327, and 3353), where peripheral VL was extremely low or undetected, condition similar to clinically viral suppressed patients, HIV-1 was detected in a broad range of tissue types, as observed in autopsy specimens of treated patients (35). Virus from these 4 animal tissues was successfully recovered from engrafted humanized mice, demonstrating that these viruses were latent and replication-competent. This may explain the failure of viral control in patients who received long-term suppressive treatment and went through ATI (55, 57). On the other hand, when virus is eliminated from all the sanctuaries it could not be recovered even after adoptive transfer (# 3319 and # 3336).

Viral amplification levels in the donors are not associated with that of recipients as previously observed (213), which can be attributed to multiple factors including donor viral burden, numbers of adoptively transferred cells, and recipient environment. One drawback in the present study is lack of comparison on detection sensitivity between qVOA and mVOA due to sample insufficiency and will be pursued in the future. We posit MVOA should be conducted only after repetitive qVOA presenting negative to reduce animal numbers. Sufficient number of cells should be engrafted to prevent false negative result. MVOA is not always viable when HIV-1 reservoir size is extremely small. For example,

in a recent report, patient A who initiated ART 10 days after infection remained viral negative (by PCR and qVOA) by extensive scrutinization from blood, colorectum, lymph node, cerebral spinal fluid, and BM for 2 years. More than 500 million CD4+ T cells were isolated and engrafted into 10 NSG mice (53 million per mouse) but only one mouse displayed minimal viremia (201 copies/ml). The patient underwent ATI and maintained HIV-1 remission for 7.4 months before viral rebound. An estimated reservoir size of 200 cells resided, before ATI, which might be missed even after 1 billion CD4+ T cells were scrutinized (96), resulting in rebound.

In summary, this study describes an hu-HSC mouse-based MVOA that successfully recovered virus from donor infected humanized mouse tissues. Notably these animals possessed either detectable or undetectable plasma VL. This observation emphasizes the 'untouchable' tissue HIV-1 reservoirs as a major obstacle to viral cure even under highly suppressive ART (154). Sensitivity of mVOA can be improved by using humanized instead of non-humanized NSG mice, in vitro stimulation (e.g. anti CD3/CD28 antibodies or latency reversing agents) before transplant, and in vivo CD8+ T cells depletion after engraftment (222). In addition, mVOA can be successfully employed to interrogate HIV-1 latency from individual tissue or cell type of interest. Future work needs to be conducted to characterize mVOA which should become standard validation assay of HIV-1 eradication.

Chapter 5 Conclusions and Future Directions

Since the first case of HIV/AIDS identified in 1981, this malicious disease has led to a total of 74.9 million infections and 32 million death by 2018 according to UNAIDS. Development of highly active antiretroviral therapy (HAART) successfully halts viral spread and renders patients a nearly normal life. An HIV-1 cure has been pursued for the past decade while only realized in two patients who received aggressive procedures (47, 48). The major barrier to HIV-1 eradication rests on latent viral reservoirs containing replication-competent HIV-1 DNA that is resistant to current therapies including HAART, latency reversing agents (LRAs), broadly neutralizing antibodies (bnAbs), and immune therapy. While HIV-1 replication is efficiently inhibited under HAART, viral sequences integrated into host genome remain untouchable and resume viral production after treatment is discontinued. Therefore, HIV-1 eradication is only possible when genomic viral DNA is edited. The development of CRISPR-Cas9 system eases the design and improves the specificity and sensitivity of gene editing, making it possible for broad application on human genetic diseases including leukemia, blindness, cystic fibrosis, muscular dystrophy, and others (106, 224). While CRISPR-Cas9 designed to target specific HIV-1 sequences has successfully excised viral genomes in cellular and small animal model, it remains unclear if CRISPR-Cas9 can synergize with other treatments to achieve a complete HIV-1 eradication (165, 166). Because HIV-1 is a human-specific disease, we first developed a human CD34+ hematopoietic stem cells (HSCs)-reconstituted humanized mouse model that simulates human immune system susceptible to HIV-1 infection (43, 120). Next HIV-1 temporal and spatial dynamics during acute infection of humanized mice were identified to guide the follow-up design of HAART intervention (196). We observed early HIV-1 tissue compartments in animal spleen, lung, and liver by 3 days post-infection

and broad viral distribution by 14 days post-infection at which point HAART was determined to initiate in the following study (109). To maximize viral restriction in the setting of optimal gene-editing efficiency by CRISPR-Cas9, a combination of nanoformulated prodrugs (RPV, MDTG, MABC, and M3TC) were developed (namely LASER ART) characterized with prolonged half-life and enhanced tissue penetration (44, 45, 161, 162). Through this combinational strategy applying sequential administration of LASER ART and CRISPR Cas9, for the first time a complete HIV-1 cure was achieved in a subset of infected humanized mice which was demonstrated in three independent experiments (109). This success is attributed to a combination of factors including a suitable animal model, control of viral set points, early treatment intervention, potent LASER ART reaching viral reservoirs, and the widespread employment of CRISPR-Cas9 gene editing. To this end, these proof-of-concept results offer novel and realistic pathways toward HIV-1 elimination.

To increase the "HIV-1 cure" rate, we will first reinforce the efficacy of two components (LASER ART and CRISPR-Cas9) in the strategy. The potency of LASER ART partially lies on the lipophilic and hydrophobic properties which can be improved with chemical modification. Taking cabotegravir (CAB) as example, through adjusting various fatty acid chains, a new prodrug linking 18-carbon stearic acid onto parent CAB has shown enhanced half-life and tissue penetration compared to the first-generation prodrug myristoylated CAB (MCAB) (unpublished data). Alternative pathway to improve the efficiency of LASER ART is to direct treatment to targets through specific ligand binding. Folate acid (FA) receptors are highly expressed on activated macrophages which are the primary sites of HIV-1 infection (225). Previous studies from our group have shown

that FA-coated nanoART is superior to non-FA-coated nanoART as to extended drug half-life, higher drug concentrations, and better HIV-1 inhibition (198, 226). Whether or not this targeting strategy can boost the competence of current prodrugs needs further investigation. To improve genomic excision of HIV-1, a more efficient delivery system of CRISPR-Cas9 can be pursued. Adenovirus has been widely applied as a gene delivery vector (227). The highly effective transfection of adenovirus is attributed to a broad expression of adenovirus receptor on human cells (228). However, this also limits its specificity when it is used to deliver gene therapy to HIV-1 containing cells which are primarily CD4+ T cells and monocytes/macrophages and may cause unnecessary off-target events. To address this issue, the virus-like particles (VLPs) that possess HIV-1 envelop protein for specific CD4 binding but fail to induce infection or replication due to gene modification have been under development as novel vector for CRISPR-Cas9. Employing multiple guide RNAs that target different HIV-1 and/or host sequences may also enhance viral suppression and elimination as shown in **Figure 3.14**. While CRISPR-Cas9 is powerful in gene editing and may lead to an HIV-1 cure, researchers should always be precautious about the potential off-target effects caused by gene manipulation in general (229). Although in our humanized mouse study, no off-target effects were detected in CRISPR-Cas9 treated animals after careful scrutinization, avoiding any potential off-target effects when designing gene therapy and performing post-procedure assessment should be required. The mechanisms of HIV-1 persistence are complicated. To maximize viral restriction and elimination of HIV-1 latency, one or multiple therapies can be employed such as LRAs, bnAbs, immune checkpoint inhibitors, CAR-T cells, etc. Lastly, observation in small animal models cannot fully predict the outcomes in human beings. Our

combinational strategy of HIV-1 eradication need to be readjusted and tested in larger animals such as non-human primates and eventually in human patients. To this end, we make an important first step towards a longer journey of HIV-1 eradication.

References

1. Palella FJ, Jr., Delaney KM, Moorman AC, Loveless MO, Fuhrer J, Satten GA, Aschman DJ, Holmberg SD. 1998. Declining morbidity and mortality among patients with advanced human immunodeficiency virus infection. HIV Outpatient Study Investigators. N Engl J Med 338:853-60.
2. Barre-Sinoussi F, Ross AL, Delfraissy JF. 2013. Past, present and future: 30 years of HIV research. Nat Rev Microbiol 11:877-83.
3. Maartens G, Celum C, Lewin SR. 2014. HIV infection: epidemiology, pathogenesis, treatment, and prevention. Lancet 384:258-71.
4. Yazdanpanah Y, Fagard C, Descamps D, Taburet AM, Colin C, Roquebert B, Katlama C, Pialoux G, Jacomet C, Piketty C, Bollens D, Molina JM, Chene G, Group ATT. 2009. High rate of virologic suppression with raltegravir plus etravirine and darunavir/ritonavir among treatment-experienced patients infected with multidrug-resistant HIV: results of the ANRS 139 TRIO trial. Clin Infect Dis 49:1441-9.
5. Guihot A, Bourgarit A, Carcelain G, Autran B. 2011. Immune reconstitution after a decade of combined antiretroviral therapies for human immunodeficiency virus. Trends Immunol 32:131-7.
6. Siliciano JD, Kajdas J, Finzi D, Quinn TC, Chadwick K, Margolick JB, Kovacs C, Gange SJ, Siliciano RF. 2003. Long-term follow-up studies confirm the stability of the latent reservoir for HIV-1 in resting CD4+ T cells. Nat Med 9:727-8.
7. Davey RT, Jr., Bhat N, Yoder C, Chun TW, Metcalf JA, Dewar R, Natarajan V, Lempicki RA, Adelsberger JW, Miller KD, Kovacs JA, Polis MA, Walker RE, Falloon J, Masur H, Gee D, Baseler M, Dimitrov DS, Fauci AS, Lane HC. 1999. HIV-1 and T cell dynamics after interruption of highly active antiretroviral therapy (HAART) in patients with a history of sustained viral suppression. Proc Natl Acad Sci U S A 96:15109-14.
8. Fischer M, Hafner R, Schneider C, Trkola A, Joos B, Joller H, Hirschel B, Weber R, Gunthard HF, Swiss HIVCS. 2003. HIV RNA in plasma rebounds within days during structured treatment interruptions. AIDS 17:195-9.
9. Harrigan PR, Whaley M, Montaner JS. 1999. Rate of HIV-1 RNA rebound upon stopping antiretroviral therapy. Aids 13:F59-62.
10. Kulpa DA, Chomont N. 2015. HIV persistence in the setting of antiretroviral therapy: when, where and how does HIV hide? J Virus Erad 1:59-66.
11. Barton K, Winckelmann A, Palmer S. 2016. HIV-1 Reservoirs During Suppressive Therapy. Trends Microbiol 24:345-355.
12. Ganor Y, Real F, Sennepin A, Dutertre CA, Prevedel L, Xu L, Tudor D, Charmeteau B, Couedel-Courteille A, Marion S, Zenak AR, Jourdain JP, Zhou Z, Schmitt A, Capron C, Eugenin EA, Cheynier R, Revol M, Cristofari S, Hosmalin A, Bomsel M. 2019. HIV-1 reservoirs in urethral macrophages of patients under suppressive antiretroviral therapy. Nat Microbiol 4:633-644.
13. Ko A, Kang G, Hattler JB, Galadima HI, Zhang J, Li Q, Kim WK. 2019. Macrophages but not Astrocytes Harbor HIV DNA in the Brains of HIV-1-Infected Aviremic Individuals on Suppressive Antiretroviral Therapy. J Neuroimmune Pharmacol 14:110-119.

14. Clayton KL, Collins DR, Lengieza J, Ghebremichael M, Dotiwala F, Lieberman J, Walker BD. 2018. Resistance of HIV-infected macrophages to CD8(+) T lymphocyte-mediated killing drives activation of the immune system. Nat Immunol 19:475-486.
15. Kandathil AJ, Sugawara S, Balagopal A. 2016. Are T cells the only HIV-1 reservoir? Retrovirology 13:86.
16. Thompson CG, Rosen EP, Prince HMA, White N, Sykes C, de la Cruz G, Mathews M, Deleage C, Estes JD, Charlins P, Mulder LR, Kovarova M, Adamson L, Arora S, Dellon ES, Peery AF, Shaheen NJ, Gay C, Muddiman DC, Akkina R, Garcia JV, Luciw P, Kashuba ADM. 2019. Heterogeneous antiretroviral drug distribution and HIV/SHIV detection in the gut of three species. Sci Transl Med 11.
17. Svicher V, Ceccherini-Silberstein F, Antinori A, Aquaro S, Perno CF. 2014. Understanding HIV compartments and reservoirs. Curr HIV/AIDS Rep 11:186-94.
18. Wong JK, Yukl SA. 2016. Tissue reservoirs of HIV. Curr Opin HIV AIDS 11:362-70.
19. Honeycutt JB, Thayer WO, Baker CE, Ribeiro RM, Lada SM, Cao Y, Cleary RA, Hudgens MG, Richman DD, Garcia JV. 2017. HIV persistence in tissue macrophages of humanized myeloid-only mice during antiretroviral therapy. Nat Med 23:638-643.
20. Mattapallil JJ, Douek DC, Hill B, Nishimura Y, Martin M, Roederer M. 2005. Massive infection and loss of memory CD4+ T cells in multiple tissues during acute SIV infection. Nature 434:1093-7.
21. Chun TW, Nickle DC, Justement JS, Meyers JH, Roby G, Hallahan CW, Kottilil S, Moir S, Mican JM, Mullins JI, Ward DJ, Kovacs JA, Mannon PJ, Fauci AS. 2008. Persistence of HIV in gut-associated lymphoid tissue despite long-term antiretroviral therapy. J Infect Dis 197:714-20.
22. Deere JD, Kauffman RC, Cannavo E, Higgins J, Villalobos A, Adamson L, Schinazi RF, Luciw PA, North TW. 2014. Analysis of multiply spliced transcripts in lymphoid tissue reservoirs of rhesus macaques infected with RT-SHIV during HAART. PLoS One 9:e87914.
23. Kroon E SM, Chottanapund S, Anderson J, Manasnayakorn S, Jorstad S, David C, Conner A, Helgeson E, Reilly C, Robb ML, Douek D, Ananworanich J, Schacker TW. 2018. PERSISTENT DETECTION OF HIV RNA+ CELLS WITH ART STARTED IN FIEBIG 1&2 VS FIEBIG 3-5.
24. Licht A, Alter G. 2016. A Drug-Free Zone--Lymph Nodes as a Safe Haven for HIV. Cell Host Microbe 19:275-6.
25. Aid M, Dupuy FP, Moysi E, Moir S, Haddad EK, Estes JD, Sekaly RP, Petrovas C, Ribeiro SP. 2018. Follicular CD4 T Helper Cells As a Major HIV Reservoir Compartment: A Molecular Perspective. Front Immunol 9:895.
26. Rocco J, Mellors JW, Macatangay BJ. 2018. Regulatory T cells: the ultimate HIV reservoir? J Virus Erad 4:209-214.
27. Dinoso JB, Rabi SA, Blankson JN, Gama L, Mankowski JL, Siliciano RF, Zink MC, Clements JE. 2009. A simian immunodeficiency virus-infected macaque model to study viral reservoirs that persist during highly active antiretroviral therapy. J Virol 83:9247-57.

28. Rose RM, Krivine A, Pinkston P, Gillis JM, Huang A, Hammer SM. 1991. Frequent identification of HIV-1 DNA in bronchoalveolar lavage cells obtained from individuals with the acquired immunodeficiency syndrome. Am Rev Respir Dis 143:850-4.
29. Blackard JT, Ma G, Martin CM, Rouster SD, Shata MT, Sherman KE. 2011. HIV variability in the liver and evidence of possible compartmentalization. AIDS Res Hum Retroviruses 27:1117-26.
30. Itescu S, Simonelli PF, Winchester RJ, Ginsberg HS. 1994. Human immunodeficiency virus type 1 strains in the lungs of infected individuals evolve independently from those in peripheral blood and are highly conserved in the C-terminal region of the envelope V3 loop. Proc Natl Acad Sci U S A 91:11378-82.
31. Cribbs SK, Lennox J, Caliendo AM, Brown LA, Guidot DM. 2015. Healthy HIV-1-infected individuals on highly active antiretroviral therapy harbor HIV-1 in their alveolar macrophages. AIDS Res Hum Retroviruses 31:64-70.
32. Sebastian NT, Zaikos TD, Terry V, Taschuk F, McNamara LA, Onafuwa-Nuga A, Yucha R, Signer RAJ, Riddell JI, Bixby D, Markowitz N, Morrison SJ, Collins KL. 2017. CD4 is expressed on a heterogeneous subset of hematopoietic progenitors, which persistently harbor CXCR4 and CCR5-tropic HIV proviral genomes in vivo. PLoS Pathog 13:e1006509.
33. Alexaki A, Wigdahl B. 2008. HIV-1 infection of bone marrow hematopoietic progenitor cells and their role in trafficking and viral dissemination. PLoS Pathog 4:e1000215.
34. Bruggeman LA. 2017. HIV-1 Infection of Renal Cells in HIV-Associated Nephropathy. J Am Soc Nephrol 28:719-721.
35. Lamers SL, Rose R, Maidji E, Agsalda-Garcia M, Nolan DJ, Fogel GB, Salemi M, Garcia DL, Bracci P, Yong W, Commins D, Said J, Khanlou N, Hinkin CH, Sueiras MV, Mathisen G, Donovan S, Shiramizu B, Stoddart CA, McGrath MS, Singer EJ. 2016. HIV DNA Is Frequently Present within Pathologic Tissues Evaluated at Autopsy from Combined Antiretroviral Therapy-Treated Patients with Undetectable Viral Loads. J Virol 90:8968-83.
36. Watanabe M, Ringler DJ, Fultz PN, MacKey JJ, Boyson JE, Levine CG, Letvin NL. 1991. A chimpanzee-passaged human immunodeficiency virus isolate is cytopathic for chimpanzee cells but does not induce disease. J Virol 65:3344-8.
37. Alter HJ, Eichberg JW, Masur H, Saxinger WC, Gallo R, Macher AM, Lane HC, Fauci AS. 1984. Transmission of HTLV-III infection from human plasma to chimpanzees: an animal model for AIDS. Science 226:549-52.
38. Gajdusek DC, Amyx HL, Gibbs CJ, Jr., Asher DM, Rodgers-Johnson P, Epstein LG, Sarin PS, Gallo RC, Maluish A, Arthur LO, et al. 1985. Infection of chimpanzees by human T-lymphotropic retroviruses in brain and other tissues from AIDS patients. Lancet 1:55-6.
39. Williams KC, Burdo TH. 2009. HIV and SIV infection: the role of cellular restriction and immune responses in viral replication and pathogenesis. APMIS 117:400-12.
40. Kumar N, Chahroudi A, Silvestri G. 2016. Animal models to achieve an HIV cure. Curr Opin HIV AIDS 11:432-41.

41. Hatziioannou T, Evans DT. 2012. Animal models for HIV/AIDS research. Nature reviews Microbiology 10:852-867.
42. Marsden MD, Zack JA. 2017. Humanized Mouse Models for Human Immunodeficiency Virus Infection. Annu Rev Virol 4:393-412.
43. Arainga M, Su H, Poluektova LY, Gorantla S, Gendelman HE. 2016. HIV-1 cellular and tissue replication patterns in infected humanized mice. Sci Rep 6:23513.
44. Sillman B, Bade AN, Dash PK, Bhargavan B, Kocher T, Mathews S, Su H, Kanmogne GD, Poluektova LY, Gorantla S, McMillan J, Gautam N, Alnouti Y, Edagwa B, Gendelman HE. 2018. Creation of a long-acting nanoformulated dolutegravir. Nat Commun 9:443.
45. Zhou T, Su H, Dash P, Lin Z, Dyavar Shetty BL, Kocher T, Szlachetka A, Lamberty B, Fox HS, Poluektova L, Gorantla S, McMillan J, Gautam N, Mosley RL, Alnouti Y, Edagwa B, Gendelman HE. 2018. Creation of a nanoformulated cabotegravir prodrug with improved antiretroviral profiles. Biomaterials 151:53-65.
46. Hill AL. 2018. Mathematical Models of HIV Latency. Curr Top Microbiol Immunol 417:131-156.
47. Hutter G, Nowak D, Mossner M, Ganepola S, Mussig A, Allers K, Schneider T, Hofmann J, Kucherer C, Blau O, Blau IW, Hofmann WK, Thiel E. 2009. Long-term control of HIV by CCR5 Delta32/Delta32 stem-cell transplantation. N Engl J Med 360:692-8.
48. Gupta RK, Abdul-Jawad S, McCoy LE, Mok HP, Peppa D, Salgado M, Martinez-Picado J, Nijhuis M, Wensing AMJ, Lee H, Grant P, Nastouli E, Lambert J, Pace M, Salasc F, Monit C, Innes AJ, Muir L, Waters L, Frater J, Lever AML, Edwards SG, Gabriel IH, Olavarria E. 2019. HIV-1 remission following CCR5Delta32/Delta32 haematopoietic stem-cell transplantation. Nature 568:244-248.
49. Hutter G. 2014. More on shift of HIV tropism in stem-cell transplantation with CCR5 delta32/delta32 mutation. N Engl J Med 371:2437-8.
50. Luzuriaga K, Gay H, Ziemniak C, Sanborn KB, Somasundaran M, Rainwater-Lovett K, Mellors JW, Rosenbloom D, Persaud D. 2015. Viremic relapse after HIV-1 remission in a perinatally infected child. N Engl J Med 372:786-8.
51. Ananworanich J, Chomont N, Eller LA, Kroon E, Tovanabutra S, Bose M, Nau M, Fletcher JLK, Tipsuk S, Vandergeeten C, O'Connell RJ, Pinyakorn S, Michael N, Phanuphak N, Robb ML, Rv, groups RSs. 2016. HIV DNA Set Point is Rapidly Established in Acute HIV Infection and Dramatically Reduced by Early ART. EBioMedicine 11:68-72.
52. Li JZ, Etemad B, Ahmed H, Aga E, Bosch RJ, Mellors JW, Kuritzkes DR, Lederman MM, Para M, Gandhi RT. 2016. The size of the expressed HIV reservoir predicts timing of viral rebound after treatment interruption. AIDS 30:343-53.
53. Saez-Cirion A, Bacchus C, Hocqueloux L, Avettand-Fenoel V, Girault I, Lecuroux C, Potard V, Versmisse P, Melard A, Prazuck T, Descours B, Guergnon J, Viard JP, Boufassa F, Lambotte O, Goujard C, Meyer L, Costagliola D, Venet A, Pancino G, Autran B, Rouzioux C, Group AVS. 2013. Post-treatment HIV-1 controllers with a long-term virological remission after the interruption of early initiated antiretroviral therapy ANRS VISCONTI Study. PLoS Pathog 9:e1003211.

54. Fiebig EW, Wright DJ, Rawal BD, Garrett PE, Schumacher RT, Peddada L, Heldebrant C, Smith R, Conrad A, Kleinman SH, Busch MP. 2003. Dynamics of HIV viremia and antibody seroconversion in plasma donors: implications for diagnosis and staging of primary HIV infection. AIDS 17:1871-9.
55. Colby DJ, Trautmann L, Pinyakorn S, Leyre L, Pagliuzza A, Kroon E, Rolland M, Takata H, Buranapraditkun S, Intasan J, Chomchey N, Muir R, Haddad EK, Tovanabutra S, Ubolyam S, Bolton DL, Fullmer BA, Gorelick RJ, Fox L, Crowell TA, Trichavaroj R, O'Connell R, Chomont N, Kim JH, Michael NL, Robb ML, Phanuphak N, Ananworanich J, group RVs. 2018. Rapid HIV RNA rebound after antiretroviral treatment interruption in persons durably suppressed in Fiebig I acute HIV infection. Nat Med 24:923-926.
56. Palich R, Ghosn J, Chaillon A, Boilet V, Nere ML, Chaix ML, Delobel P, Molina JM, Lucht F, Bouchaud O, Rieux V, Thiebaut R, Levy Y, Delaugerre C, Lelievre JD, Group VALVT. 2019. Viral rebound in semen after antiretroviral treatment interruption in an HIV therapeutic vaccine double-blind trial. AIDS 33:279-284.
57. Calin R, Hamimi C, Lambert-Niclot S, Carcelain G, Bellet J, Assoumou L, Tubiana R, Calvez V, Dudoit Y, Costagliola D, Autran B, Katlama C, Group US. 2016. Treatment interruption in chronically HIV-infected patients with an ultralow HIV reservoir. AIDS 30:761-9.
58. Vanhamel J, Bruggemans A, Debyser Z. 2019. Establishment of latent HIV-1 reservoirs: what do we really know? J Virus Erad 5:3-9.
59. Abner E, Jordan A. 2019. HIV "shock and kill" therapy: In need of revision. Antiviral Res 166:19-34.
60. Siliciano RF, Greene WC. 2011. HIV latency. Cold Spring Harb Perspect Med 1:a007096.
61. Darcis G, Das AT, Berkhout B. 2018. Tackling HIV Persistence: Pharmacological versus CRISPR-Based Shock Strategies. Viruses 10.
62. Spivak AM, Planelles V. 2018. Novel Latency Reversal Agents for HIV-1 Cure. Annu Rev Med 69:421-436.
63. Kim Y, Anderson JL, Lewin SR. 2018. Getting the "Kill" into "Shock and Kill": Strategies to Eliminate Latent HIV. Cell Host Microbe 23:14-26.
64. Darcis G, Van Driessche B, Van Lint C. 2017. HIV Latency: Should We Shock or Lock? Trends Immunol 38:217-228.
65. Gutierrez C, Serrano-Villar S, Madrid-Elena N, Perez-Elias MJ, Martin ME, Barbas C, Ruiperez J, Munoz E, Munoz-Fernandez MA, Castor T, Moreno S. 2016. Bryostatin-1 for latent virus reactivation in HIV-infected patients on antiretroviral therapy. AIDS 30:1385-92.
66. Cummins NW, Sainski AM, Dai H, Natesampillai S, Pang YP, Bren GD, de Araujo Correia MCM, Sampath R, Rizza SA, O'Brien D, Yao JD, Kaufmann SH, Badley AD. 2016. Prime, Shock, and Kill: Priming CD4 T Cells from HIV Patients with a BCL-2 Antagonist before HIV Reactivation Reduces HIV Reservoir Size. J Virol 90:4032-4048.
67. Hosmane NN, Kwon KJ, Bruner KM, Capoferri AA, Beg S, Rosenbloom DI, Keele BF, Ho YC, Siliciano JD, Siliciano RF. 2017. Proliferation of latently infected CD4(+) T cells carrying replication-competent HIV-1: Potential role in latent reservoir dynamics. J Exp Med 214:959-972.

68. Gendelman HE, McMillan J, Bade AN, Edagwa B, Kevadiya BD. 2019. The Promise of Long-Acting Antiretroviral Therapies: From Need to Manufacture. Trends Microbiol doi:10.1016/j.tim.2019.02.009.
69. Cao S, Woodrow KA. 2019. Nanotechnology approaches to eradicating HIV reservoirs. Eur J Pharm Biopharm 138:48-63.
70. Boyd MA, Cooper DA. 2017. Long-acting injectable ART: next revolution in HIV? Lancet 390:1468-1470.
71. Sillman B, Bade AN, Dash PK, Bhargavan B, Kocher T, Mathews S, Su H, Kanmogne GD, Poluektova LY, Gorantla S, McMillan J, Gautam N, Alnouti Y, Edagwa B, Gendelman HE. 2018. Creation of a long-acting nanoformulated dolutegravir. Nature Communications 9:443.
72. Ferretti F, Boffito M. 2018. Rilpivirine long-acting for the prevention and treatment of HIV infection. Curr Opin HIV AIDS 13:300-307.
73. Landovitz RJ, Li S, Grinsztejn B, Dawood H, Liu AY, Magnus M, Hosseinipour MC, Panchia R, Cottle L, Chau G, Richardson P, Marzinke MA, Hendrix CW, Eshleman SH, Zhang Y, Tolley E, Sugarman J, Kofron R, Adeyeye A, Burns D, Rinehart AR, Margolis D, Spreen WR, Cohen MS, McCauley M, Eron JJ. 2018. Safety, tolerability, and pharmacokinetics of long-acting injectable cabotegravir in low-risk HIV-uninfected individuals: HPTN 077, a phase 2a randomized controlled trial. PLoS Med 15:e1002690.
74. Buehler DC, Marsden MD, Shen S, Toso DB, Wu X, Loo JA, Zhou ZH, Kickhoefer VA, Wender PA, Zack JA, Rome LH. 2014. Bioengineered vaults: self-assembling protein shell-lipophilic core nanoparticles for drug delivery. ACS Nano 8:7723-32.
75. Kovochich M, Marsden MD, Zack JA. 2011. Activation of latent HIV using drug-loaded nanoparticles. PLoS One 6:e18270.
76. Jayant RD, Atluri VS, Agudelo M, Sagar V, Kaushik A, Nair M. 2015. Sustained-release nanoART formulation for the treatment of neuroAIDS. Int J Nanomedicine 10:1077-93.
77. Darcis G, Bouchat S, Kula A, Van Driessche B, Delacourt N, Vanhulle C, Avettand-Fenoel V, De Wit S, Rohr O, Rouzioux C, Van Lint C. 2017. Reactivation capacity by latency-reversing agents ex vivo correlates with the size of the HIV-1 reservoir. AIDS 31:181-189.
78. Battivelli E, Dahabieh MS, Abdel-Mohsen M, Svensson JP, Tojal Da Silva I, Cohn LB, Gramatica A, Deeks S, Greene WC, Pillai SK, Verdin E. 2018. Distinct chromatin functional states correlate with HIV latency reactivation in infected primary CD4(+) T cells. Elife 7.
79. Darcis G, Kula A, Bouchat S, Fujinaga K, Corazza F, Ait-Ammar A, Delacourt N, Melard A, Kabeya K, Vanhulle C, Van Driessche B, Gatot JS, Cherrier T, Pianowski LF, Gama L, Schwartz C, Vila J, Burny A, Clumeck N, Moutschen M, De Wit S, Peterlin BM, Rouzioux C, Rohr O, Van Lint C. 2015. An In-Depth Comparison of Latency-Reversing Agent Combinations in Various In Vitro and Ex Vivo HIV-1 Latency Models Identified Bryostatin-1+JQ1 and Ingenol-B+JQ1 to Potently Reactivate Viral Gene Expression. PLoS Pathog 11:e1005063.
80. Laird GM, Bullen CK, Rosenbloom DI, Martin AR, Hill AL, Durand CM, Siliciano JD, Siliciano RF. 2015. Ex vivo analysis identifies effective HIV-1 latency-reversing drug combinations. J Clin Invest 125:1901-12.

81. McBrien JB, Kumar NA, Silvestri G. 2018. Mechanisms of CD8(+) T cell-mediated suppression of HIV/SIV replication. Eur J Immunol 48:898-914.
82. Porichis F, Kaufmann DE. 2012. Role of PD-1 in HIV pathogenesis and as target for therapy. Curr HIV/AIDS Rep 9:81-90.
83. Pardoll DM. 2012. The blockade of immune checkpoints in cancer immunotherapy. Nat Rev Cancer 12:252-64.
84. Topalian SL, Hodi FS, Brahmer JR, Gettinger SN, Smith DC, McDermott DF, Powderly JD, Carvajal RD, Sosman JA, Atkins MB, Leming PD, Spigel DR, Antonia SJ, Horn L, Drake CG, Pardoll DM, Chen L, Sharfman WH, Anders RA, Taube JM, McMiller TL, Xu H, Korman AJ, Jure-Kunkel M, Agrawal S, McDonald D, Kollia GD, Gupta A, Wigginton JM, Sznol M. 2012. Safety, activity, and immune correlates of anti-PD-1 antibody in cancer. N Engl J Med 366:2443-54.
85. Goulder PJ, Jeena P, Tudor-Williams G, Burchett S. 2001. Paediatric HIV infection: correlates of protective immunity and global perspectives in prevention and management. Br Med Bull 58:89-108.
86. Trautmann L, Janbazian L, Chomont N, Said EA, Gimmig S, Bessette B, Boulassel MR, Delwart E, Sepulveda H, Balderas RS, Routy JP, Haddad EK, Sekaly RP. 2006. Upregulation of PD-1 expression on HIV-specific CD8+ T cells leads to reversible immune dysfunction. Nat Med 12:1198-202.
87. Cockerham LR, Jain V, Sinclair E, Glidden DV, Hartogenesis W, Hatano H, Hunt PW, Martin JN, Pilcher CD, Sekaly R, McCune JM, Hecht FM, Deeks SG. 2014. Programmed death-1 expression on CD4(+) and CD8(+) T cells in treated and untreated HIV disease. AIDS 28:1749-58.
88. Velu V, Titanji K, Zhu B, Husain S, Pladevega A, Lai L, Vanderford TH, Chennareddi L, Silvestri G, Freeman GJ, Ahmed R, Amara RR. 2009. Enhancing SIV-specific immunity in vivo by PD-1 blockade. Nature 458:206-10.
89. Gay CL, Bosch RJ, Ritz J, Hataye JM, Aga E, Tressler RL, Mason SW, Hwang CK, Grasela DM, Ray N, Cyktor JC, Coffin JM, Acosta EP, Koup RA, Mellors JW, Eron JJ, Team ACTS. 2017. Clinical Trial of the Anti-PD-L1 Antibody BMS-936559 in HIV-1 Infected Participants on Suppressive Antiretroviral Therapy. J Infect Dis 215:1725-1733.
90. Hatano H, Jain V, Hunt PW, Lee TH, Sinclair E, Do TD, Hoh R, Martin JN, McCune JM, Hecht F, Busch MP, Deeks SG. 2013. Cell-based measures of viral persistence are associated with immune activation and programmed cell death protein 1 (PD-1)-expressing CD4+ T cells. J Infect Dis 208:50-6.
91. Chomont N, El-Far M, Ancuta P, Trautmann L, Procopio FA, Yassine-Diab B, Boucher G, Boulassel MR, Ghattas G, Brenchley JM, Schacker TW, Hill BJ, Douek DC, Routy JP, Haddad EK, Sekaly RP. 2009. HIV reservoir size and persistence are driven by T cell survival and homeostatic proliferation. Nat Med 15:893-900.
92. Bruel T, Guivel-Benhassine F, Amraoui S, Malbec M, Richard L, Bourdic K, Donahue DA, Lorin V, Casartelli N, Noel N, Lambotte O, Mouquet H, Schwartz O. 2016. Elimination of HIV-1-infected cells by broadly neutralizing antibodies. Nat Commun 7:10844.
93. Caskey M, Klein F, Lorenzi JC, Seaman MS, West AP, Jr., Buckley N, Kremer G, Nogueira L, Braunschweig M, Scheid JF, Horwitz JA, Shimeliovich I, Ben-

Avraham S, Witmer-Pack M, Platten M, Lehmann C, Burke LA, Hawthorne T, Gorelick RJ, Walker BD, Keler T, Gulick RM, Fatkenheuer G, Schlesinger SJ, Nussenzweig MC. 2015. Viraemia suppressed in HIV-1-infected humans by broadly neutralizing antibody 3BNC117. Nature 522:487-91.

94. Lynch RM, Boritz E, Coates EE, DeZure A, Madden P, Costner P, Enama ME, Plummer S, Holman L, Hendel CS, Gordon I, Casazza J, Conan-Cibotti M, Migueles SA, Tressler R, Bailer RT, McDermott A, Narpala S, O'Dell S, Wolf G, Lifson JD, Freemire BA, Gorelick RJ, Pandey JP, Mohan S, Chomont N, Fromentin R, Chun TW, Fauci AS, Schwartz RM, Koup RA, Douek DC, Hu Z, Capparelli E, Graham BS, Mascola JR, Ledgerwood JE, Team VRCS. 2015. Virologic effects of broadly neutralizing antibody VRC01 administration during chronic HIV-1 infection. Sci Transl Med 7:319ra206.
95. Borducchi EN, Liu J, Nkolola JP, Cadena AM, Yu WH, Fischinger S, Broge T, Abbink P, Mercado NB, Chandrashekar A, Jetton D, Peter L, McMahan K, Moseley ET, Bekerman E, Hesselgesser J, Li W, Lewis MG, Alter G, Geleziunas R, Barouch DH. 2018. Antibody and TLR7 agonist delay viral rebound in SHIV-infected monkeys. Nature 563:360-364.
96. Henrich TJ, Hatano H, Bacon O, Hogan LE, Rutishauser R, Hill A, Kearney MF, Anderson EM, Buchbinder SP, Cohen SE, Abdel-Mohsen M, Pohlmeyer CW, Fromentin R, Hoh R, Liu AY, McCune JM, Spindler J, Metcalf-Pate K, Hobbs KS, Thanh C, Gibson EA, Kuritzkes DR, Siliciano RF, Price RW, Richman DD, Chomont N, Siliciano JD, Mellors JW, Yukl SA, Blankson JN, Liegler T, Deeks SG. 2017. HIV-1 persistence following extremely early initiation of antiretroviral therapy (ART) during acute HIV-1 infection: An observational study. PLoS Med 14:e1002417.
97. Brodin J, Zanini F, Thebo L, Lanz C, Bratt G, Neher RA, Albert J. 2016. Establishment and stability of the latent HIV-1 DNA reservoir. Elife 5.
98. Petravic J, Martyushev A, Reece JC, Kent SJ, Davenport MP. 2014. Modeling the timing of antilatency drug administration during HIV treatment. J Virol 88:14050-6.
99. Chomont N, Okoye AA, Favre D, Trautmann L. 2018. Wake me up before you go: a strategy to reduce the latent HIV reservoir. AIDS 32:293-298.
100. Gunst JD, Tolstrup M, Sogaard OS. 2017. Beyond antiretroviral therapy: early interventions to control HIV-1 infection. AIDS 31:1665-1667.
101. Goulder P, Deeks SG. 2018. HIV control: Is getting there the same as staying there? PLoS Pathog 14:e1007222.
102. Gaj T, Sirk SJ, Shui SL, Liu J. 2016. Genome-Editing Technologies: Principles and Applications. Cold Spring Harb Perspect Biol 8.
103. Tebas P, Stein D, Tang WW, Frank I, Wang SQ, Lee G, Spratt SK, Surosky RT, Giedlin MA, Nichol G, Holmes MC, Gregory PD, Ando DG, Kalos M, Collman RG, Binder-Scholl G, Plesa G, Hwang WT, Levine BL, June CH. 2014. Gene editing of CCR5 in autologous CD4 T cells of persons infected with HIV. N Engl J Med 370:901-10.
104. Petolino JF, Worden A, Curlee K, Connell J, Strange Moynahan TL, Larsen C, Russell S. 2010. Zinc finger nuclease-mediated transgene deletion. Plant Mol Biol 73:617-28.

105. Xu L, Yang H, Gao Y, Chen Z, Xie L, Liu Y, Liu Y, Wang X, Li H, Lai W, He Y, Yao A, Ma L, Shao Y, Zhang B, Wang C, Chen H, Deng H. 2017. CRISPR/Cas9-Mediated CCR5 Ablation in Human Hematopoietic Stem/Progenitor Cells Confers HIV-1 Resistance In Vivo. Mol Ther 25:1782-1789.
106. Doudna JA, Charpentier E. 2014. Genome editing. The new frontier of genome engineering with CRISPR-Cas9. Science 346:1258096.
107. Hu W, Kaminski R, Yang F, Zhang Y, Cosentino L, Li F, Luo B, Alvarez-Carbonell D, Garcia-Mesa Y, Karn J, Mo X, Khalili K. 2014. RNA-directed gene editing specifically eradicates latent and prevents new HIV-1 infection. Proc Natl Acad Sci U S A 111:11461-6.
108. Kaminski R, Bella R, Yin C, Otte J, Ferrante P, Gendelman HE, Li H, Booze R, Gordon J, Hu W, Khalili K. 2016. Excision of HIV-1 DNA by gene editing: a proof-of-concept in vivo study. Gene Ther 23:696.
109. Dash PK, Kaminski R, Bella R, Su H, Mathews S, Ahooyi TM, Chen C, Mancuso P, Sariyer R, Ferrante P, Donadoni M, Robinson JA, Sillman B, Lin Z, Hilaire JR, Banoub M, Elango M, Gautam N, Mosley RL, Poluektova LY, McMillan J, Bade AN, Gorantla S, Sariyer IK, Burdo TH, Young WB, Amini S, Gordon J, Jacobson JM, Edagwa B, Khalili K, Gendelman HE. 2019. Sequential LASER ART and CRISPR Treatments Eliminate HIV-1 in a Subset of Infected Humanized Mice. Nat Commun 10:2753.
110. Richman DD, Margolis DM, Delaney M, Greene WC, Hazuda D, Pomerantz RJ. 2009. The challenge of finding a cure for HIV infection. Science 323:1304-7.
111. Colby DJ, Trautmann L, Pinyakorn S, Leyre L, Pagliuzza A, Kroon E, Rolland M, Takata H, Buranapraditkun S, Intasan J, Chomchey N, Muir R, Haddad EK, Tovanabutra S, Ubolyam S, Bolton DL, Fullmer BA, Gorelick RJ, Fox L, Crowell TA, Trichavaroj R, O'Connell R, Chomont N, Kim JH, Michael NL, Robb ML, Phanuphak N, Ananworanich J, group RVs. 2018. Rapid HIV RNA rebound after antiretroviral treatment interruption in persons durably suppressed in Fiebig I acute HIV infection. Nat Med doi:10.1038/s41591-018-0026-6.
112. Denton PW, Sogaard OS, Tolstrup M. 2016. Using animal models to overcome temporal, spatial and combinatorial challenges in HIV persistence research. J Transl Med 14:44.
113. Miller CJ, Li Q, Abel K, Kim EY, Ma ZM, Wietgrefe S, La Franco-Scheuch L, Compton L, Duan L, Shore MD, Zupancic M, Busch M, Carlis J, Wolinsky S, Haase AT. 2005. Propagation and dissemination of infection after vaginal transmission of simian immunodeficiency virus. J Virol 79:9217-27.
114. Barouch DH, Ghneim K, Bosche WJ, Li Y, Berkemeier B, Hull M, Bhattacharyya S, Cameron M, Liu J, Smith K, Borducchi E, Cabral C, Peter L, Brinkman A, Shetty M, Li H, Gittens C, Baker C, Wagner W, Lewis MG, Colantonio A, Kang HJ, Li W, Lifson JD, Piatak M, Jr., Sekaly RP. 2016. Rapid Inflammasome Activation following Mucosal SIV Infection of Rhesus Monkeys. Cell 165:656-67.
115. Akkina R, Allam A, Balazs AB, Blankson JN, Burnett JC, Casares S, Garcia JV, Hasenkrug KJ, Kashanchi F, Kitchen SG, Klein F, Kumar P, Luster AD, Poluektova LY, Rao M, Sanders-Beer BE, Shultz LD, Zack JA. 2016. Improvements and Limitations of Humanized Mouse Models for HIV Research:

NIH/NIAID "Meet the Experts" 2015 Workshop Summary. AIDS Res Hum Retroviruses 32:109-19.
116. Dash PK, Gendelman HE, Roy U, Balkundi S, Alnouti Y, Mosley RL, Gelbard HA, McMillan J, Gorantla S, Poluektova LY. 2012. Long-acting nanoformulated antiretroviral therapy elicits potent antiretroviral and neuroprotective responses in HIV-1-infected humanized mice. AIDS 26:2135-44.
117. Victor Garcia J. 2016. Humanized mice for HIV and AIDS research. Curr Opin Virol 19:56-64.
118. Kim J, Peachman KK, Jobe O, Morrison EB, Allam A, Jagodzinski L, Casares SA, Rao M. 2017. Tracking Human Immunodeficiency Virus-1 Infection in the Humanized DRAG Mouse Model. Front Immunol 8:1405.
119. Gorantla S, Makarov E, Finke-Dwyer J, Gebhart CL, Domm W, Dewhurst S, Gendelman HE, Poluektova LY. 2010. CD8+ cell depletion accelerates HIV-1 immunopathology in humanized mice. J Immunol 184:7082-91.
120. Gorantla S, Makarov E, Finke-Dwyer J, Castanedo A, Holguin A, Gebhart CL, Gendelman HE, Poluektova L. 2010. Links between progressive HIV-1 infection of humanized mice and viral neuropathogenesis. Am J Pathol 177:2938-49.
121. Araínga M, Su H, Poluektova LY, Gorantla S, Gendelman HE. 2016. HIV-1 cellular and tissue replication patterns in infected humanized mice. Scientific Reports 6:23513.
122. Benki S, McClelland RS, Emery S, Baeten JM, Richardson BA, Lavreys L, Mandaliya K, Overbaugh J. 2006. Quantification of genital human immunodeficiency virus type 1 (HIV-1) DNA in specimens from women with low plasma HIV-1 RNA levels typical of HIV-1 nontransmitters. J Clin Microbiol 44:4357-62.
123. Roy U, McMillan J, Alnouti Y, Gautum N, Smith N, Balkundi S, Dash P, Gorantla S, Martinez-Skinner A, Meza J, Kanmogne G, Swindells S, Cohen SM, Mosley RL, Poluektova L, Gendelman HE. 2012. Pharmacodynamic and antiretroviral activities of combination nanoformulated antiretrovirals in HIV-1-infected human peripheral blood lymphocyte-reconstituted mice. J Infect Dis 206:1577-88.
124. Ali N, Flutter B, Sanchez Rodriguez R, Sharif-Paghaleh E, Barber LD, Lombardi G, Nestle FO. 2012. Xenogeneic graft-versus-host-disease in NOD-scid IL-2Rgammanull mice display a T-effector memory phenotype. PLoS One 7:e44219.
125. Moir S, Chun TW, Fauci AS. 2011. Pathogenic mechanisms of HIV disease. Annu Rev Pathol 6:223-48.
126. Garcia S, Dadaglio G, Gougeon ML. 1997. Limits of the human-PBL-SCID mice model: severe restriction of the V beta T-cell repertoire of engrafted human T cells. Blood 89:329-36.
127. Strain MC, Little SJ, Daar ES, Havlir DV, Gunthard HF, Lam RY, Daly OA, Nguyen J, Ignacio CC, Spina CA, Richman DD, Wong JK. 2005. Effect of treatment, during primary infection, on establishment and clearance of cellular reservoirs of HIV-1. J Infect Dis 191:1410-8.
128. Buzon MJ, Martin-Gayo E, Pereyra F, Ouyang Z, Sun H, Li JZ, Piovoso M, Shaw A, Dalmau J, Zangger N, Martinez-Picado J, Zurakowski R, Yu XG, Telenti A, Walker BD, Rosenberg ES, Lichterfeld M. 2014. Long-term antiretroviral treatment initiated at primary HIV-1 infection affects the size, composition, and

decay kinetics of the reservoir of HIV-1-infected CD4 T cells. J Virol 88:10056-65.
129. Hey-Cunningham WJ, Murray JM, Natarajan V, Amin J, Moore CL, Emery S, Cooper DA, Zaunders J, Kelleher AD, Koelsch KK. 2015. Early antiretroviral therapy with raltegravir generates sustained reductions in HIV reservoirs but not lower T-cell activation levels. Aids 29:911-9.
130. Hocqueloux L, Prazuck T, Avettand-Fenoel V, Lafeuillade A, Cardon B, Viard JP, Rouzioux C. 2010. Long-term immunovirologic control following antiretroviral therapy interruption in patients treated at the time of primary HIV-1 infection. AIDS 24:1598-601.
131. Gendelman HE, Orenstein JM, Martin MA, Ferrua C, Mitra R, Phipps T, Wahl LA, Lane HC, Fauci AS, Burke DS, et al. 1988. Efficient isolation and propagation of human immunodeficiency virus on recombinant colony-stimulating factor 1-treated monocytes. J Exp Med 167:1428-41.
132. Gorantla S, Gendelman HE, Poluektova LY. 2012. Can humanized mice reflect the complex pathobiology of HIV-associated neurocognitive disorders? J Neuroimmune Pharmacol 7:352-62.
133. Mosier DE, Gulizia RJ, Baird SM, Wilson DB, Spector DH, Spector SA. 1991. Human immunodeficiency virus infection of human-PBL-SCID mice. Science 251:791-4.
134. Levy JA. 2011. Virus-host interactions in HIV pathogenesis: directions for therapy. Adv Dent Res 23:13-8.
135. Brenchley JM, Schacker TW, Ruff LE, Price DA, Taylor JH, Beilman GJ, Nguyen PL, Khoruts A, Larson M, Haase AT, Douek DC. 2004. CD4+ T cell depletion during all stages of HIV disease occurs predominantly in the gastrointestinal tract. J Exp Med 200:749-59.
136. Engsig FN, Zangerle R, Katsarou O, Dabis F, Reiss P, Gill J, Porter K, Sabin C, Riordan A, Fatkenheuer G, Gutierrez F, Raffi F, Kirk O, Mary-Krause M, Stephan C, de Olalla PG, Guest J, Samji H, Castagna A, d'Arminio Monforte A, Skaletz-Rorowski A, Ramos J, Lapadula G, Mussini C, Force L, Meyer L, Lampe F, Boufassa F, Bucher HC, De Wit S, Burkholder GA, Teira R, Justice AC, Sterling TR, H MC, Gerstoft J, Grarup J, May M, Chene G, Ingle SM, Sterne J, Obel N, Antiretroviral Therapy Cohort C, the Collaboration of Observational HIVEREiE. 2014. Long-term mortality in HIV-positive individuals virally suppressed for >3 years with incomplete CD4 recovery. Clin Infect Dis 58:1312-21.
137. Cohen MS, Shaw GM, McMichael AJ, Haynes BF. 2011. Acute HIV-1 Infection. N Engl J Med 364:1943-54.
138. Valcour V, Chalermchai T, Sailasuta N, Marovich M, Lerdlum S, Suttichom D, Suwanwela NC, Jagodzinski L, Michael N, Spudich S, van Griensven F, de Souza M, Kim J, Ananworanich J, Group RSS. 2012. Central nervous system viral invasion and inflammation during acute HIV infection. J Infect Dis 206:275-82.
139. Nolan DJ, Rose R, Rodriguez PH, Salemi M, Singer EJ, Lamers SL, McGrath MS. 2018. The Spleen Is an HIV-1 Sanctuary During Combined Antiretroviral Therapy. AIDS Res Hum Retroviruses 34:123-125.
140. Velu V, Mylvaganam G, Ibegbu C, Amara RR. 2018. Tfh1 Cells in Germinal Centers During Chronic HIV/SIV Infection. Front Immunol 9:1272.

141. Simonetti FR, Sobolewski MD, Fyne E, Shao W, Spindler J, Hattori J, Anderson EM, Watters SA, Hill S, Wu X, Wells D, Su L, Luke BT, Halvas EK, Besson G, Penrose KJ, Yang Z, Kwan RW, Van Waes C, Uldrick T, Citrin DE, Kovacs J, Polis MA, Rehm CA, Gorelick R, Piatak M, Keele BF, Kearney MF, Coffin JM, Hughes SH, Mellors JW, Maldarelli F. 2016. Clonally expanded CD4+ T cells can produce infectious HIV-1 in vivo. Proc Natl Acad Sci U S A 113:1883-8.
142. Brehm MA, Shultz LD, Luban J, Greiner DL. 2013. Overcoming current limitations in humanized mouse research. J Infect Dis 208 Suppl 2:S125-30.
143. Denton PW, Nochi T, Lim A, Krisko JF, Martinez-Torres F, Choudhary SK, Wahl A, Olesen R, Zou W, Di Santo JP, Margolis DM, Garcia JV. 2012. IL-2 receptor gamma-chain molecule is critical for intestinal T-cell reconstitution in humanized mice. Mucosal Immunol 5:555-66.
144. Joseph SB, Swanstrom R, Kashuba AD, Cohen MS. 2015. Bottlenecks in HIV-1 transmission: insights from the study of founder viruses. Nat Rev Microbiol 13:414-25.
145. Watanabe S, Ohta S, Yajima M, Terashima K, Ito M, Mugishima H, Fujiwara S, Shimizu K, Honda M, Shimizu N, Yamamoto N. 2007. Humanized NOD/SCID/IL2Rgamma(null) mice transplanted with hematopoietic stem cells under nonmyeloablative conditions show prolonged life spans and allow detailed analysis of human immunodeficiency virus type 1 pathogenesis. J Virol 81:13259-64.
146. Araínga M, Edagwa B, Mosley RL, Poluektova LY, Gorantla S, Gendelman HE. 2017. A mature macrophage is a principal HIV-1 cellular reservoir in humanized mice after treatment with long acting antiretroviral therapy. Retrovirology 14:17.
147. Koning FA, Otto SA, Hazenberg MD, Dekker L, Prins M, Miedema F, Schuitemaker H. 2005. Low-level CD4+ T cell activation is associated with low susceptibility to HIV-1 infection. J Immunol 175:6117-22.
148. Begaud E, Chartier L, Marechal V, Ipero J, Leal J, Versmisse P, Breton G, Fontanet A, Capoulade-Metay C, Fleury H, Barre-Sinoussi F, Scott-Algara D, Pancino G. 2006. Reduced CD4 T cell activation and in vitro susceptibility to HIV-1 infection in exposed uninfected Central Africans. Retrovirology 3:35.
149. Ward H, Ronn M. 2010. Contribution of sexually transmitted infections to the sexual transmission of HIV. Curr Opin HIV AIDS 5:305-10.
150. Johnson LF, Lewis DA. 2008. The effect of genital tract infections on HIV-1 shedding in the genital tract: a systematic review and meta-analysis. Sex Transm Dis 35:946-59.
151. Schacker T, Zeh J, Hu H, Shaughnessy M, Corey L. 2002. Changes in plasma human immunodeficiency virus type 1 RNA associated with herpes simplex virus reactivation and suppression. J Infect Dis 186:1718-25.
152. Selhorst P, Masson L, Ismail SD, Samsunder N, Garrett N, Mansoor LE, Abdool Karim Q, Abdool Karim SS, Passmore JS, Williamson C. 2017. Cervicovaginal Inflammation Facilitates Acquisition of Less Infectious HIV Variants. Clin Infect Dis 64:79-82.
153. Srivastava KK, Fernandez-Larsson R, Zinkus DM, Robinson HL. 1991. Human immunodeficiency virus type 1 NL4-3 replication in four T-cell lines: rate and efficiency of entry, a major determinant of permissiveness. J Virol 65:3900-2.

154. Rose R, Nolan DJ, Maidji E, Stoddart CA, Singer EJ, Lamers SL, McGrath MS. 2018. Eradication of HIV from Tissue Reservoirs: Challenges for the Cure. AIDS Res Hum Retroviruses 34:3-8.
155. Chun TW, Stuyver L, Mizell SB, Ehler LA, Mican JA, Baseler M, Lloyd AL, Nowak MA, Fauci AS. 1997. Presence of an inducible HIV-1 latent reservoir during highly active antiretroviral therapy. Proc Natl Acad Sci U S A 94:13193-7.
156. Lorenzo-Redondo R, Fryer HR, Bedford T, Kim EY, Archer J, Pond SLK, Chung YS, Penugonda S, Chipman J, Fletcher CV, Schacker TW, Malim MH, Rambaut A, Haase AT, McLean AR, Wolinsky SM. 2016. Persistent HIV-1 replication maintains the tissue reservoir during therapy. Nature 530:51-56.
157. Deeks SG, Lewin SR, Ross AL, Ananworanich J, Benkirane M, Cannon P, Chomont N, Douek D, Lifson JD, Lo YR, Kuritzkes D, Margolis D, Mellors J, Persaud D, Tucker JD, Barre-Sinoussi F, International ASTaCWG, Alter G, Auerbach J, Autran B, Barouch DH, Behrens G, Cavazzana M, Chen Z, Cohen EA, Corbelli GM, Eholie S, Eyal N, Fidler S, Garcia L, Grossman C, Henderson G, Henrich TJ, Jefferys R, Kiem HP, McCune J, Moodley K, Newman PA, Nijhuis M, Nsubuga MS, Ott M, Palmer S, Richman D, Saez-Cirion A, Sharp M, Siliciano J, Silvestri G, Singh J, Spire B, Taylor J, et al. 2016. International AIDS Society global scientific strategy: towards an HIV cure 2016. Nat Med 22:839-50.
158. Martin AR, Siliciano RF. 2016. Progress Toward HIV Eradication: Case Reports, Current Efforts, and the Challenges Associated with Cure. Annu Rev Med 67:215-28.
159. Siliciano JD, Siliciano RF. 2016. Recent developments in the effort to cure HIV infection: going beyond N = 1. J Clin Invest 126:409-14.
160. Xu W, Li H, Wang Q, Hua C, Zhang H, Li W, Jiang S, Lu L. 2017. Advancements in Developing Strategies for Sterilizing and Functional HIV Cures. Biomed Res Int 2017:6096134.
161. Guo D, Zhou T, Arainga M, Palandri D, Gautam N, Bronich T, Alnouti Y, McMillan J, Edagwa B, Gendelman HE. 2017. Creation of a Long-Acting Nanoformulated 2',3'-Dideoxy-3'-Thiacytidine. J Acquir Immune Defic Syndr 74:e75-e83.
162. Singh D, McMillan J, Hilaire J, Gautam N, Palandri D, Alnouti Y, Gendelman HE, Edagwa B. 2016. Development and characterization of a long-acting nanoformulated abacavir prodrug. Nanomedicine (Lond) 11:1913-27.
163. Edagwa BJ, Zhou T, McMillan JM, Liu XM, Gendelman HE. 2014. Development of HIV reservoir targeted long acting nanoformulated antiretroviral therapies. Curr Med Chem 21:4186-98.
164. Edagwa B, McMillan J, Sillman B, Gendelman HE. 2017. Long-acting slow effective release antiretroviral therapy. Expert Opin Drug Deliv 14:1281-1291.
165. Kaminski R, Bella R, Yin C, Otte J, Ferrante P, Gendelman HE, Li H, Booze R, Gordon J, Hu W, Khalili K. 2016. Excision of HIV-1 DNA by gene editing: a proof-of-concept in vivo study. Gene Ther 23:690-5.
166. Kaminski R, Chen Y, Fischer T, Tedaldi E, Napoli A, Zhang Y, Karn J, Hu W, Khalili K. 2016. Elimination of HIV-1 Genomes from Human T-lymphoid Cells by CRISPR/Cas9 Gene Editing. Sci Rep 6:22555.

167. Kaminski R, Chen Y, Salkind J, Bella R, Young WB, Ferrante P, Karn J, Malcolm T, Hu W, Khalili K. 2016. Negative Feedback Regulation of HIV-1 by Gene Editing Strategy. Sci Rep 6:31527.
168. White MK, Hu W, Khalili K. 2016. Gene Editing Approaches against Viral Infections and Strategy to Prevent Occurrence of Viral Escape. PLoS Pathog 12:e1005953.
169. Yin C, Zhang T, Qu X, Zhang Y, Putatunda R, Xiao X, Li F, Xiao W, Zhao H, Dai S, Qin X, Mo X, Young WB, Khalili K, Hu W. 2017. In Vivo Excision of HIV-1 Provirus by saCas9 and Multiplex Single-Guide RNAs in Animal Models. Mol Ther 25:1168-1186.
170. O'Doherty U, Swiggard WJ, Malim MH. 2000. Human immunodeficiency virus type 1 spinoculation enhances infection through virus binding. J Virol 74:10074-80.
171. Dash PK, Gorantla S, Gendelman HE, Knibbe J, Casale GP, Makarov E, Epstein AA, Gelbard HA, Boska MD, Poluektova LY. 2011. Loss of neuronal integrity during progressive HIV-1 infection of humanized mice. J Neurosci 31:3148-57.
172. Gorantla S, Sneller H, Walters L, Sharp JG, Pirruccello SJ, West JT, Wood C, Dewhurst S, Gendelman HE, Poluektova L. 2007. Human immunodeficiency virus type 1 pathobiology studied in humanized BALB/c-Rag2-/-gammac-/- mice. J Virol 81:2700-12.
173. Arainga M, Edagwa B, Mosley RL, Poluektova LY, Gorantla S, Gendelman HE. 2017. A mature macrophage is a principal HIV-1 cellular reservoir in humanized mice after treatment with long acting antiretroviral therapy. Retrovirology 14:17.
174. Pasternak AO, Adema KW, Bakker M, Jurriaans S, Berkhout B, Cornelissen M, Lukashov VV. 2008. Highly sensitive methods based on seminested real-time reverse transcription-PCR for quantitation of human immunodeficiency virus type 1 unspliced and multiply spliced RNA and proviral DNA. J Clin Microbiol 46:2206-11.
175. Buzon MJ, Sun H, Li C, Shaw A, Seiss K, Ouyang Z, Martin-Gayo E, Leng J, Henrich TJ, Li JZ, Pereyra F, Zurakowski R, Walker BD, Rosenberg ES, Yu XG, Lichterfeld M. 2014. HIV-1 persistence in CD4+ T cells with stem cell-like properties. Nat Med 20:139-42.
176. Laird GM, Eisele EE, Rabi SA, Lai J, Chioma S, Blankson JN, Siliciano JD, Siliciano RF. 2013. Rapid quantification of the latent reservoir for HIV-1 using a viral outgrowth assay. PLoS Pathog 9:e1003398.
177. Hunsucker SA, Mitchell BS, Spychala J. 2005. The 5'-nucleotidases as regulators of nucleotide and drug metabolism. Pharmacol Ther 107:1-30.
178. Yuen GJ, Weller S, Pakes GE. 2008. A review of the pharmacokinetics of abacavir. Clin Pharmacokinet 47:351-71.
179. Singh H, Kaur M, Kakkar AK, Kumar H. 2016. The Promise of Dolutegravir: A Novel Second Generation Integrase Strand Transfer Inhibitor. Curr Clin Pharmacol 11:88-94.
180. Ford N, Lee J, Andrieux-Meyer I, Calmy A. 2011. Safety, efficacy, and pharmacokinetics of rilpivirine: systematic review with an emphasis on resource-limited settings. HIV AIDS (Auckl) 3:35-44.

181. Charlins P, Schmitt K, Remling-Mulder L, Hogan LE, Hanhauser E, Hobbs KS, Hecht F, Deeks SG, Henrich TJ, Akkina R. 2017. A humanized mouse-based HIV-1 viral outgrowth assay with higher sensitivity than in vitro qVOA in detecting latently infected cells from individuals on ART with undetectable viral loads. Virology 507:135-139.
182. Littman DR. 1998. Chemokine receptors: keys to AIDS pathogenesis? Cell 93:677-80.
183. Murphy PM. 2001. Viral exploitation and subversion of the immune system through chemokine mimicry. Nat Immunol 2:116-22.
184. Dean M, Carrington M, Winkler C, Huttley GA, Smith MW, Allikmets R, Goedert JJ, Buchbinder SP, Vittinghoff E, Gomperts E, Donfield S, Vlahov D, Kaslow R, Saah A, Rinaldo C, Detels R, O'Brien SJ. 1996. Genetic restriction of HIV-1 infection and progression to AIDS by a deletion allele of the CKR5 structural gene. Hemophilia Growth and Development Study, Multicenter AIDS Cohort Study, Multicenter Hemophilia Cohort Study, San Francisco City Cohort, ALIVE Study. Science 273:1856-62.
185. Samson M, Libert F, Doranz BJ, Rucker J, Liesnard C, Farber CM, Saragosti S, Lapoumeroulie C, Cognaux J, Forceille C, Muyldermans G, Verhofstede C, Burtonboy G, Georges M, Imai T, Rana S, Yi Y, Smyth RJ, Collman RG, Doms RW, Vassart G, Parmentier M. 1996. Resistance to HIV-1 infection in caucasian individuals bearing mutant alleles of the CCR-5 chemokine receptor gene. Nature 382:722-5.
186. Li C, Guan X, Du T, Jin W, Wu B, Liu Y, Wang P, Hu B, Griffin GE, Shattock RJ, Hu Q. 2015. Inhibition of HIV-1 infection of primary CD4+ T-cells by gene editing of CCR5 using adenovirus-delivered CRISPR/Cas9. J Gen Virol 96:2381-93.
187. Boska MD, Dash PK, Knibbe J, Epstein AA, Akhter SP, Fields N, High R, Makarov E, Bonasera S, Gelbard HA, Poluektova LY, Gendelman HE, Gorantla S. 2014. Associations between brain microstructures, metabolites, and cognitive deficits during chronic HIV-1 infection of humanized mice. Mol Neurodegener 9:58.
188. Gorantla S, Poluektova L, Gendelman HE. 2012. Rodent models for HIV-associated neurocognitive disorders. Trends Neurosci 35:197-208.
189. Puligujja P, Arainga M, Dash P, Palandri D, Mosley RL, Gorantla S, Poluektova L, McMillan J, Gendelman HE. 2015. Pharmacodynamics of folic acid receptor targeted antiretroviral nanotherapy in HIV-1-infected humanized mice. Antiviral Res 120:85-8.
190. Gnanadhas DP, Dash PK, Sillman B, Bade AN, Lin Z, Palandri DL, Gautam N, Alnouti Y, Gelbard HA, McMillan J, Mosley RL, Edagwa B, Gendelman HE, Gorantla S. 2017. Autophagy facilitates macrophage depots of sustained-release nanoformulated antiretroviral drugs. J Clin Invest 127:857-873.
191. Ottemann BM, Helmink AJ, Zhang W, Mukadam I, Woldstad C, Hilaire JR, Liu Y, McMillan JM, Edagwa BJ, Mosley RL, Garrison JC, Kevadiya BD, Gendelman HE. 2018. Bioimaging predictors of rilpivirine biodistribution and antiretroviral activities. Biomaterials 185:174-193.
192. Herskovitz J, Gendelman HE. 2019. HIV and the Macrophage: From Cell Reservoirs to Drug Delivery to Viral Eradication. J Neuroimmune Pharmacol 14:52-67.

193. McMillan J, Szlachetka A, Zhou T, Morsey B, Lamberty B, Callen S, Gautam N, Alnouti Y, Edagwa B, Gendelman HE, Fox HS. 2019. Pharmacokinetic testing of a first-generation cabotegravir prodrug in rhesus macaques. AIDS 33:585-588.
194. Dou H, Destache CJ, Morehead JR, Mosley RL, Boska MD, Kingsley J, Gorantla S, Poluektova L, Nelson JA, Chaubal M, Werling J, Kipp J, Rabinow BE, Gendelman HE. 2006. Development of a macrophage-based nanoparticle platform for antiretroviral drug delivery. Blood 108:2827-35.
195. Dou H, Grotepas CB, McMillan JM, Destache CJ, Chaubal M, Werling J, Kipp J, Rabinow B, Gendelman HE. 2009. Macrophage delivery of nanoformulated antiretroviral drug to the brain in a murine model of neuroAIDS. J Immunol 183:661-9.
196. Su H, Cheng Y, Sravanam S, Mathews S, Gorantla S, Poluektova LY, Dash PK, Gendelman HE. 2019. Immune Activations and Viral Tissue Compartmentalization During Progressive HIV-1 Infection of Humanized Mice. Front Immunol 10:340.
197. Zhang G, Guo D, Dash PK, Arainga M, Wiederin JL, Haverland NA, Knibbe-Hollinger J, Martinez-Skinner A, Ciborowski P, Goodfellow VS, Wysocki TA, Wysocki BJ, Poluektova LY, Liu XM, McMillan JM, Gorantla S, Gelbard HA, Gendelman HE. 2016. The mixed lineage kinase-3 inhibitor URMC-099 improves therapeutic outcomes for long-acting antiretroviral therapy. Nanomedicine 12:109-22.
198. Zhou T, Lin Z, Puligujja P, Palandri D, Hilaire J, Arainga M, Smith N, Gautam N, McMillan J, Alnouti Y, Liu X, Edagwa B, Gendelman HE. 2018. Optimizing the preparation and stability of decorated antiretroviral drug nanocrystals. Nanomedicine (Lond) 13:871-885.
199. Guo D, Zhang G, Wysocki TA, Wysocki BJ, Gelbard HA, Liu XM, McMillan JM, Gendelman HE. 2014. Endosomal trafficking of nanoformulated antiretroviral therapy facilitates drug particle carriage and HIV clearance. J Virol 88:9504-13.
200. Nowacek AS, Balkundi S, McMillan J, Roy U, Martinez-Skinner A, Mosley RL, Kanmogne G, Kabanov AV, Bronich T, Gendelman HE. 2011. Analyses of nanoformulated antiretroviral drug charge, size, shape and content for uptake, drug release and antiviral activities in human monocyte-derived macrophages. J Control Release 150:204-11.
201. Balkundi S, Nowacek AS, Roy U, Martinez-Skinner A, McMillan J, Gendelman HE. 2010. Methods development for blood borne macrophage carriage of nanoformulated antiretroviral drugs. J Vis Exp doi:10.3791/2460.
202. Nowacek AS, McMillan J, Miller R, Anderson A, Rabinow B, Gendelman HE. 2010. Nanoformulated antiretroviral drug combinations extend drug release and antiretroviral responses in HIV-1-infected macrophages: implications for neuroAIDS therapeutics. J Neuroimmune Pharmacol 5:592-601.
203. Eriksson S, Graf EH, Dahl V, Strain MC, Yukl SA, Lysenko ES, Bosch RJ, Lai J, Chioma S, Emad F, Abdel-Mohsen M, Hoh R, Hecht F, Hunt P, Somsouk M, Wong J, Johnston R, Siliciano RF, Richman DD, O'Doherty U, Palmer S, Deeks SG, Siliciano JD. 2013. Comparative analysis of measures of viral reservoirs in HIV-1 eradication studies. PLoS Pathog 9:e1003174.
204. Rouzioux C, Richman D. 2013. How to best measure HIV reservoirs? Curr Opin HIV AIDS 8:170-5.

205. Gupta P, Sanyal A, Mailliard RB. 2017. TZA: a novel assay for measuring the latent HIV-1 reservoir. Expert Rev Mol Diagn 17:1033-1035.
206. Sanyal A, Mailliard RB, Rinaldo CR, Ratner D, Ding M, Chen Y, Zerbato JM, Giacobbi NS, Venkatachari NJ, Patterson BK, Chargin A, Sluis-Cremer N, Gupta P. 2017. Novel assay reveals a large, inducible, replication-competent HIV-1 reservoir in resting CD4(+) T cells. Nat Med 23:885-889.
207. Bruner KM, Hosmane NN, Siliciano RF. 2015. Towards an HIV-1 cure: measuring the latent reservoir. Trends Microbiol 23:192-203.
208. Massanella M, Richman DD. 2016. Measuring the latent reservoir in vivo. J Clin Invest 126:464-72.
209. Bruner KM, Murray AJ, Pollack RA, Soliman MG, Laskey SB, Capoferri AA, Lai J, Strain MC, Lada SM, Hoh R, Ho YC, Richman DD, Deeks SG, Siliciano JD, Siliciano RF. 2016. Defective proviruses rapidly accumulate during acute HIV-1 infection. Nat Med 22:1043-9.
210. Siliciano JD, Siliciano RF. 2005. Enhanced culture assay for detection and quantitation of latently infected, resting CD4+ T-cells carrying replication-competent virus in HIV-1-infected individuals. Methods Mol Biol 304:3-15.
211. Ho YC, Shan L, Hosmane NN, Wang J, Laskey SB, Rosenbloom DI, Lai J, Blankson JN, Siliciano JD, Siliciano RF. 2013. Replication-competent noninduced proviruses in the latent reservoir increase barrier to HIV-1 cure. Cell 155:540-51.
212. Policicchio BB, Pandrea I, Apetrei C. 2016. Animal Models for HIV Cure Research. Front Immunol 7:12.
213. Metcalf Pate KA, Pohlmeyer CW, Walker-Sperling VE, Foote JB, Najarro KM, Cryer CG, Salgado M, Gama L, Engle EL, Shirk EN, Queen SE, Chioma S, Vermillion MS, Bullock B, Li M, Lyons CE, Adams RJ, Zink MC, Clements JE, Mankowski JL, Blankson JN. 2015. A Murine Viral Outgrowth Assay to Detect Residual HIV Type 1 in Patients With Undetectable Viral Loads. J Infect Dis 212:1387-96.
214. Yuan Z, Kang G, Lu W, Li Q. 2017. Reactivation of HIV-1 proviruses in immune-compromised mice engrafted with human VOA-negative CD4+ T cells. J Virus Erad 3:61-65.
215. Adachi A, Gendelman HE, Koenig S, Folks T, Willey R, Rabson A, Martin MA. 1986. Production of acquired immunodeficiency syndrome-associated retrovirus in human and nonhuman cells transfected with an infectious molecular clone. J Virol 59:284-91.
216. Gendelman HE, Baca LM, Kubrak CA, Genis P, Burrous S, Friedman RM, Jacobs D, Meltzer MS. 1992. Induction of IFN-alpha in peripheral blood mononuclear cells by HIV-infected monocytes. Restricted antiviral activity of the HIV-induced IFN. J Immunol 148:422-9.
217. Lu W, Mehraj V, Vyboh K, Cao W, Li T, Routy JP. 2015. CD4:CD8 ratio as a frontier marker for clinical outcome, immune dysfunction and viral reservoir size in virologically suppressed HIV-positive patients. J Int AIDS Soc 18:20052.
218. Bruner KM, Wang Z, Simonetti FR, Bender AM, Kwon KJ, Sengupta S, Fray EJ, Beg SA, Antar AAR, Jenike KM, Bertagnolli LN, Capoferri AA, Kufera JT, Timmons A, Nobles C, Gregg J, Wada N, Ho YC, Zhang H, Margolick JB, Blankson JN, Deeks SG, Bushman FD, Siliciano JD, Laird GM, Siliciano RF. 2019.

A quantitative approach for measuring the reservoir of latent HIV-1 proviruses. Nature 566:120-125.
219. Procopio FA, Fromentin R, Kulpa DA, Brehm JH, Bebin AG, Strain MC, Richman DD, O'Doherty U, Palmer S, Hecht FM, Hoh R, Barnard RJ, Miller MD, Hazuda DJ, Deeks SG, Sekaly RP, Chomont N. 2015. A Novel Assay to Measure the Magnitude of the Inducible Viral Reservoir in HIV-infected Individuals. EBioMedicine 2:874-83.
220. Henrich TJ, Hanhauser E, Marty FM, Sirignano MN, Keating S, Lee TH, Robles YP, Davis BT, Li JZ, Heisey A, Hill AL, Busch MP, Armand P, Soiffer RJ, Altfeld M, Kuritzkes DR. 2014. Antiretroviral-free HIV-1 remission and viral rebound after allogeneic stem cell transplantation: report of 2 cases. Ann Intern Med 161:319-27.
221. Dubrocq G, Rakhmanina N. 2018. Antiretroviral therapy interruptions: impact on HIV treatment and transmission. HIV AIDS (Auckl) 10:91-101.
222. Schmitt K, Akkina R. 2018. Ultra-Sensitive HIV-1 Latency Viral Outgrowth Assays Using Humanized Mice. Front Immunol 9:344.
223. Darcis G, Coombs RW, Van Lint C. 2016. Exploring the anatomical HIV reservoirs: role of the testicular tissue. AIDS 30:2891-2893.
224. Sander JD, Joung JK. 2014. CRISPR-Cas systems for editing, regulating and targeting genomes. Nat Biotechnol 32:347-55.
225. Xia W, Hilgenbrink AR, Matteson EL, Lockwood MB, Cheng JX, Low PS. 2009. A functional folate receptor is induced during macrophage activation and can be used to target drugs to activated macrophages. Blood 113:438-46.
226. Puligujja P, Balkundi SS, Kendrick LM, Baldridge HM, Hilaire JR, Bade AN, Dash PK, Zhang G, Poluektova LY, Gorantla S, Liu XM, Ying T, Feng Y, Wang Y, Dimitrov DS, McMillan JM, Gendelman HE. 2015. Pharmacodynamics of long-acting folic acid-receptor targeted ritonavir-boosted atazanavir nanoformulations. Biomaterials 41:141-50.
227. Lee CS, Bishop ES, Zhang R, Yu X, Farina EM, Yan S, Zhao C, Zheng Z, Shu Y, Wu X, Lei J, Li Y, Zhang W, Yang C, Wu K, Wu Y, Ho S, Athiviraham A, Lee MJ, Wolf JM, Reid RR, He TC. 2017. Adenovirus-Mediated Gene Delivery: Potential Applications for Gene and Cell-Based Therapies in the New Era of Personalized Medicine. Genes Dis 4:43-63.
228. Crystal RG. 2014. Adenovirus: the first effective in vivo gene delivery vector. Hum Gene Ther 25:3-11.
229. Kimberland ML, Hou W, Alfonso-Pecchio A, Wilson S, Rao Y, Zhang S, Lu Q. 2018. Strategies for controlling CRISPR/Cas9 off-target effects and biological variations in mammalian genome editing experiments. J Biotechnol 284:91-101.